Synthesis, electronic structure and interaction of rhodium(I) and iridium(I) bisimine-acenaphthalene complexes with CO_2.

Electronic Supplementary Information

Wynand J. Louw,[a] Shankara G. Radhakrishnan,[a,‡] Frederick P. Malan,[a] Daniela I. Bezuidenhout.[b,‡]

[a] Department of Chemistry, University of Pretoria, Private Bag X20, Hatfield 0028, Pretoria, South Africa, shankara.radhakrishnan@up.ac.za

[b] Laboratory of Inorganic Chemistry, Environmental and Chemical Engineering, University of Oulu, P.O. BOX 3000, FI-90014 Oulu, Finland, daniela.bezuidenhout@oulu.fi

[‡] Corresponding authors: shankara.radhakrishnan@up.ac.za, daniela.bezuidenhout@oulu.fi

TABLE OF CONTENT

S1) SYNTHESIS AND CHARACTERISATION DATA

S1.1) Complex **1a** [RhDB(cod)]PF_6

To 0.148 g (0.3 mmol, 1eq) $[Rh(cod)Cl]_2$, 0.301 g (0.6 mmol, 2eq) DippBIAN and 0.135 g (0.7 mmol, 2.44eq) KPF_6 in a Schlenk tube was added 20 mL CH_2Cl_2 at RT and the brown solution stirred overnight. The dark brown solution was filtered and dried *in vacuo*. The resulting brown powder was washed with 50 mL hexane, and **1a** was isolated as a dark brown solid. (0.437 g, 85 % yield).

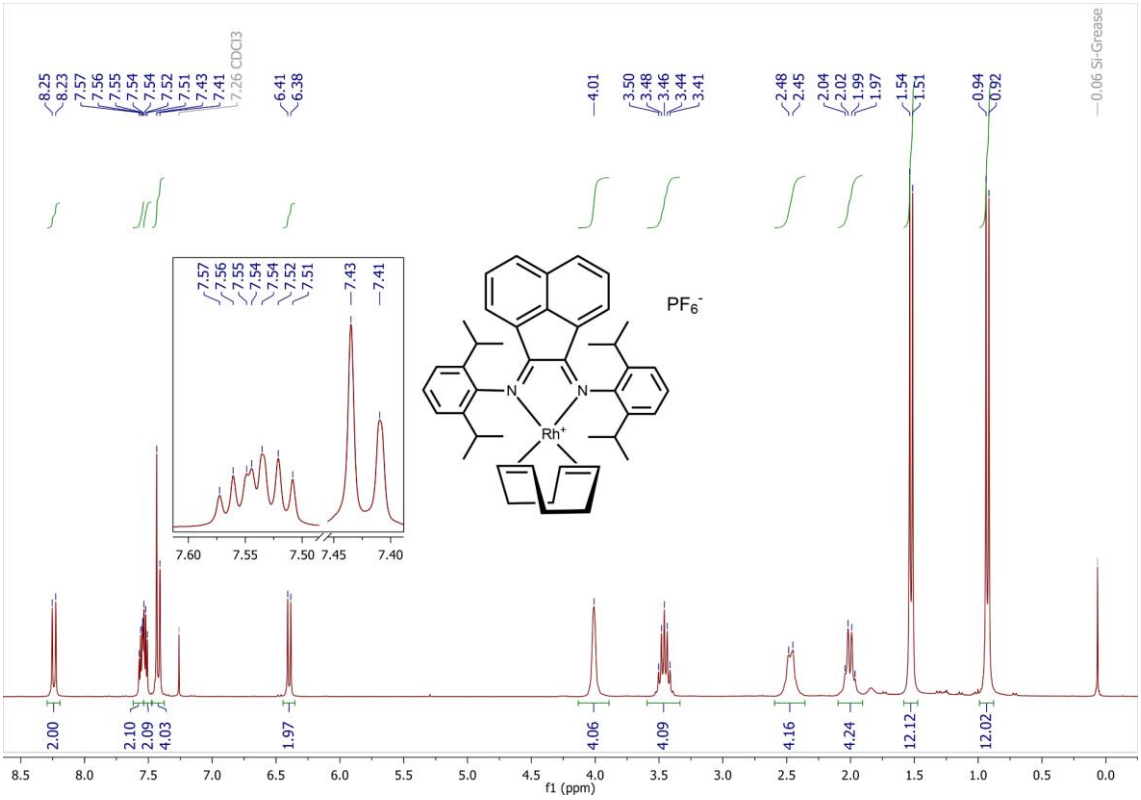

*Figure S1: ^1H NMR spectrum of complex **1a** in $CDCl_3$.*

^{1}H NMR (300 MHz, $CDCl_3$) δ 8.24 (d, *J* = 8.3 Hz, 2H, BIAN-Ar-C**H**), 7.56 (dd, *J* = 7.3, 3.6 Hz, 2H, BIAN-Ar-C**H**), 7.53 (dd, *J* = 7.5, 3.3 Hz, 2H, Dipp-Ar-C**H**), 7.42 (d, *J* = 7.5 Hz, 4H, Dipp-Ar-C**H**), 6.40 (d, *J* = 7.3 Hz, 2H, BIAN-Ar-C**H**), 4.01 (br, 4H, cod-C**H**), 3.46 (sept, *J* = 6.7 Hz, 4H, Dipp(iso)-C**H**), 2.59–2.36 (m, 4H, cod-C$\mathbf{H}_2$), 2.10–1.91 (m, 4H, cod-C$\mathbf{H}_2$), 1.52 (d, *J* = 6.8 Hz, 12H, Dipp(iso)-C$\mathbf{H}_3$), 0.93 (d, *J* = 6.8 Hz, 12H, Dipp(iso)-C$\mathbf{H}_3$).

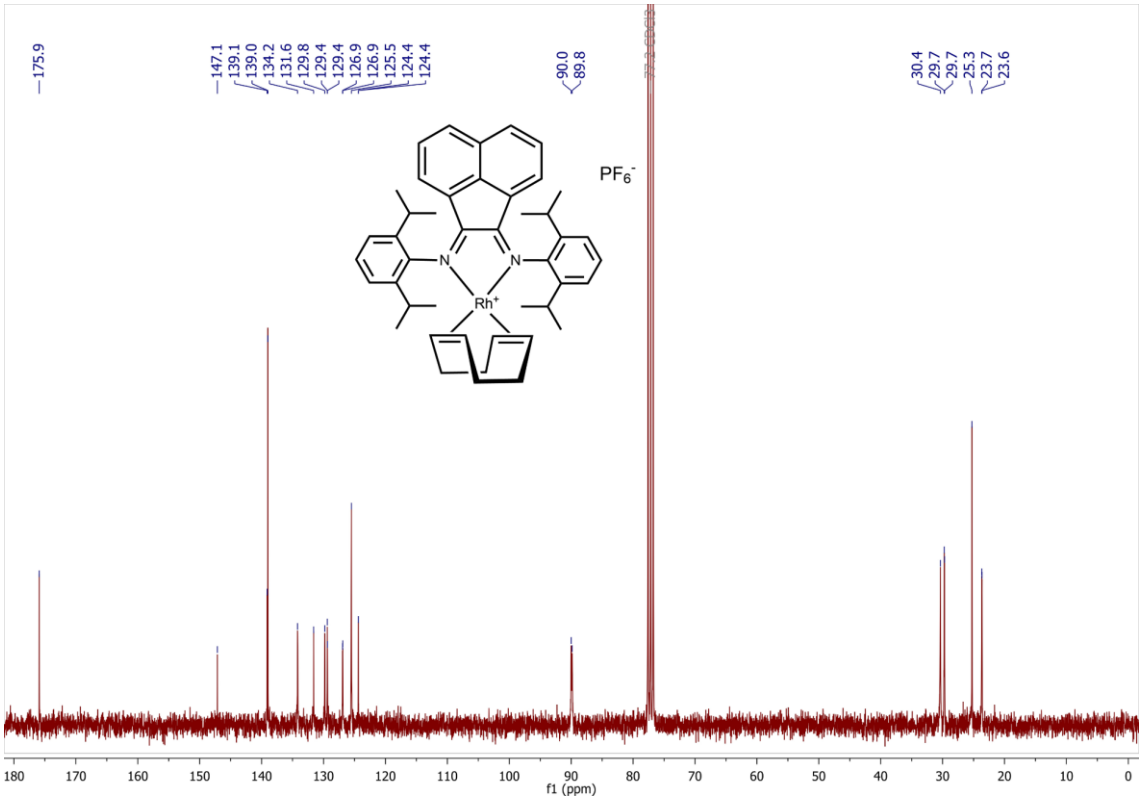

*Figure S2: ^{13}C NMR spectrum of complex **1a** in $CDCl_3$.*

^{13}C NMR (75 MHz, $CDCl_3$) δ 175.9 (BIAN-N=**C**$_q$), 147.1 (Dipp-N-**C**$_q$), 139.1 (BIAN-**C**$_q$), 139.00 (Dipp(iso)-**C**$_q$), 134.2 (BIAN-**C**H), 131.6 (**C**$_q$), 129.8 (**C**$_q$), 129.4 (Dipp-**C**H), 129.4 (Dipp-**C**H), 126.9 (BIAN-**C**H), 126.9 (BIAN-**C**H), 125.5 (Dipp-**C**H), 124.4 (BIAN-**C**$_q$), 124.4 (BIAN-**C**$_q$), 89.9 (d, $J_{C\text{-}Rh}$ = 12.2 Hz, cod-**C**H), 30.4 (cod-**C**H$_2$), 29.7 (Dipp(iso)-**C**H), 29.7 (cod-**C**H$_2$), 25.3 (Dipp(iso)-**C**H$_3$), 23.7, 23.6 (Dipp(iso)-**C**H$_3$).

^{19}F NMR (282 MHz, $CDCl_3$) δ –73.8 (d, $J_{F\text{-}P}$ = 712.3 Hz, P**F**$_6$). **^{31}P NMR** (121 MHz, $CDCl_3$) δ –144.3 (sept, $J_{P\text{-}F}$ = 712.4 Hz, **P**F$_6$).

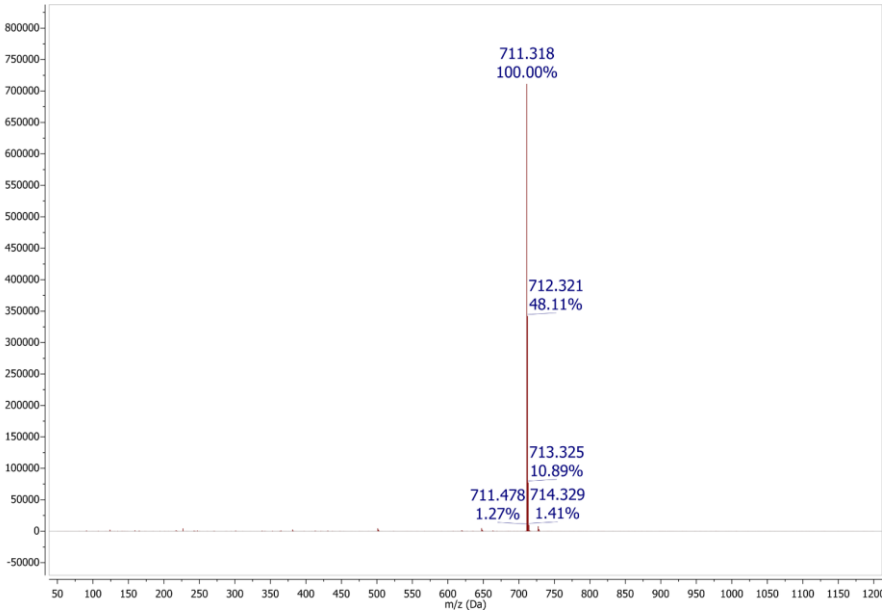

*Figure S3: Mass Spectroscopy spectrum of **1a** recorded in methanol: Positive mode, Electron Spray Ionisation.*

MS (ESI+, CH_3OH): m/z [**1a**]$^+$ calculated 711.31855; found 711.318.

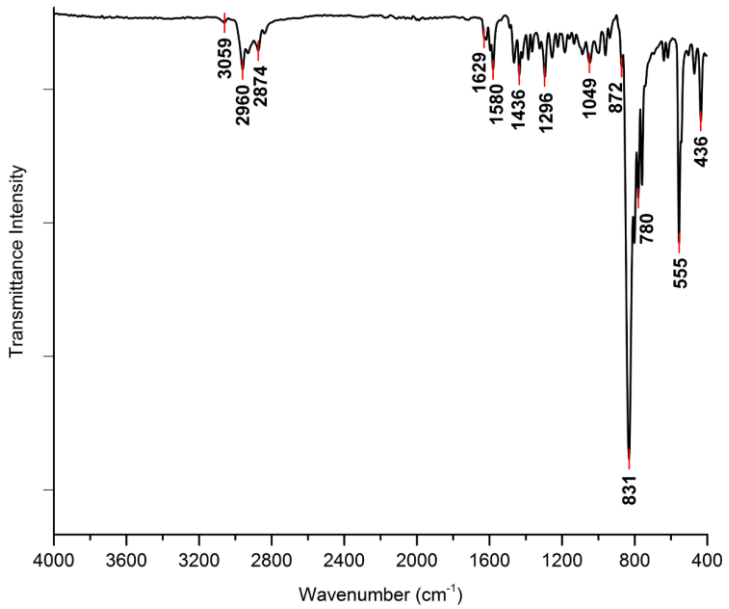

*Figure S4: Solid state infrared transmittance spectrum of **1a** recorded with a platinum-ATR module (monolithic diamond crystal window).*

IR (cm^{-1}) **ν(C=N)** 1629 (wv), 1580 (w); **ν(P–F)** 831 (vs); **δ(P–F)** 555 (vs).

S1.2) Complex **1b** [RhMB(cod)]PF_6

Complex **1b** was prepared in a procedure similar to that reported for **1a**. 0.291 g (0.6 mmol, 1.01eq) $[Rh(cod)Cl]_2$, 0.0.4731 g (1.16 mmol, 2eq) MesBIAN and 0.243 g (1.3 mmol, 2.2eq) KPF_6 were employed, and **1b** was isolated as an iridescent dark brown solid. (0.821 g, 92 % yield).

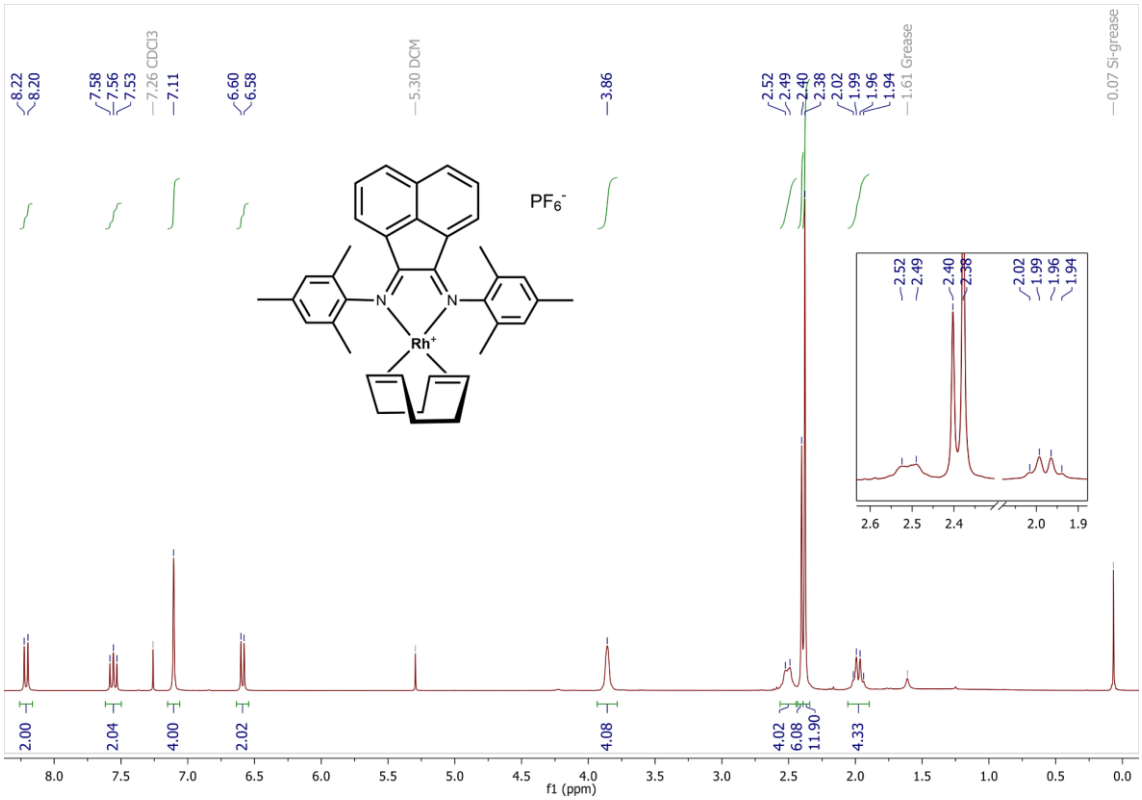

*Figure S5: ^1H NMR spectrum of complex **1b** in $CDCl_3$.*

^1H NMR (300 MHz, $CDCl_3$) δ 8.21 (d, *J* = 8.3 Hz, 2H, BIAN-C**H**), 7.56 (dd, *J* = 8.3, 7.3 Hz, 2H, BIAN-C**H**), 7.11 (s, 3H, Mes-C**H**), 6.59 (d, *J* = 7.3 Hz, 2H, BIAN-C**H**), 3.86 (br, 4H, cod-C**H**), 2.51 (br, 4H, cod-C$\mathbf{H}_2$), 2.40 (s, 6H, Mes-C$\mathbf{H}_3$), 2.38 (s, 12H, Mes-C$\mathbf{H}_3$), 2.06–1.90 (m, 4H, cod-C$\mathbf{H}_2$).

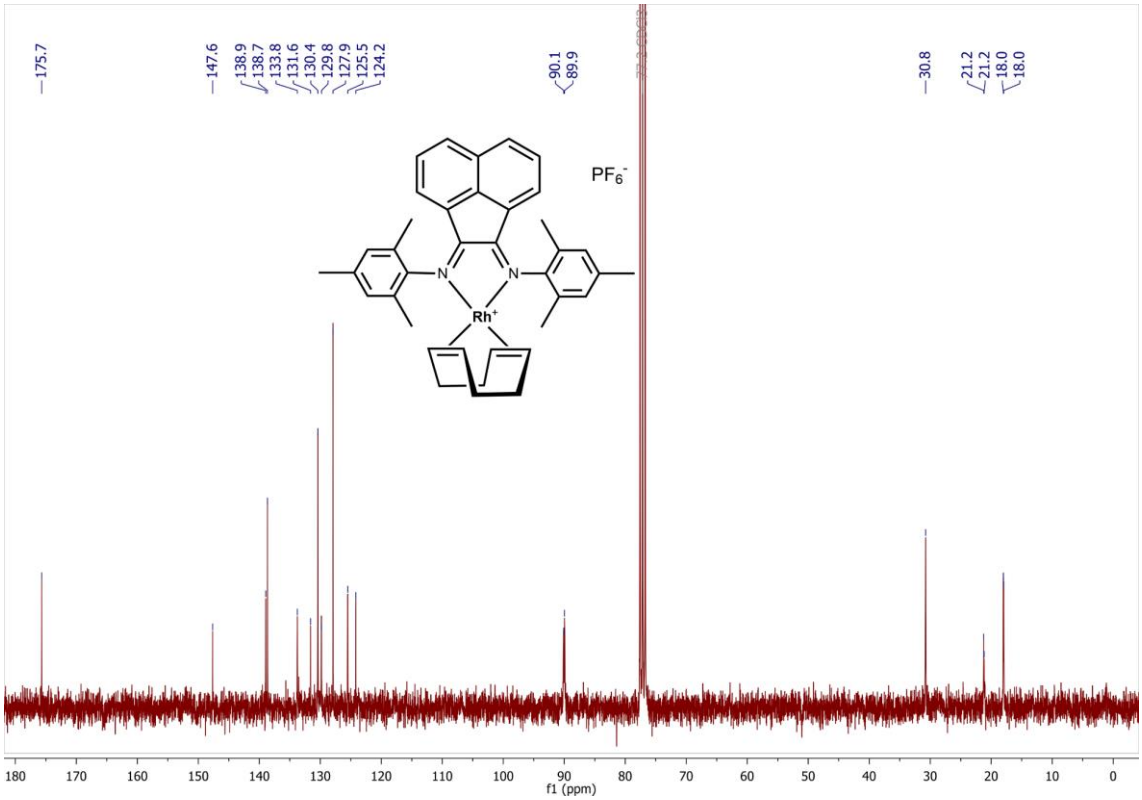

*Figure S6: ^{13}C NMR spectrum of complex **1b** in $CDCl_3$.*

^{13}C NMR (75 MHz, $CDCl_3$) δ 175.7 (BIAN-N=**C**$_q$), 147.6 (Mes-N-**C**$_q$), 138.9 (BIAN-**C**$_q$), 138.7 (BIAN-**C**H), 133.8 (BIAN-**C**H), 131.6 (**C**$_q$), 130.4 (BIAN-**C**H), 129.8 (**C**$_q$), 127.9 (Mes-**C**H), 125.5 (**C**$_q$), 124.2 (BIAN-**C**$_q$), 90.0 (d, $J_{C\text{-}Rh}$ = 10.1 Hz, cod-**C**H), 30.8 (cod-**C**H$_2$), 21.22, 21.17, 18.00, 17.95 (Mes-**C**H$_3$).

^{19}F NMR (282 MHz, $CDCl_3$) δ –73.9 (d, $J_{F\text{-}P}$ = 712.4 Hz, P**F**$_6$). **^{31}P NMR** (121 MHz, $CDCl_3$) δ –144.4 (sept, $J_{P\text{-}F}$ = 712.1 Hz, **P**F$_6$).

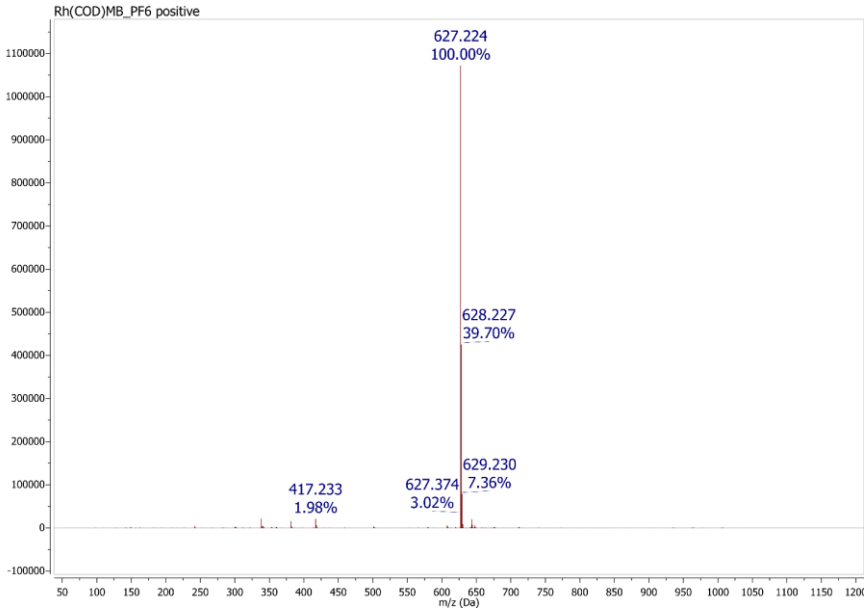

*Figure S7: Mass Spectroscopy spectrum of **1b** recorded in methanol: Positive mode, Electron Spray Ionisation.*

MS (ESI+, CH_3OH): m/z [**1b**]$^+$ calculated 627.225; found 627.224.

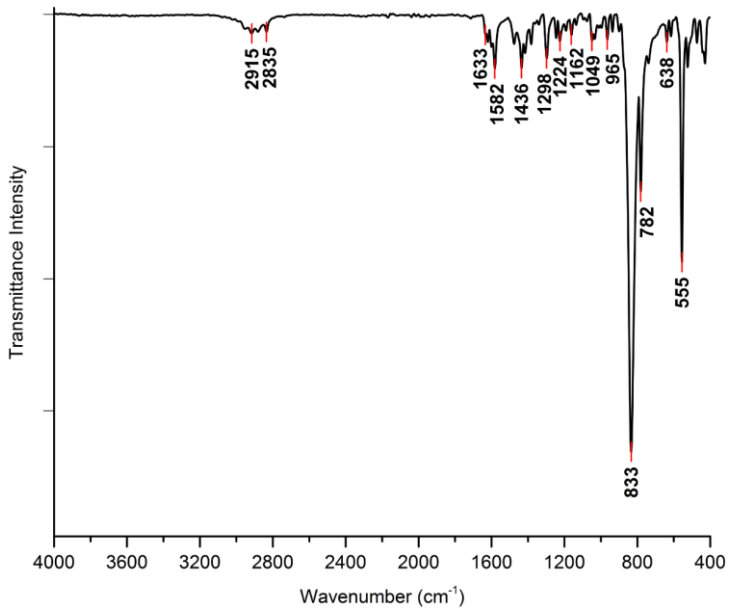

*Figure S8: Solid state infrared transmittance spectrum of **1b** recorded with a platinum-ATR module (monolithic diamond crystal window).*

IR (cm^{-1}) **ν(C=N)** 1627–1580 (m); **ν(P–F)** 833 (vs); **δ(P–F)** 555 (s).

S1.3) Complex **1c** [IrDB(cod)]PF_6

To 0.327 g (0.48 mmol, 1.01 eq) $[Ir(cod)Cl]_2$, 0.474 g (0.7 mmol, 2 eq) DippBIAN and 0.220 g (1.2 mmol, 2.5 eq) KPF_6 in a Schlenk tube was added 10 mL CH_2Cl_2 at RT and the orange suspension stirred for four days. The dark green solution was filtered and dried *in vacuo*. The resulting dark green powder was washed with 50 mL hexane, and **1c** was isolated as a dark green solid. (0.648 g, 72 % yield).

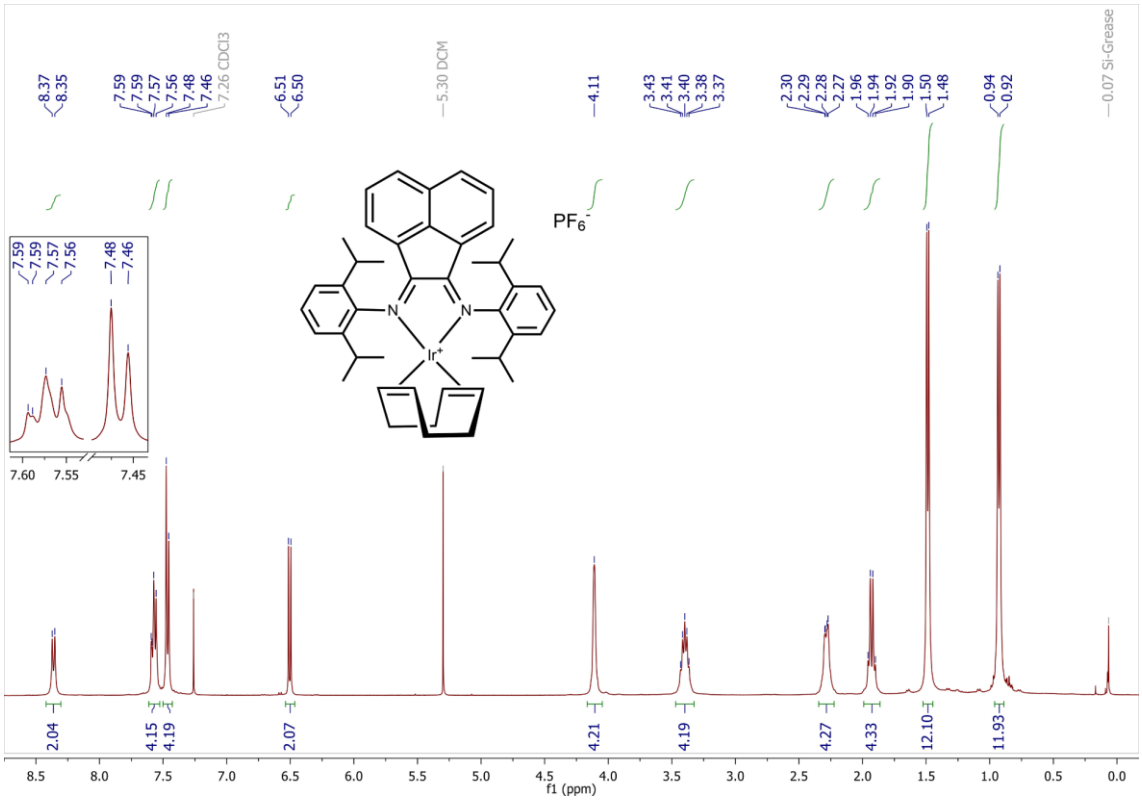

*Figure S9: ^{1}H NMR spectrum of complex **1c** in $CDCl_3$.*

^{1}H NMR (300 MHz, $CDCl_3$) δ 8.36 (d, *J* = 8.2 Hz, 2H, BIAN-C**H**), 7.61–7.53 (m, 4H, Dipp-C**H** and BIAN-C**H**), 7.47 (d, *J* = 7.8 Hz, 4H, Dipp-C**H**), 6.50 (d, *J* = 7.3 Hz, 2H, BIAN-C**H**), 4.11 (br, 4H, cod-C**H**), 3.40 (sept, *J* = 6.4 Hz, 4H, Dipp(iso)C**H**), 2.35–2.22 (m, 4H, cod-C$\mathbf{H}_2$), 1.99–1.86 (m, 4H, cod-C$\mathbf{H}_2$), 1.49 (d, *J* = 6.7 Hz, 12H, Dipp(iso)C$\mathbf{H}_3$), 0.93 (d, *J* = 6.7 Hz, 12H, Dipp(iso)C$\mathbf{H}_3$).

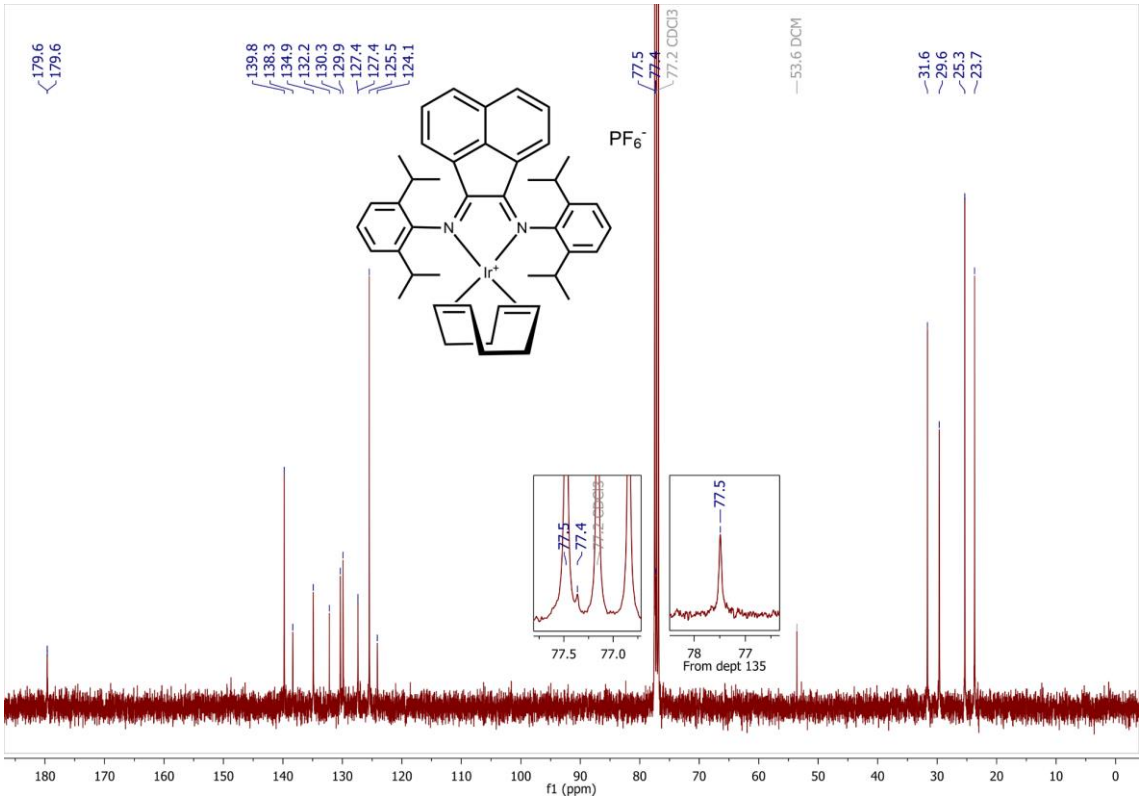

*Figure S10: ^{13}C NMR spectrum of complex **1c** in $CDCl_3$.*

^{13}C NMR (75 MHz, $CDCl_3$) δ 179.6 (BIAN-N=**C**$_q$), 179.6 (BIAN-N=**C**$_q$), 139.8 (Dipp(iso)-**C**$_q$), 138.3 (Dipp-N-**C**$_q$), 134.9 (BIAN-**C**H), 132.2 (BIAN-**C**$_q$), 130.3 (Dipp-**C**H), 129.9 (BIAN-**C**H), 127.4 (BIAN-**C**H), 127.4 (BIAN-**C**H), 125.5 (Dipp-**C**H), 124.1 (BIAN-**C**$_q$), 77.5 (from dept135, cod-**C**H), 77.4 (cod-**C**H), 31.6 (cod-**C**H_2), 29.6 (Dipp(iso)-**C**H), 25.3 (Dipp(iso)-**C**H_3), 23.7 (Dipp(iso)-**C**H_3).

^{19}F NMR (282 MHz, $CDCl_3$) δ –73.8 (d, $J_{F\text{-}P}$ = 712.5 Hz, P**F**$_6$). **^{31}P NMR** (121 MHz, $CDCl_3$) δ –144.4 (sept, $J_{P\text{-}F}$ = 712.6 Hz, **P**F_6).

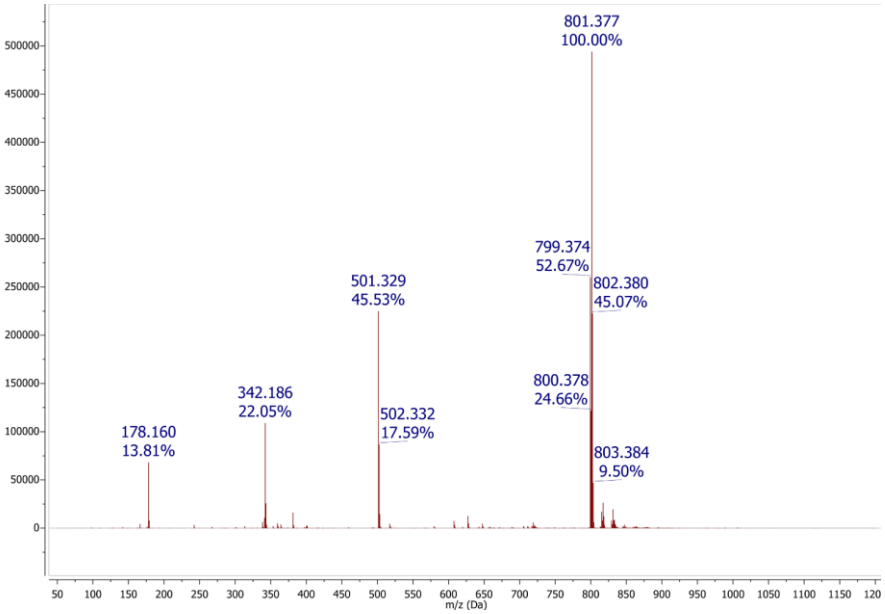

*Figure S11: Mass Spectroscopy spectrum of **1c** recorded in methanol: Positive mode, Electron Spray Ionisation.*

MS (ESI+, CH_3OH): m/z $[\mathbf{1c}]^+$ calculated 801.3759; found 801.377.

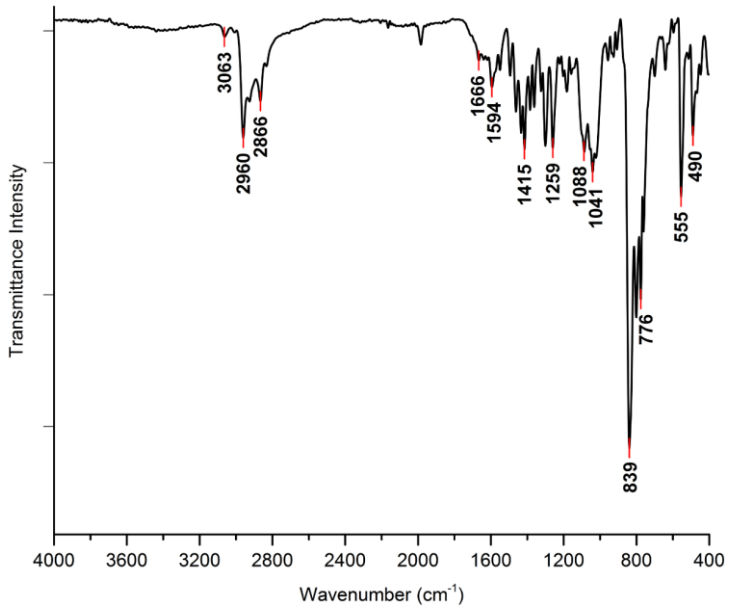

*Figure S12: Solid state infrared transmittance spectrum of **1c** recorded with a platinum-ATR module (monolithic diamond crystal window).*

IR (cm^{-1}) **ν(C=N)** 1666 (vw), 1594(w); **ν(P–F)** 839 (vs); **δ(P–F)** 555 (s).

S1.4) Complex **1d** [IrMB(cod)]PF_6

Complex **1d** was prepared in a procedure similar to that reported for **1c**. 0.282 g (0.4 mmol, 1.01 eq) $[Ir(COD)Cl]_2$, 0.349 g (0.84 mmol, 2 eq) MesBIAN and 0.217 g (1.2 mmol, 2.8 eq) KPF_6 were employed, and **1d** was isolated as an iridescent dark brown solid. (0.632 g, 88 % yield).

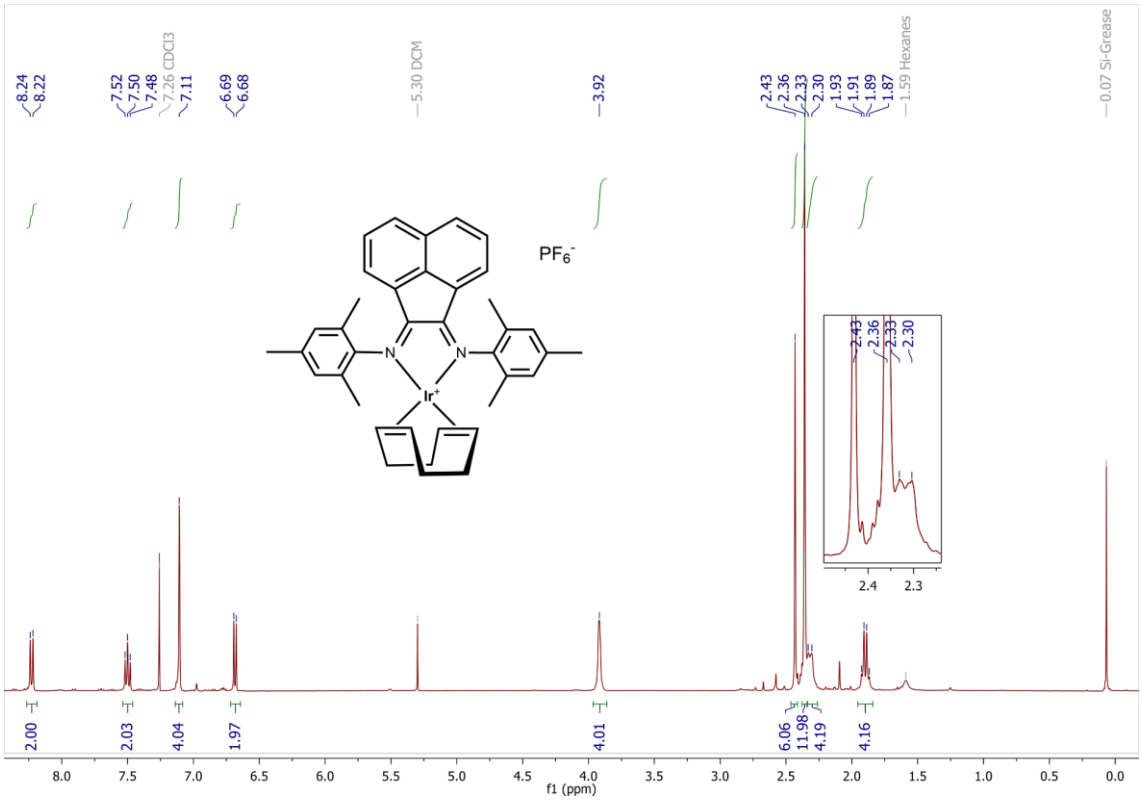

*Figure S13: ^{1}H NMR spectrum of complex **1d** in $CDCl_3$.*

^{1}H NMR (300 MHz, $CDCl_3$) δ 8.23 (d, *J* = 8.3 Hz, 2H, BIAN-C**H**), 7.50 (dd, *J* = 8.3, 7.2 Hz, 2H, BIAN-C**H**), 7.11 (s, 4H, Mes-C**H**), 6.68 (d, *J* = 7.2 Hz, 2H, BIAN-C**H**), 3.92 (br, 4H, cod-C**H**), 2.43 (s, 6H, Mes-C**H**$_3$), 2.36 (s, 12H, Mes-C**H**$_3$), 2.32 (br, 4H, cod-C**H**$_2$), 1.90 (br, 4H, cod-C**H**$_2$).

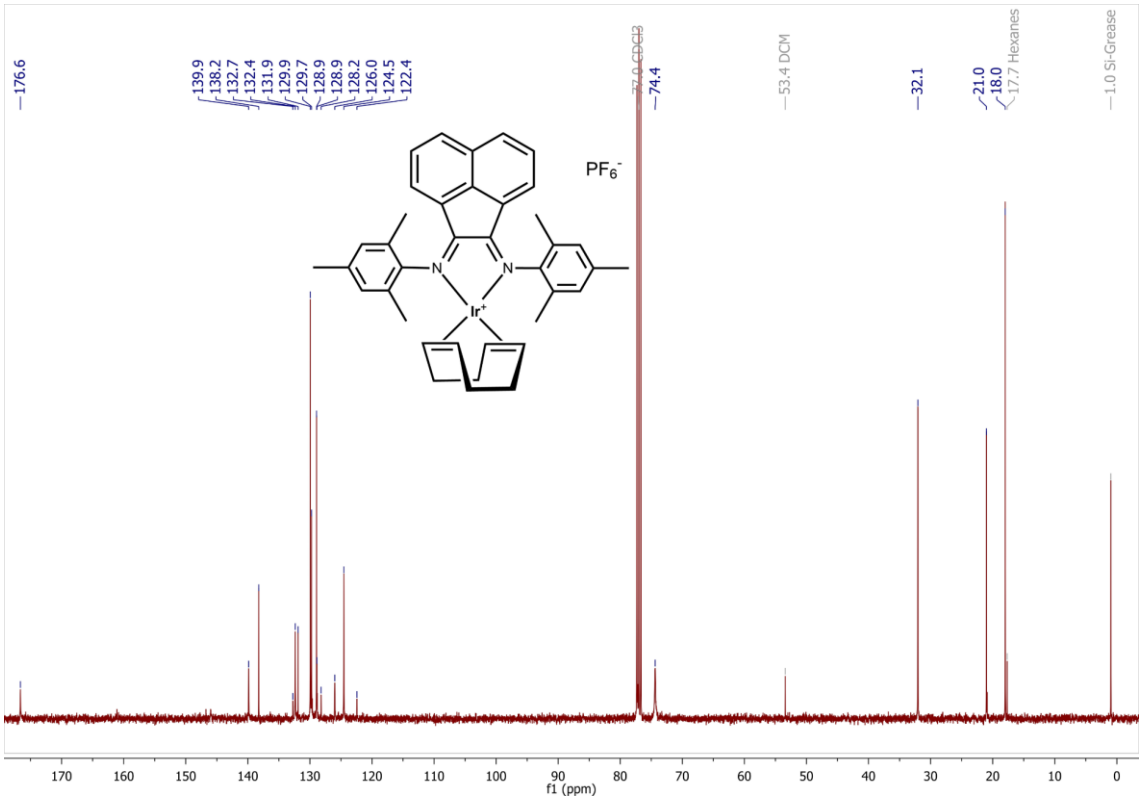

*Figure S14: ^{13}C NMR spectrum of complex **1d** in $CDCl_3$.*

^{13}C NMR (75 MHz, $CDCl_3$) δ 176.6 (BIAN-N=**C**$_q$), 139.9 (Mes-N-**C**$_q$), 138.2 (BIAN-**C**$_q$), 132.7 (BIAN-**C**H), 132.4, 131.9, 129.9 (Mes-**C**H), 129.7 (BIAN-**C**H), 128.93, 128.87, 128.2, 126.0, 124.5 (BIAN-**C**H), 122.4 (BIAN-**C**$_q$), 74.4 (cod-**C**H), 32.1 (cod-**C**H$_2$), 21.0, 18.0 (Mes-**C**H$_3$).

^{19}F NMR (282 MHz, $CDCl_3$) δ –73.8 (d, $J_{F\text{-}P}$ = 712.6 Hz, P**F**$_6$). **^{31}P NMR** (121 MHz, $CDCl_3$) δ –144.5 (sept, $J_{P\text{-}F}$ = 712.2 Hz, **P**F$_6$).

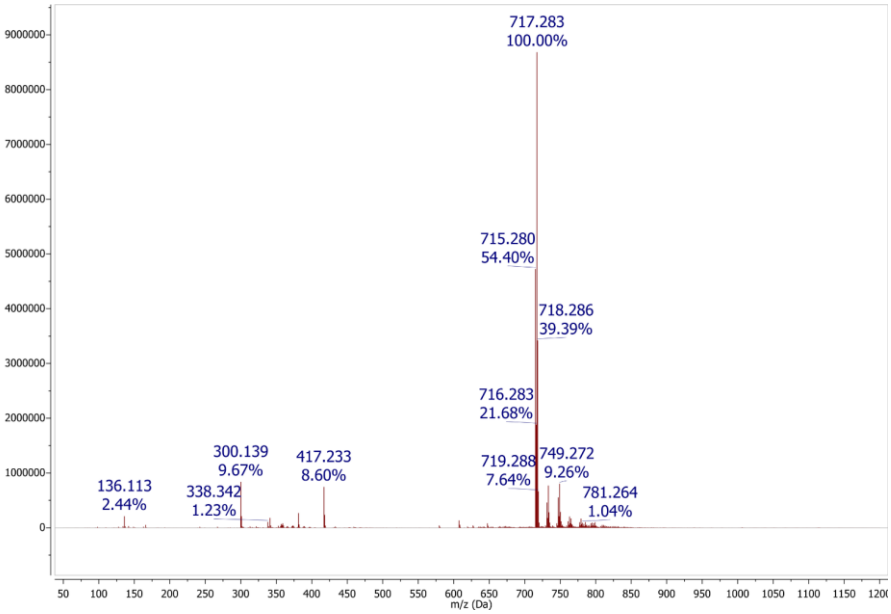

*Figure S15: Mass Spectroscopy spectrum of **1d** recorded in methanol: Positive mode, Electron Spray Ionisation.*

MS (ESI+, CH_3OH): m/z [**1d**]$^+$ calculated 717.28207; found 717.283.

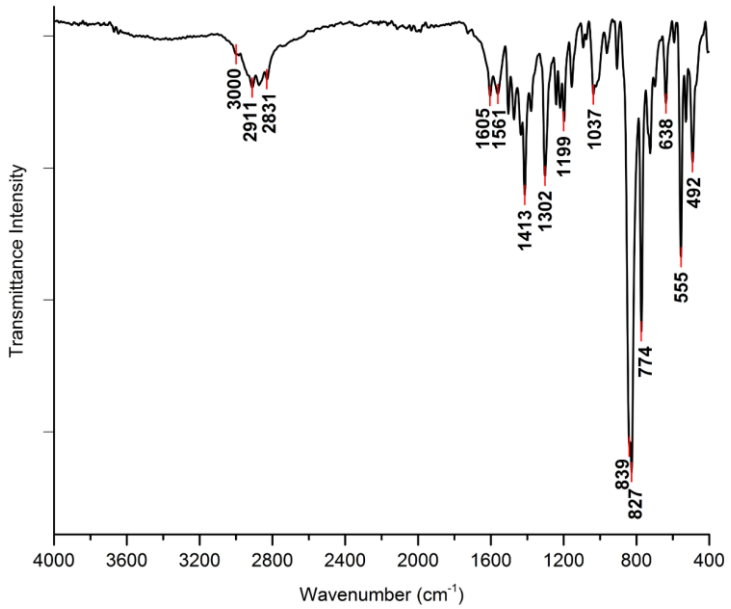

*Figure S16: Solid state infrared transmittance spectrum of **1d** recorded with a platinum-ATR module (monolithic diamond crystal window).*

IR (cm^{-1}) **ν(C=N)** 1605 (w), 1561 (w), 1504 (w); **ν(P–F)** overlapped; **δ(P–F)** 555 (s).

S1.5) Complex **2a** $[RhDB(CO)_2]PF_6$

Complex **2a** was prepared from complex **1a** generated *in situ*. To 0.266 g (0.53 mmol, 1.01eq) $[Rh(cod)Cl]_2$, 0.519 g (1.05 mmol, 2eq) DippBIAN and 0.219 g (1.2 mmol, 2.2eq) KPF_6 in a Schlenk tube, was added 15 mL CH_2Cl_2 at RT and the brown solution stirred overnight. The dark brown solution was cannula filtered and dried *in vacuo*. The residue was dissolved in a minimum of CH_2Cl_2 (2 mL) and CO (g) was bubbled through the solution for 5 minutes, resulting in a slow colour change from dark brown to brick red. Hexane was added slowly while passing CO (g) through the solution for 45 minutes to form a brown precipitate. The lightly green coloured solution was decanted off and the solids rinsed with hexane whilst under a flow of CO (g). The brown solid was dried *in vacuo*, and **2a** isolated as a dark brown solid. (0.735 g, 98 % yield).

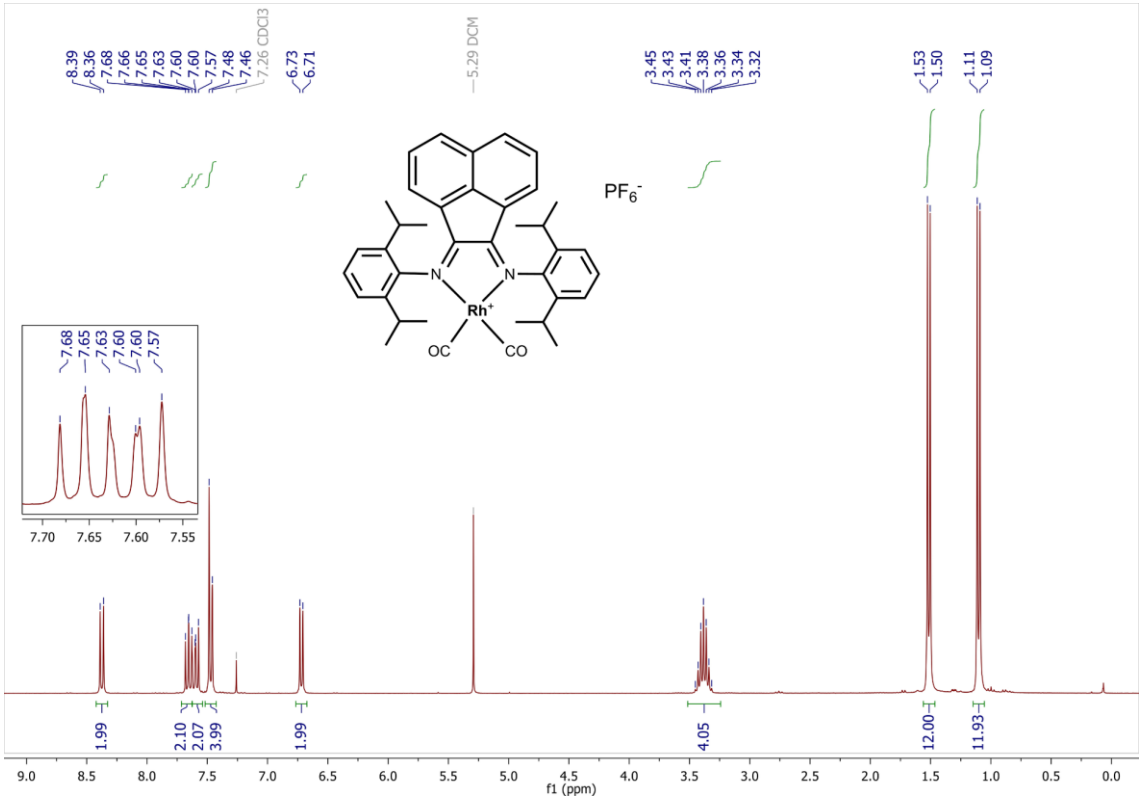

*Figure S17: ^{1}H NMR spectrum of complex **2a** in $CDCl_3$.*

^{1}H NMR (300 MHz, $CDCl_3$) δ 8.37 (d, *J* = 8.3 Hz, 2H, BIAN-C**H**), 7.66 (dd, *J* = 8.3, 7.4 Hz, 2H, BIAN-C**H**), 7.60 (dd, *J* = 8.7, 7.1 Hz, 2H, Dipp-C**H**), 7.47 (d, *J* = 7.9 Hz, 2H, Dipp-C**H**), 6.72 (d, *J* = 7.4 Hz, 2H, BIAN-C**H**), 3.38 (sept, *J* = 6.7 Hz, 4H, Dipp(iso)C**H**), 1.51 (d, *J* = 6.8 Hz, 12H, Dipp(iso)C**H**$_3$), 1.10 (d, *J* = 6.8 Hz, 12H, Dipp(iso)C**H**$_3$).

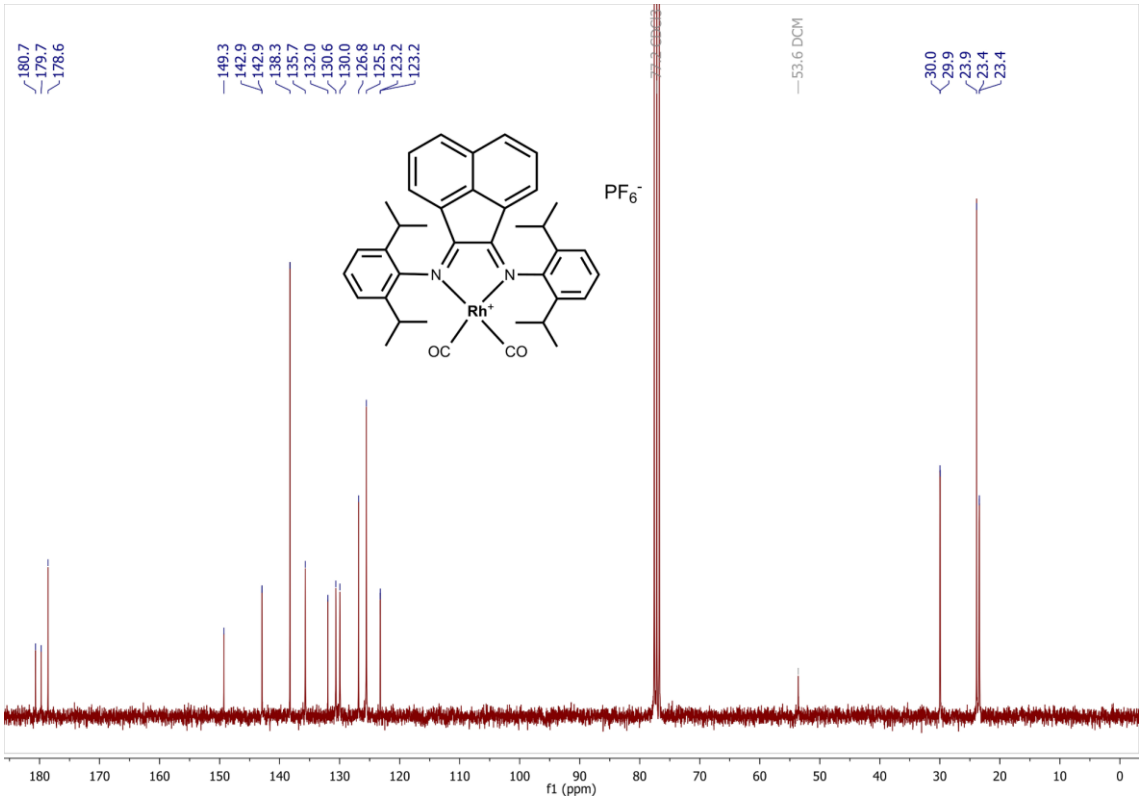

*Figure S18: ^{13}C NMR spectrum of complex **2a** in $CDCl_3$.*

^{13}C NMR (75 MHz, $CDCl_3$) δ 180.2 (d, $J_{CO\text{-}Rh}$ = 70.3 Hz, **C**O), 178.6 (BIAN-N=**C**$_q$), 149.3 (Dipp-N-**C**$_q$), 142.9 (BIAN-**C**$_q$), 142.9 (BIAN-**C**$_q$), 138.3 (Dipp-**C**H), 135.7 (BIAN-**C**H), 132.0 (Dipp-**C**H), 130.6 (Dipp(iso)-**C**$_q$), 130.0 (Dipp(iso)-**C**$_q$), 126.8 (BIAN-**C**H), 125.5 (BIAN-**C**H), 123.2 (Dipp-**C**H), 123.2 (Dipp-**C**H), 30.0, 29.9 (Dipp(iso)-**C**H), 23.9, 23.4, 23.4 (Dipp(iso)-**C**H).

^{19}F NMR (377 MHz, $CDCl_3$) δ –73.7 (d, $J_{F\text{-}P}$ = 712.6 Hz, P**F**$_6$). **^{31}P NMR** (162 MHz, $CDCl_3$) δ –144.5 (sept, $J_{P\text{-}F}$ = 712.4 Hz, **P**F$_6$).

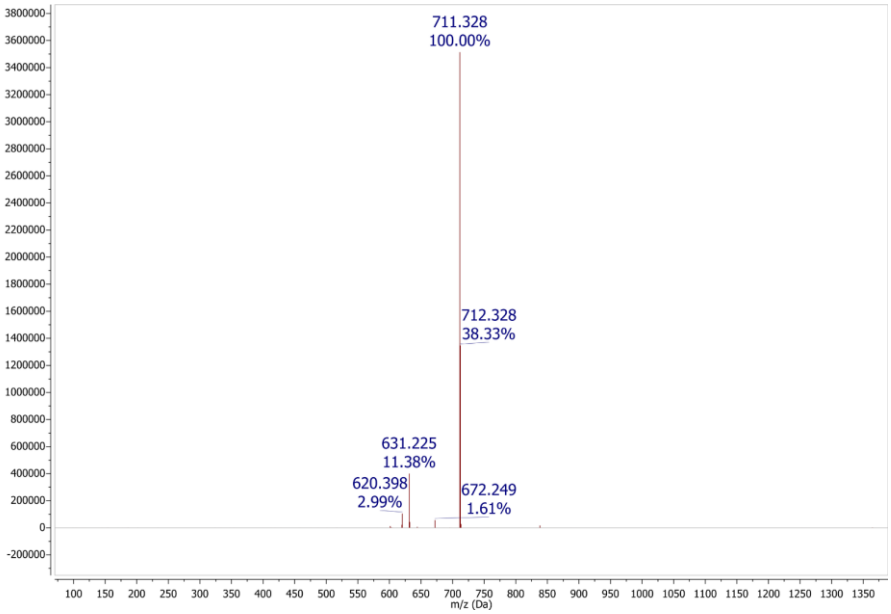

*Figure S19: Mass Spectroscopy spectrum of **2a** recorded in methanol: Positive mode, Electron Spray Ionisation.*

MS (ESI+, CH_3OH): m/z [**2a**-CO]$^+$ calculated 631.220; found 631.225.

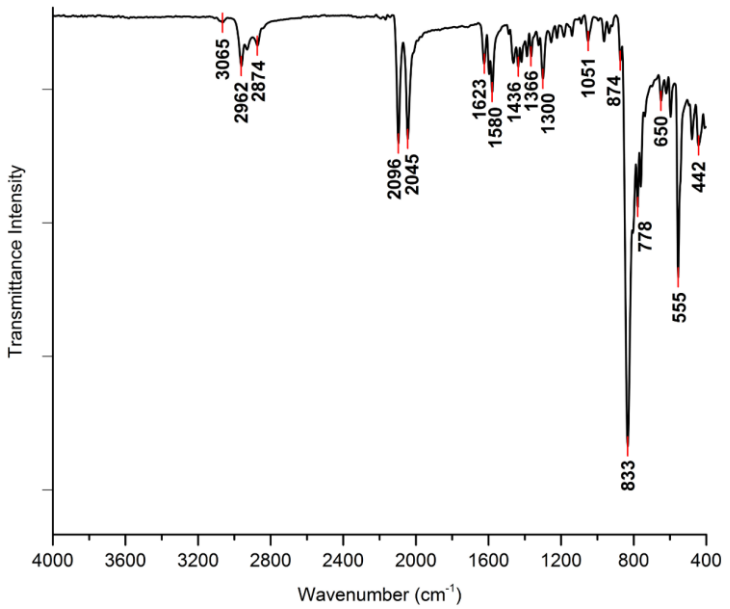

*Figure S20: Solid state infrared transmittance spectrum of **2a** recorded with a platinum-ATR module (monolithic diamond crystal window).*

IR (cm^{-1}) **ν(CO)** 2096 (m), 2045 (m); **ν(C=N)** 1625–1580 (m); **ν(P–F)** 833 (vs) ; **δ(P–F)** 555 (s).

S1.6) Complex **2b** $[RhMB(CO)_2]PF_6$

Complex **2b** was prepared in a procedure similar to that reported for **2a**. 0.247 g (0.5 mmol, 1.01eq) $[Rh(cod)Cl]_2$, 0.414 g (1.0 mmol, 2eq) MesBIAN and 0.225 g (1.2 mmol, 2.4eq) KPF_6 were used, and **2b** was isolated as an iridescent brown solid. (0.670 g, 93 % yield).

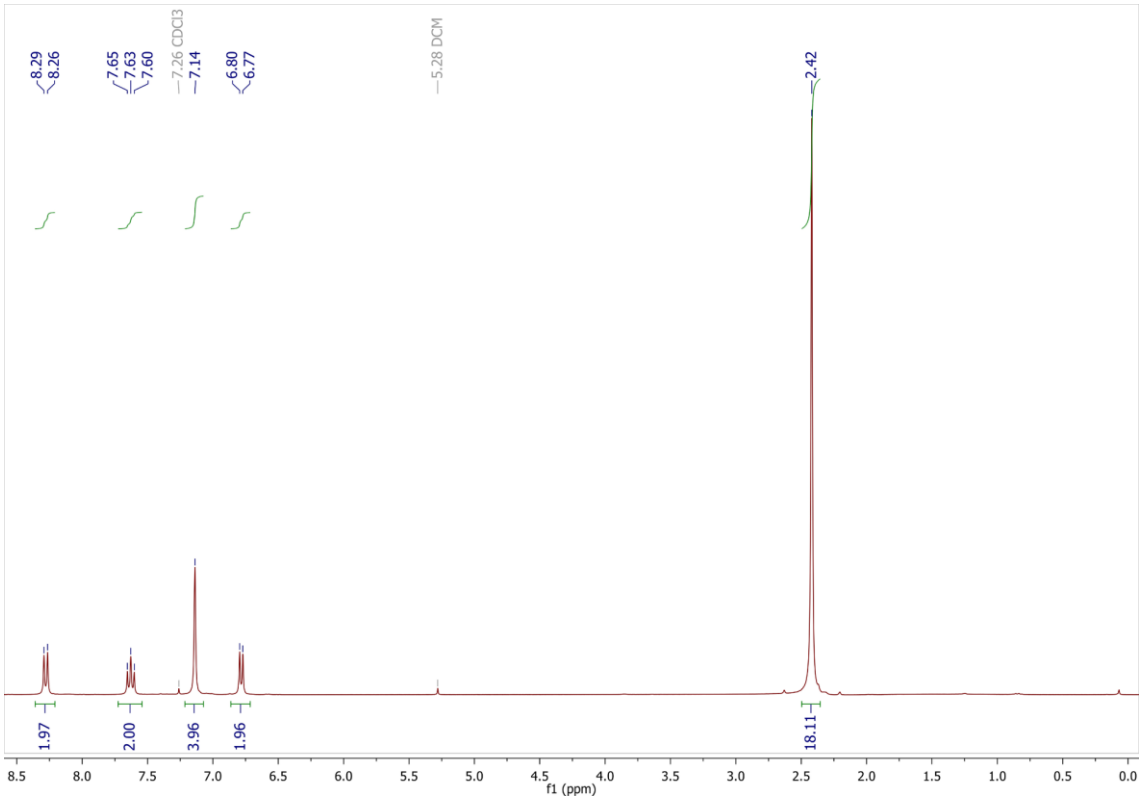

*Figure S21: ^{1}H NMR spectrum of complex **2b** in $CDCl_3$.*

^{1}H NMR (300 MHz, $CDCl_3$) δ 8.28 (d, *J* = 8.3 Hz, 2H, BIAN-C**H**), 7.63 (dd, *J* = 8.3, 7.3 Hz, 2H, BIAN-C**H**), 7.14 (s, 4H, Mes-C**H**), 6.78 (d, *J* = 7.3 Hz, 2H, BIAN-C**H**), 2.42 (s, 18H, Mes-C**H**$_3$).

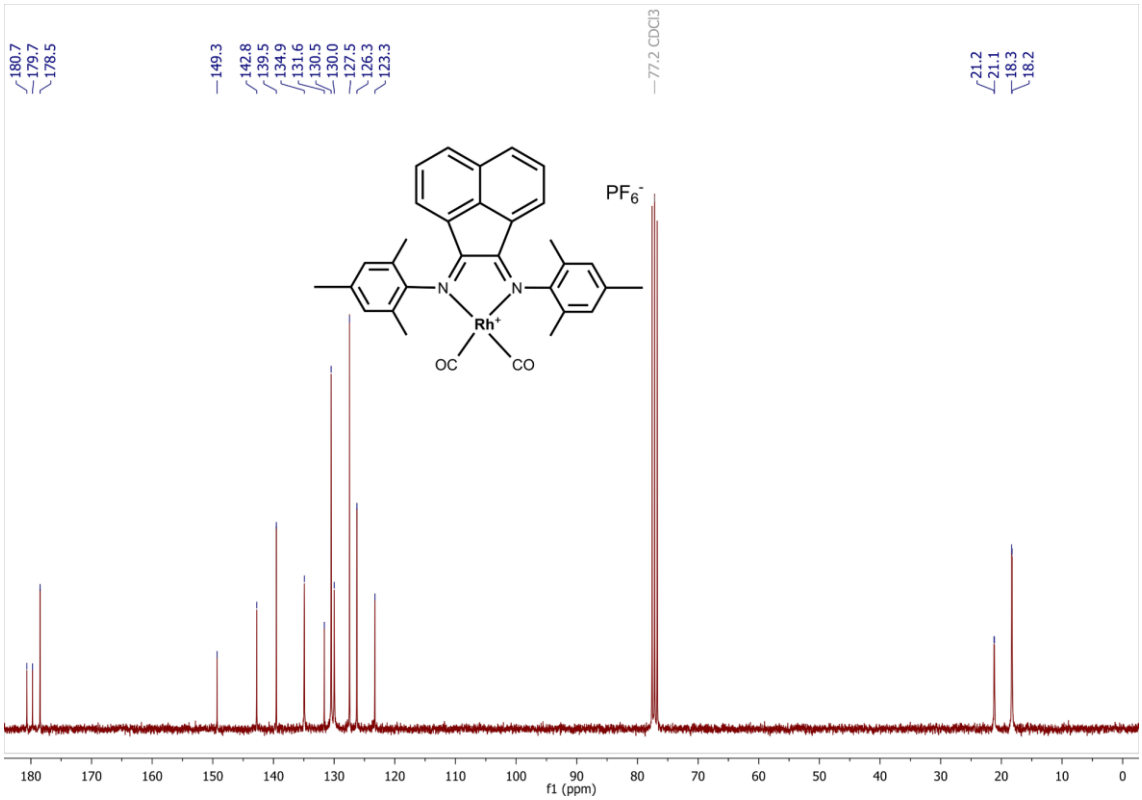

*Figure S22: ^{13}C NMR spectrum of complex **2b** in $CDCl_3$.*

^{13}C NMR (75 MHz, $CDCl_3$) δ 180.19 (d, $J_{C\text{-}Rh}$ = 70.1 Hz, Rh=**C**=O), 178.5 (BIAN-N=**C**$_q$), 149.3 (Mes-N-**C**$_q$), 142.8 (BIAN-**C**$_q$), 139.5 (BIAN-**C**H), 134.9 (BIAN-**C**H), 131.6 (**C**$_q$), 130.5 (Mes-**C**H), 130.0 (**C**$_q$), 127.5 (BIAN-**C**H), 126.3 (BIAN-**C**$_q$), 123.3 (**C**$_q$), 21.2, 21.1, 18.3, 18.2 (Mes-**C**H_3).

^{19}F NMR (282 MHz, $CDCl_3$) δ –73.7 (d, $J_{F\text{-}P}$ = 712.9 Hz, P**F**$_6$). **^{31}P NMR** (121 MHz, $CDCl_3$) δ –144.6 (sept, $J_{P\text{-}F}$ = 713.3 Hz, **P**F_6).

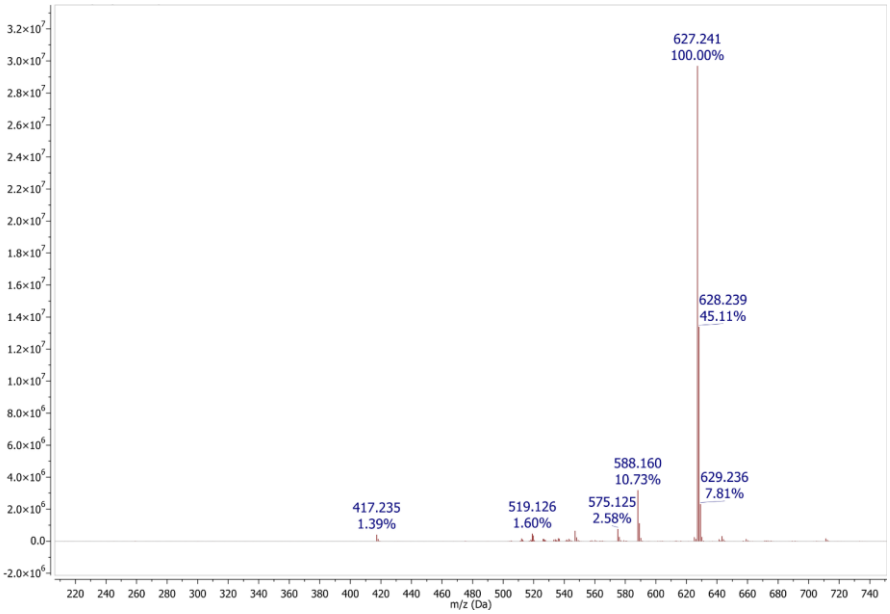

*Figure S23: Mass Spectroscopy spectrum of **2b** recorded in methanol: Positive mode, Electron Spray Ionisation.*

MS (ESI+, CH_3OH): m/z [**2b**]$^+$ calculated 575.121; found 575.125, [**2b**-CO]$^+$ calculated 547.126; found 547.125, [**2b**-$(CO)_2$]$^+$ calculated 519.131; found 519.126.

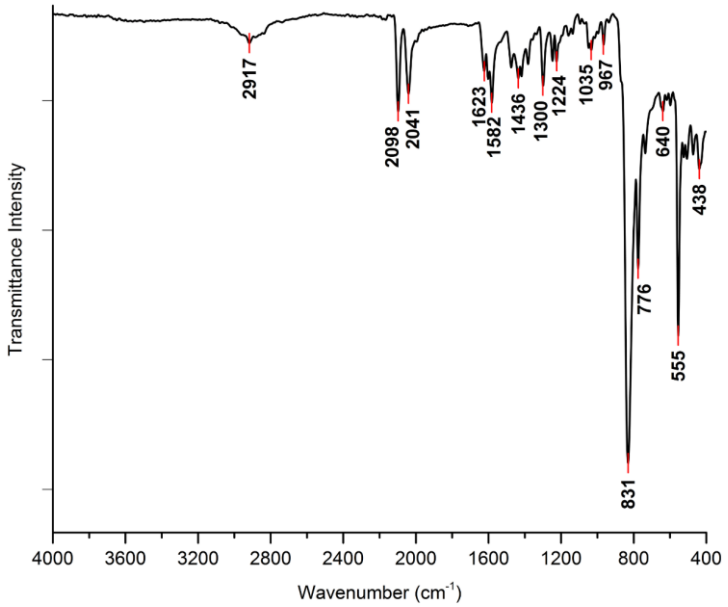

*Figure S24: Solid state infrared transmittance spectrum of **2b** recorded with a platinum-ATR module (monolithic diamond crystal window).*

IR (cm^{-1}) **ν(CO)** 2098 (w), 2041 (w); **ν(C=N)** 1625–1582 (w); **ν(P–F)** 831 (vs) ; **δ(P–F)** 555 (vs).

S1.7) Complex **2c** $[IrDB(CO)_2]PF_6$

Complex **2c** was prepared in a procedure similar to that reported for **2a**. To 0.269 g (0.4 mmol, 1.01 eq) $[Ir(cod)Cl]_2$, 0.399 g (0.8 mmol, 2 eq) DippBIAN and 0.198 g (1.01 mmol, 2.7 eq) KPF_6 were used, and **2c** isolated as a dark brown solid. (0.407 g, 57 % yield).

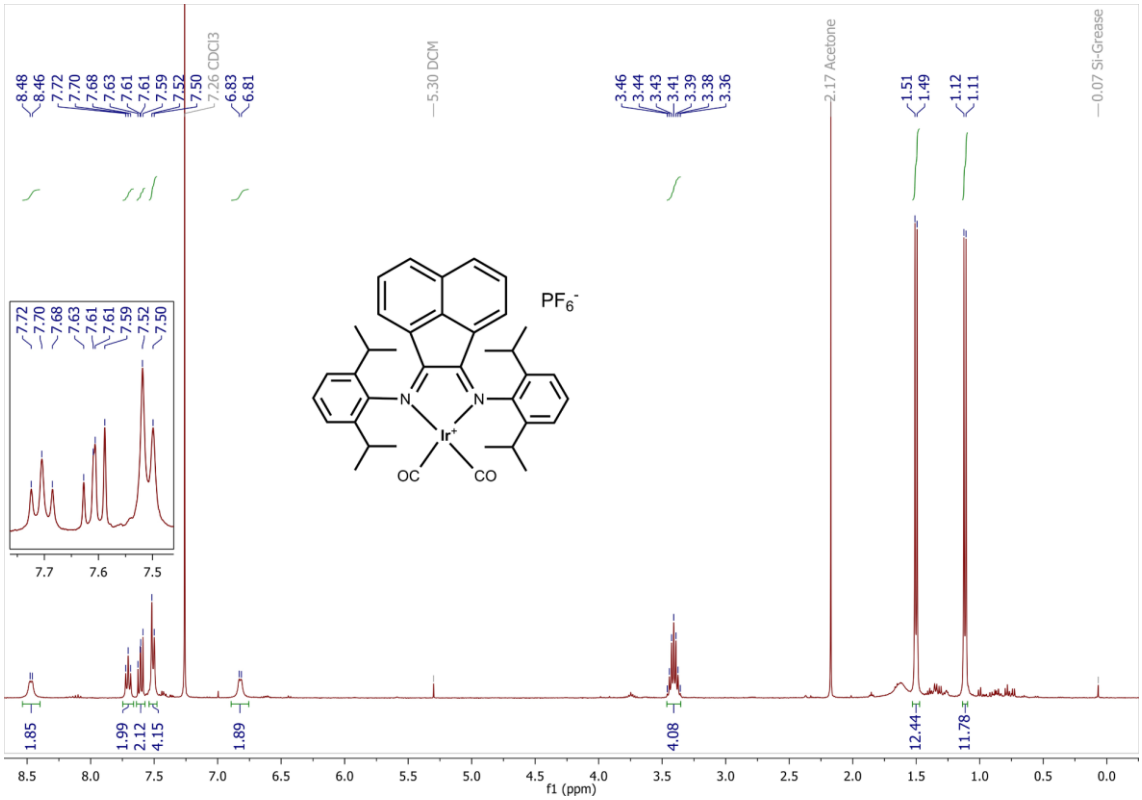

*Figure S25: ^{1}H NMR spectrum of complex **2c** in $CDCl_3$.*

^{1}H NMR (300 MHz, $CDCl_3$) δ 8.45 (br, 2H, BIAN-C**H**), 7.70 (dd, *J* = 7.9, 7.3 Hz, 2H, BIAN-C**H**), 7.61 (dd, *J* = 8.7, 6.8 Hz, 2H, Dipp-C**H**), 7.51 (d, *J* = 7.7 Hz, 4H, Dipp-C**H**), 6.82 (d, *J* = 7.3 Hz, 2H, BIAN-C**H**), 3.39 (sept, *J* = 6.8 Hz, 4H, Dipp(iso)C**H**), 1.50 (d, *J* = 6.8 Hz, 12H, Dipp(iso)C**H**$_3$), 1.11 (d, *J* = 6.8 Hz, 12H, Dipp(iso)C**H**$_3$).

No well-resolved **^{13}C NMR** spectrum of this compound could be obtained, even after extended data acquisition times.

^{19}F NMR (282 MHz, $CDCl_3$) δ –73.7 (d, J_{F-P} = 712.7 Hz, P**F**$_6$). **^{31}P NMR** (121 MHz, $CDCl_3$) δ –144.5 (sept, J_{P-F} = 712.3 Hz, **P**F_6).

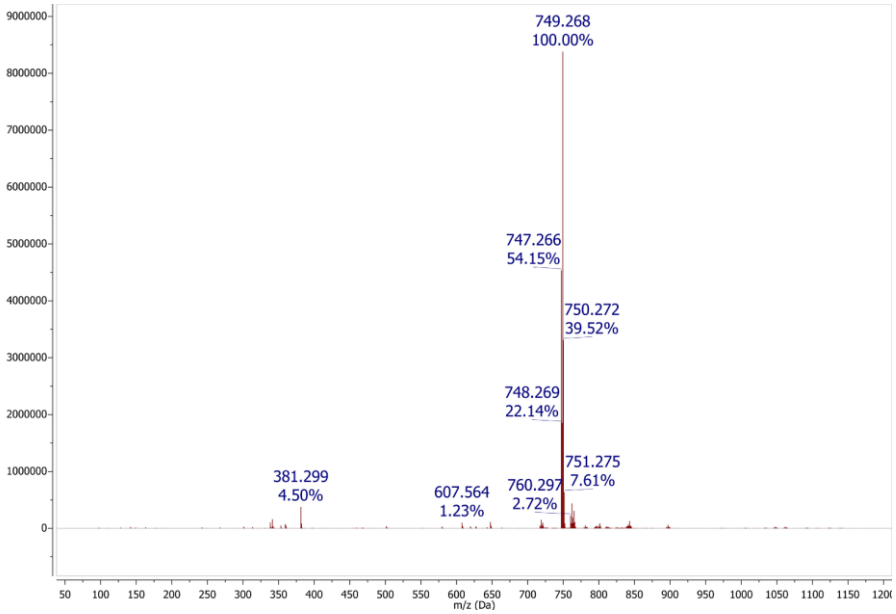

*Figure S26: Mass Spectroscopy spectrum of **2c** recorded in methanol: Positive mode, Electron Spray Ionisation.*

MS (ESI+, CH_3OH): m/z [**2c**]$^+$ calculated 749.27190; found 749.268.

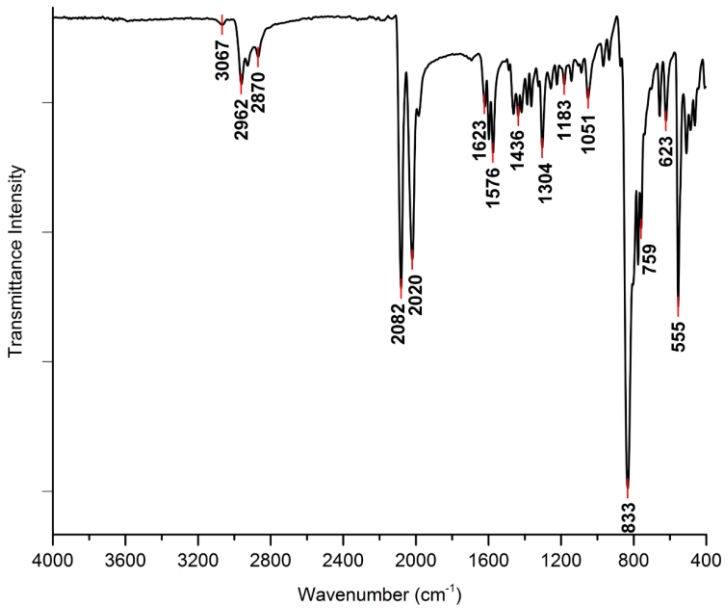

*Figure S27: Solid state infrared transmittance spectrum of **2c** recorded with a platinum-ATR module (monolithic diamond crystal window).*

IR (cm^{-1}) **ν(CO)** 2082 (s), 2020 (s), 1983 (vw, sh); **ν(C=N)** 1623 (w), 1599 (w), 1576 (w); **ν(P–F)** 833 (vs); **δ(P–F)** 555 (s).

S1.8) Complex **2d** [IrMB(CO)$_2$]PF$_6$

Complex **2d** was prepared in a procedure similar to that reported for **2a**. To 0.284 g (0.42 mmol, 1.01 eq) [Ir(COD)Cl]$_2$, 0.349 g (0.84 mmol, 2 eq) MesBIAN and 0.184 g (1.0 mmol, 2.4 eq) KPF$_6$ were used, and **2d** isolated as an iridescent brown solid. (0.478 g, 70 % yield).

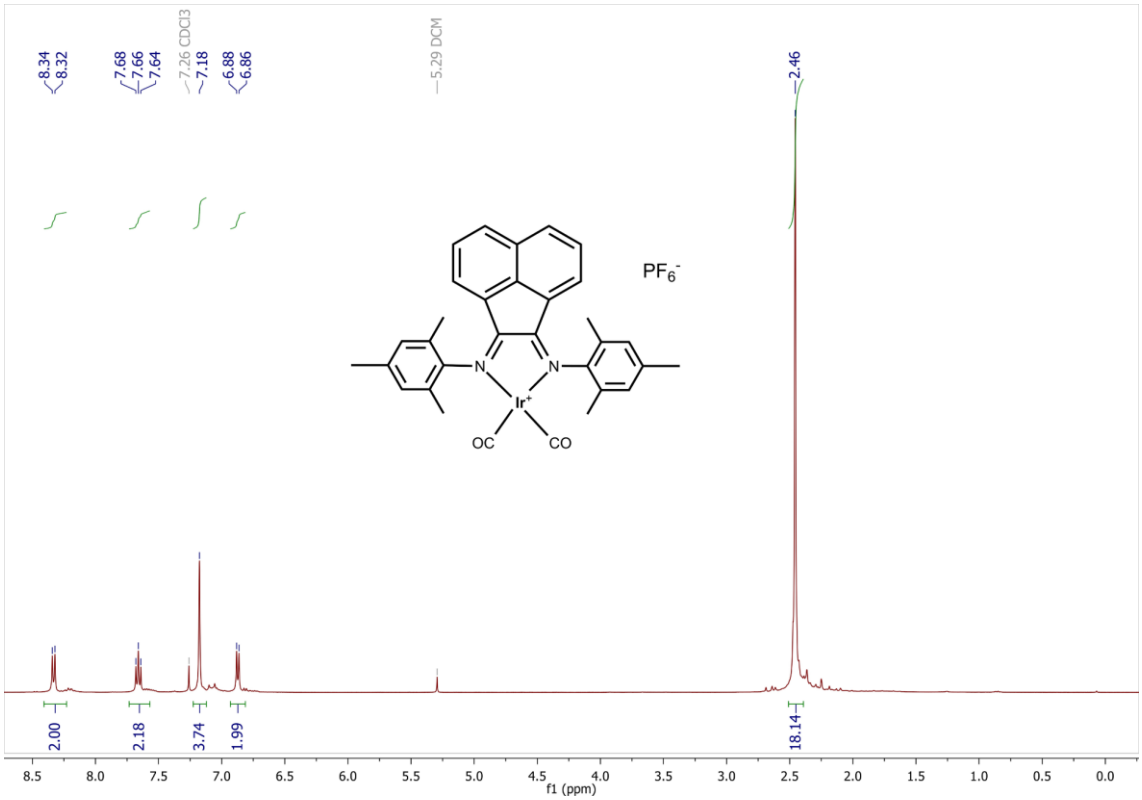

*Figure S28: ^{1}H NMR spectrum of complex **2d** in CDCl$_3$.*

^{1}H NMR (300 MHz, $CDCl_3$) δ 8.33 (d, *J* = 8.3 Hz, 2H, BIAN-C**H**), 7.66 (dd, *J* = 8.3, 7.3 Hz, 2H, BIAN-C**H**), 7.18 (s, 4H, Mes-C**H**), 6.87 (d, *J* = 7.3 Hz, 2H, BIAN-C**H**), 2.46 (s, 18H, Mes-C**H**$_3$).

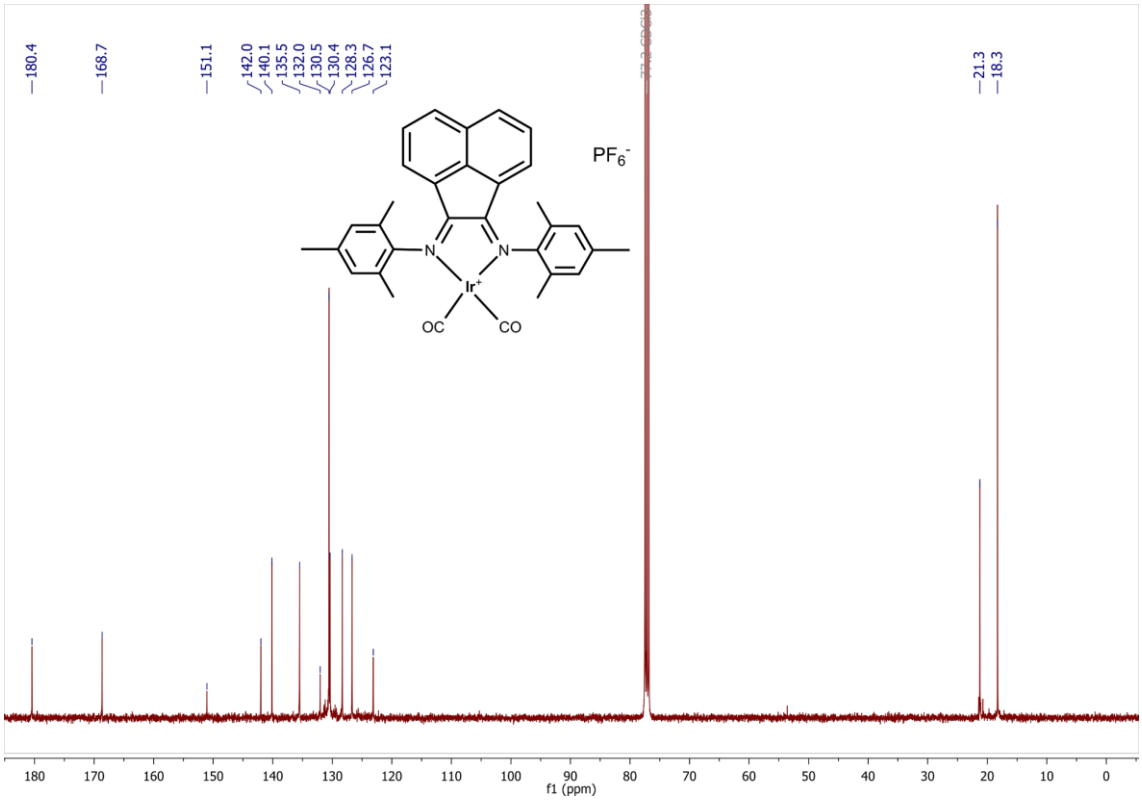

*Figure S29: ^{13}C NMR spectrum of complex **2d** in $CDCl_3$.*

^{13}C NMR (75 MHz, $CDCl_3$) δ 180.4 (Ir=**C**=O), 168.7 (BIAN-N=**C**$_q$), 151.1 (Mes-N-**C**$_q$), 142.0 (BIAN-**C**$_q$), 140.1 (BIAN-**C**H), 135.5 (BIAN-**C**H), 132.0, 130.5 (Mes-**C**H), 130.4, 128.3 (BIAN-**C**H), 126.7, 123.1, 21.3, 18.3 (Mes-**C**H_3).

^{19}F NMR (282 MHz, $CDCl_3$) δ –73.7 (d, $J_{F\text{-}P}$ = 712.9 Hz, P**F**$_6$). **^{31}P NMR** (121 MHz, $CDCl_3$) δ –144.8 (sept, $J_{P\text{-}F}$ = 712.9 Hz, **P**F_6).

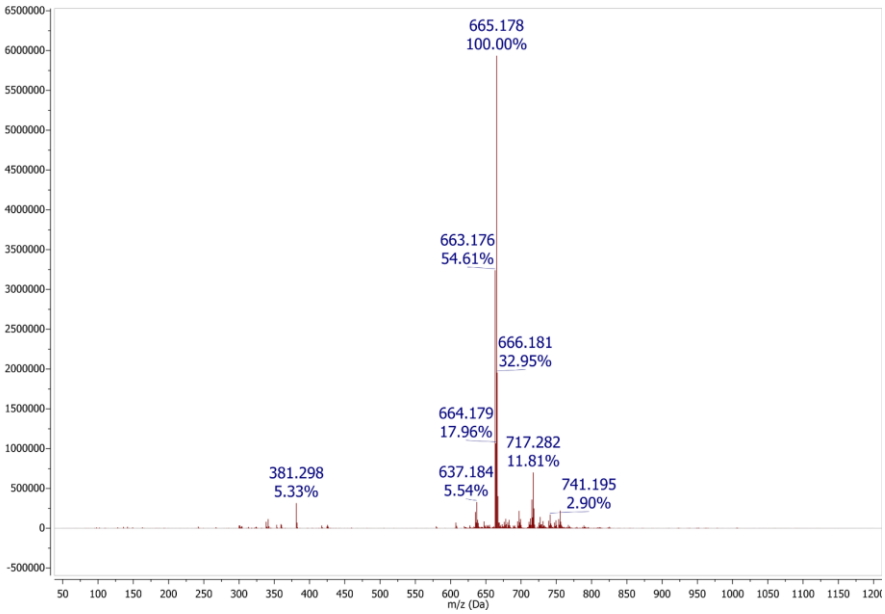

*Figure S30: Mass Spectroscopy spectrum of **2d** recorded in methanol: Positive mode, Electron Spray Ionisation.*

MS (ESI+, CH_3OH): m/z [**2d**]$^+$ calculated 665.178; found 665.178.

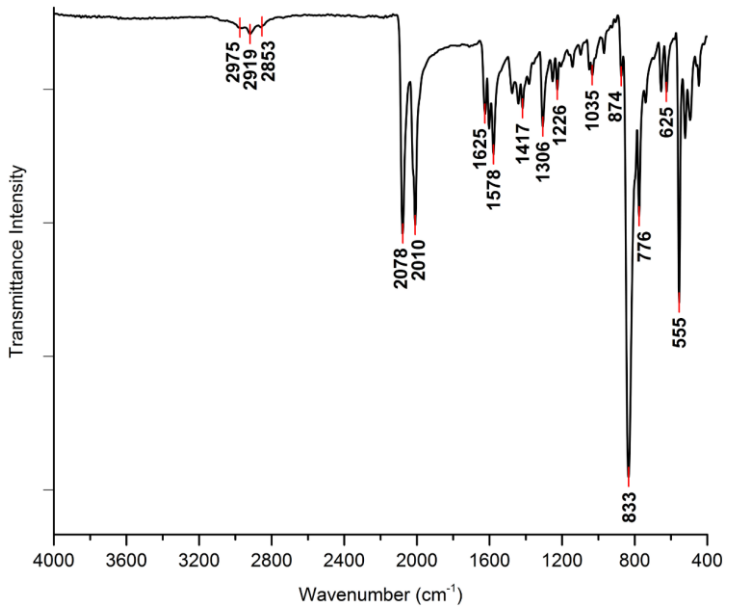

*Figure S31: Solid state infrared transmittance spectrum of **2d** recorded with a platinum-ATR module (monolithic diamond crystal window).*

IR (cm^{-1}) **ν(C=O)** 2078 (s), 2010 (s); **ν(C=N)** 1627–1570 (m); **ν(P–F)** 833 (vs); **δ(P–F)** 555 (vs).

S1.9) Complex **3a** [RhDB(CO)(PEt_3)]PF_6

Complex **3a** was prepared from complex **2a**. To 0.569 g (0.7 mmol, 1eq) **2a** dissolved in 15 mL CH_2Cl_2 was added drop wise 0.714 mL (0.71 mmol, 1.1eq) triethylphosphine (PEt_3) solution (1.0 M in THF), and the reaction mixture stirred for 3 hours. The solvent was evaporated and the residue was washed with small portions of Et_2O. The solids were dried *in vacuo*, and **3a** isolated as a dark brown solid. (0.550 g, 87 % yield).

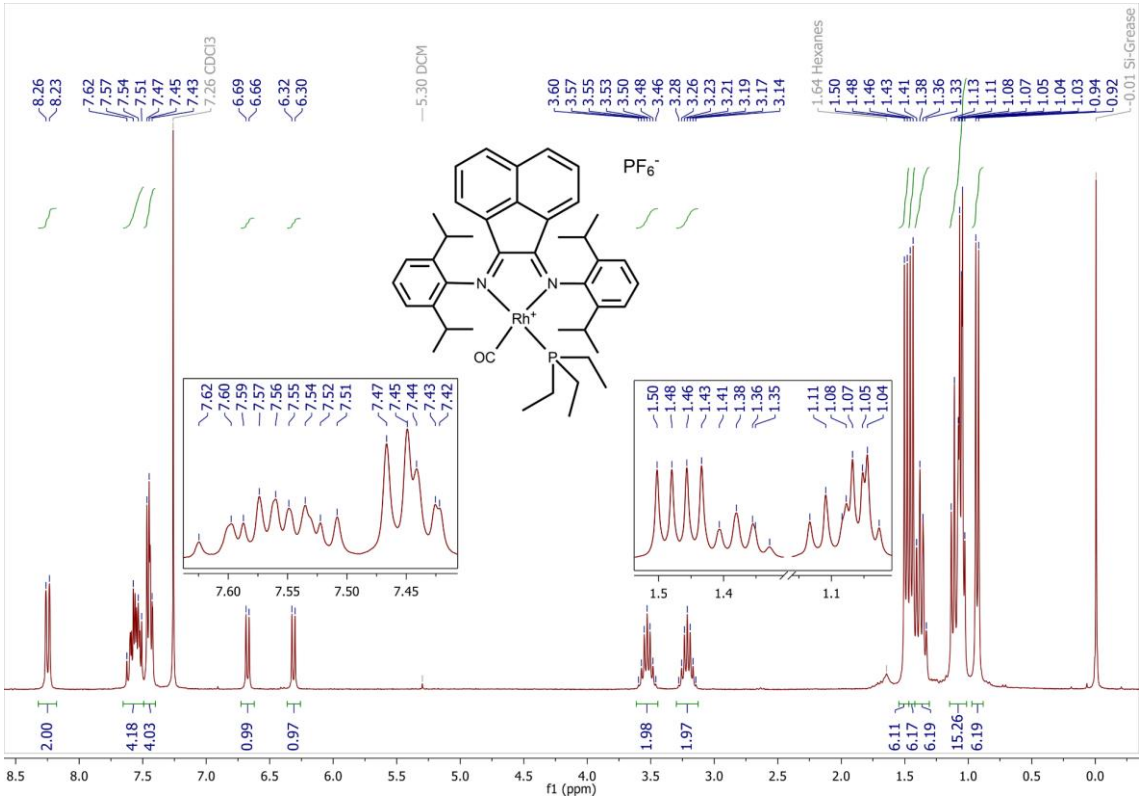

*Figure S32: ^{1}H NMR spectrum of complex **3a** in $CDCl_3$.*

^{1}H NMR (300 MHz, $CDCl_3$) δ 8.25 (d, *J* = 8.4 Hz, 2H, BIAN-C**H**), 7.63–7.50 (m, 4H, Dipp-C**H** and BIAN-C**H**), 7.48–7.41 (m, 4H, Dipp-C**H** and BIAN-C**H**), 6.67 (d, *J* = 7.3 Hz, 1H, BIAN-C**H**), 6.31 (d, *J* = 7.4 Hz, 1H, BIAN-C**H**), 3.53 (sept, *J* = 6.9 Hz, 2H, Dipp(iso)C**H**), 3.21 (sept, *J* = 6.7 Hz, 2H, Dipp(iso)C**H**), 1.49 (d, *J* = 6.8 Hz, 6H, Dipp(iso)C**H**$_3$), 1.45 (d, *J* = 6.8 Hz, 6H, Dipp(iso)C**H**$_3$), 1.37 (q, *J* = 7.9 Hz, 6H, PEt_3-C**H**$_2$), 1.15–1.01 (m, 15H, Dipp(iso)C**H**$_3$ and PEt_3-C**H**$_3$), 0.93 (d, *J* = 6.8 Hz, 6H, Dipp(iso)C**H**$_3$).

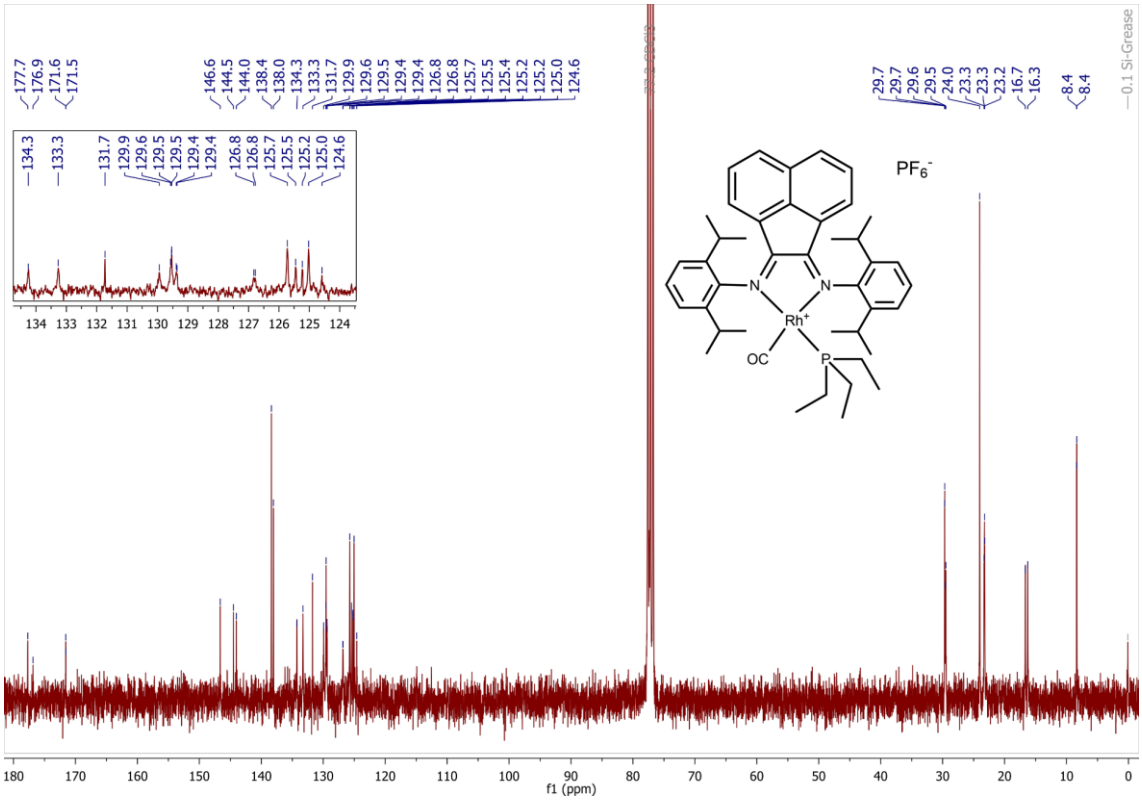

*Figure S33: ^{13}C NMR spectrum of complex **3a** in $CDCl_3$.*

^{13}C NMR (75 MHz, $CDCl_3$) δ 177.27 (d, $J_{C\text{-}Rh}$ = 63.2 Hz, **C**O), 171.6 (BIAN-N=**C**$_q$), 171.5 (BIAN-N=**C**$_q$), 146.6 (BIAN-**C**$_q$), 144.5 (Dipp-N-**C**$_q$), 144.0(Dipp-N-**C**$_q$), 138.4 (BIAN-**C**$_q$), 138.0 (BIAN-**C**$_q$), 134.3 (BIAN-**C**H), 133.3 (BIAN-**C**H), 131.7 (BIAN-**C**$_q$), 129.9 (Dipp-**C**H), 129.6, 129.5 (Dipp-**C**H), 129.4 (Dipp-**C**H), 129.4 (BIAN-**C**$_q$), 126.83 (BIAN-**C**H), 126.78 (BIAN-**C**H), 125.7 (BIAN-**C**H), 125.5 (Dipp(iso)-**C**$_q$), 125.4 (Dipp(iso)-**C**$_q$), 125.23 (Dipp-**C**H), 125.21 (BIAN-**C**H), 125.0 (Dipp-**C**H), 124.6 (Dipp-**C**H), 29.69, 29.66, 29.6, 29.5 (Dipp(iso)-**C**H), 24.0, 23.31, 23.26, 23.21 (Dipp(iso)-**C**H$_3$), 16.45 (d, $J_{C\text{-}P}$ = 30.1 Hz, PEt_3-**C**H$_2$), 8.38, 8.35 (PEt_3-**C**H$_3$).

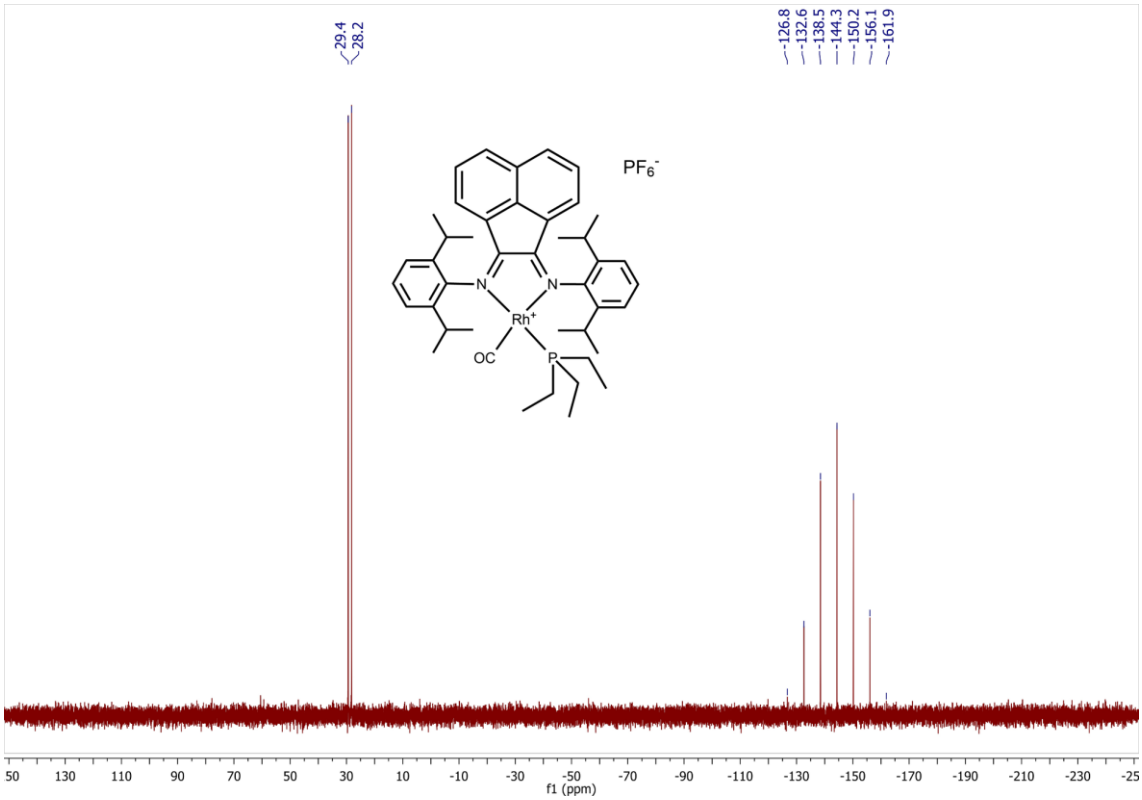

*Figure S34: ^{31}P NMR spectrum of complex **3a** in $CDCl_3$.*

^{19}F NMR (282 MHz, $CDCl_3$) δ –73.8 (d, $J_{F\text{-}P}$ = 712.5 Hz, P**F**$_6$). **^{31}P NMR** (121 MHz, $CDCl_3$) δ 28.8 (d, $J_{P\text{-}Rh}$ = 141.4 Hz, **P**Et$_3$), –144.4 (sept, $J_{P\text{-}F}$ = 712.2 Hz, **P**F$_6$).

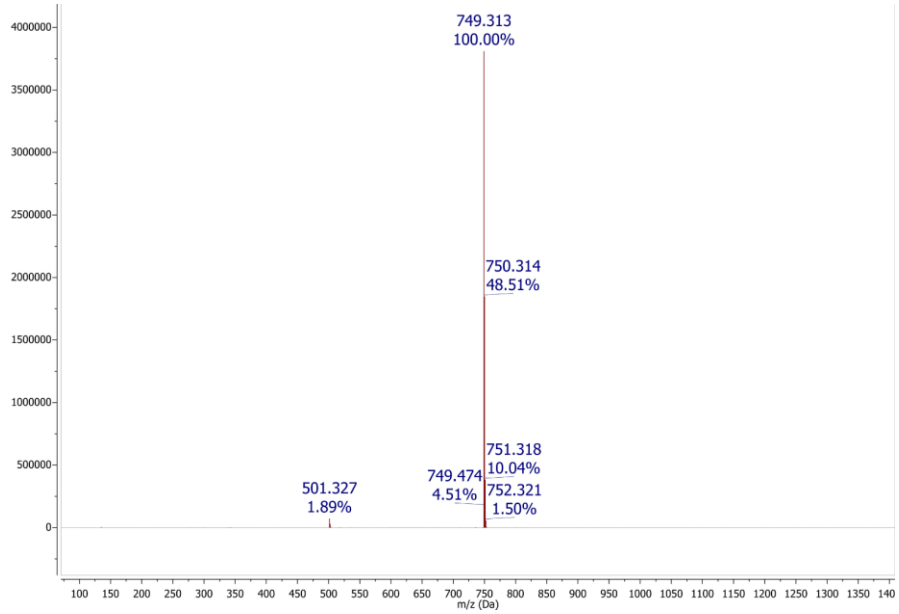

*Figure S35: Mass Spectroscopy spectrum of **3a** recorded in methanol: Positive mode, Electron Spray Ionisation.*

MS (ESI+, CH_3OH): m/z [**3a**]$^+$ calculated 749.310; found 749.313.

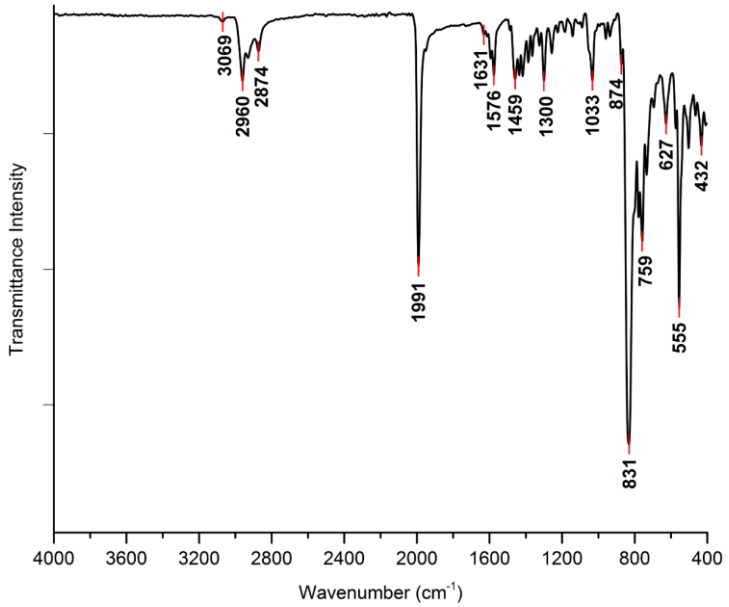

*Figure S36: Solid state infrared transmittance spectrum of **3a** recorded with a platinum-ATR module (monolithic diamond crystal window).*

IR (cm^{-1}) **ν(CO)** 1991 (s); **ν(C=N)** 1654–1555 (vw-w); **ν(P–F)** 831 (vs); **δ(P–F)** 555 (s).

S1.10) Complex **3b** [RhMB(CO)(PEt_3)]PF_6

Complex **3b** was prepared in a procedure similar to that reported for **3a**. 0.526 g (0.73 mmol, 1eq) **2b** and 0.714 mL (0.71 mmol, 1.1 eq) PEt_3 solution (1.0 M in THF) were used and **3b** isolated as a dark brown powder. (0.437 g, 74 % yield).

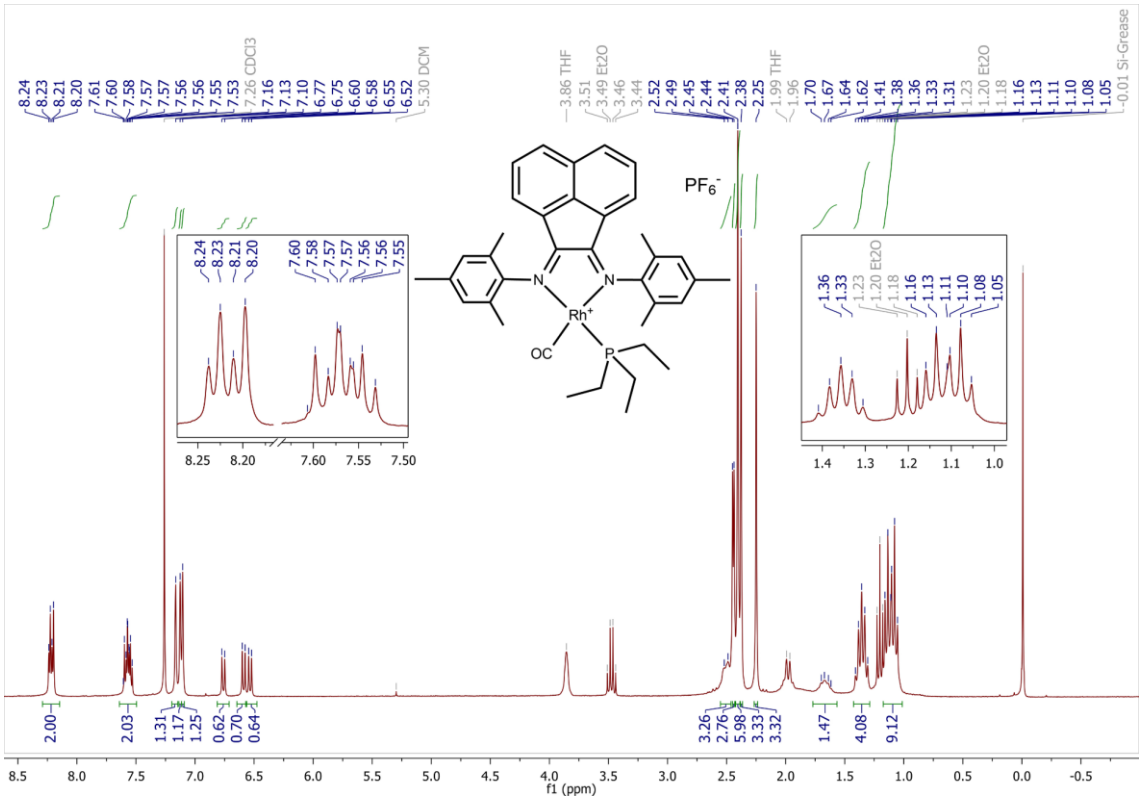

*Figure S37: ^{1}H NMR spectrum of complex **3b** in $CDCl_3$.*

^{1}H NMR (300 MHz, $CDCl_3$) δ 8.22 (dd, *J* = 8.3, 3.9 Hz, 2H, BIAN-C**H**), 7.56 (m, 2H, Mes-C**H** and BIAN-C**H**), 7.16 (s, 1H, Mes-C**H**), 7.13 (s, 1H, Mes-C**H**), 7.10 (s, 1H, Mes-C**H**), 6.76 (d, *J* = 7.2 Hz, 1H, BIAN-C**H**), 6.59 (d, *J* = 7.2 Hz, 1H, BIAN-C**H**), 6.53 (d, *J* = 7.3 Hz, 1H, BIAN-C**H**), 2.55–2.46 (m, 3H, Mes-C$\mathbf{H}_3$), 2.44 (d, *J* = 3.8 Hz, 3H, Mes-C$\mathbf{H}_3$), 2.41 (s, 6H, Mes-C$\mathbf{H}_3$), 2.38 (s, 3H, Mes-C$\mathbf{H}_3$), 2.25 (s, 3H, Mes-C$\mathbf{H}_3$), 1.66 (br, 2H, PEt_3-C$\mathbf{H}_2$), 1.36 (dq, $J_{P\text{-}H}$ = 8.0 Hz, $J_{H\text{-}H}$ = 7.6, 7.4 Hz, 4H, PEt_3-C$\mathbf{H}_2$), 1.11 (dt, $J_{P\text{-}H}$ = 17.0 Hz, $J_{H\text{-}H}$ = 7.4, 7.4 Hz, 9H, PEt_3-C$\mathbf{H}_3$).

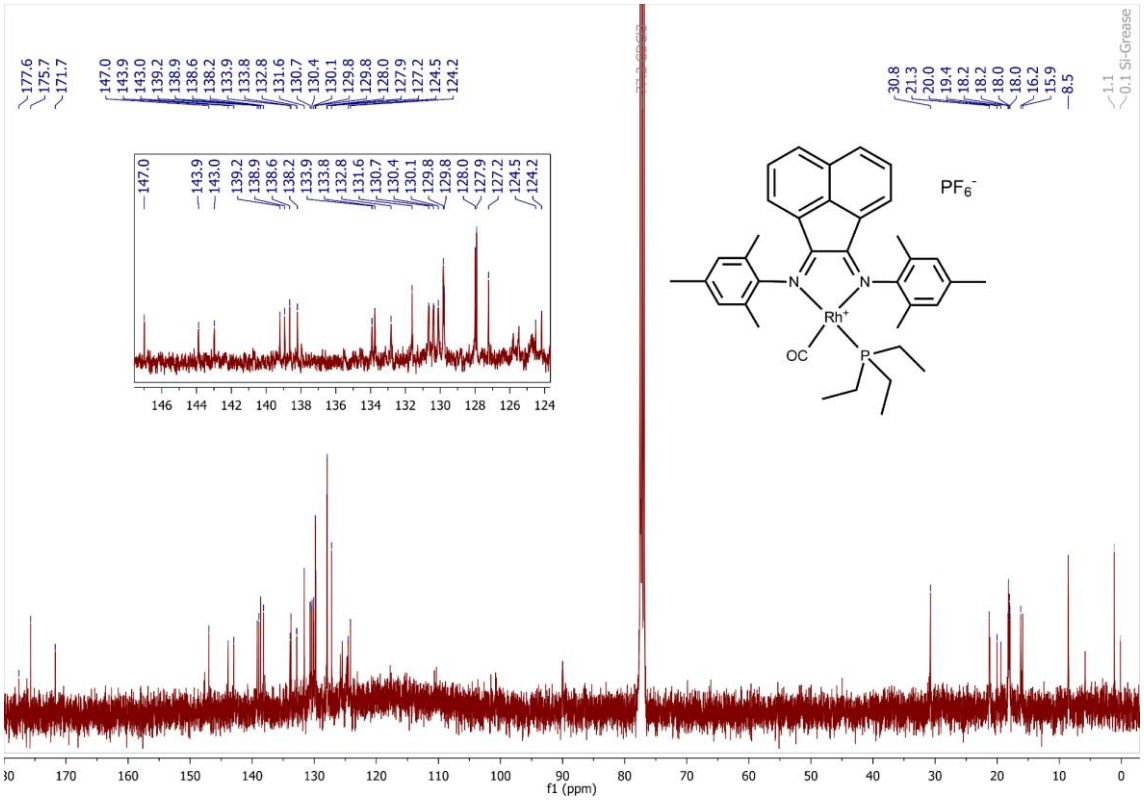

*Figure S38: ^{13}C NMR spectrum of complex **3b** in $CDCl_3$.*

^{13}C NMR (75 MHz, $CDCl_3$) δ 177.6 (Rh=**C**=O), 175.7 (BIAN-N=**C**$_q$), 171.7 (BIAN-N=**C**$_q$), 147.0 (BIAN-**C**$_q$), 143.9 (Mes-N-**C**$_q$), 143.0 (Dipp-N-**C**$_q$), 139.2, 138.9, 138.6, 138.2, 133.9 (BIAN-**C**H), 133.8, 132.8 (BIAN-**C**H), 131.6, 130.7 (Mes-**C**H), 130.4 (Mes-**C**H), 130.1 (Mes-**C**H), 129.82 (Mes-**C**H), 129.77 (BIAN-**C**H), 128.0, 127.9, 127.2 (BIAN-**C**$_q$), 125.8 (BIAN-**C**H), 125.5 (BIAN-**C**H), 124.5 (BIAN-**C**H), 124.2, 30.88, 21.3, 21.2 (Mes-**C**H$_3$), 19.71 (d, $J_{C\text{-}P}$ = 65.8 Hz, PEt$_3$-**C**H$_2$), 18.24, 18.19, 17.96 (Mes-**C**H$_3$), 16.06 (d, $J_{C\text{-}P}$ = 29.7 Hz, PEt$_3$-**C**H$_2$), 8.5, 5.8 (PEt$_3$-**C**H$_3$).

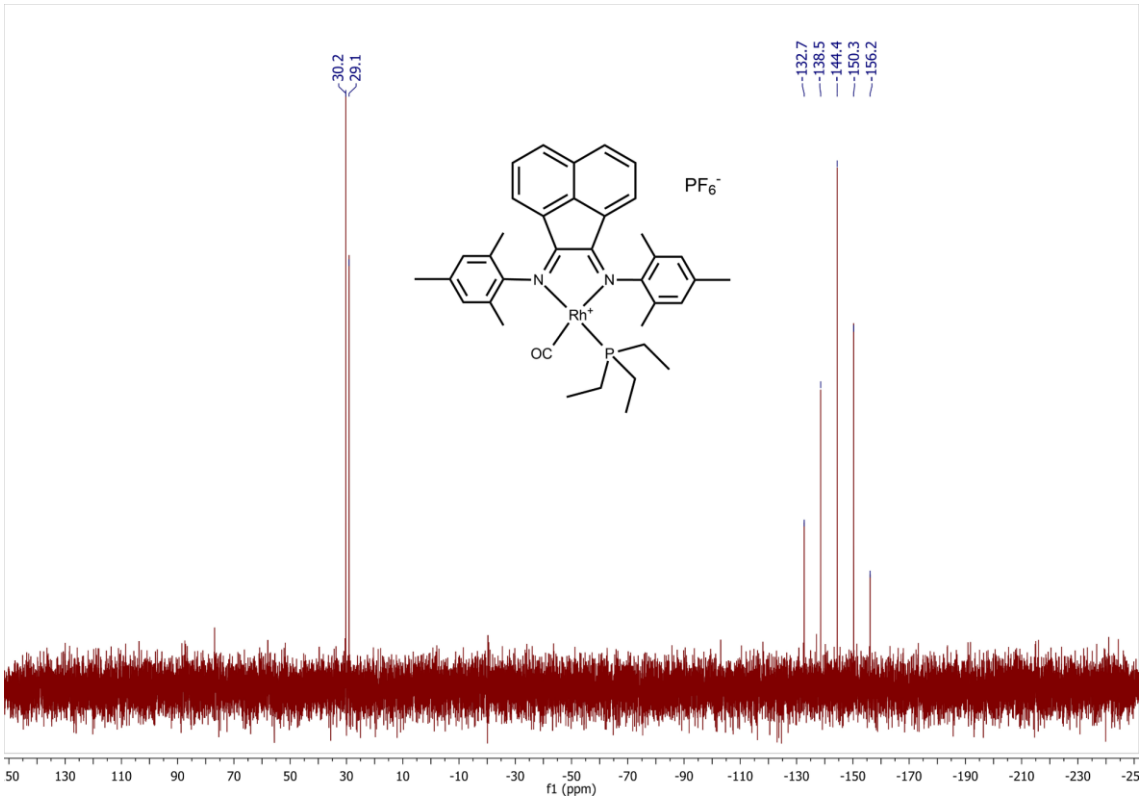

*Figure S39: ^{31}P NMR spectrum of complex **3b** in $CDCl_3$.*

^{19}F NMR (282 MHz, $CDCl_3$) δ –73.5 (d, $J_{F\text{-}P}$ = 713.1 Hz, P**F**$_6$). **^{31}P NMR** (121 MHz, $CDCl_3$) δ 29.7 (d, $J_{P\text{-}Rh}$ = 143.0 Hz), –144.4 (sept, $J_{P\text{-}F}$ = 712.4 Hz, **P**F$_6$).

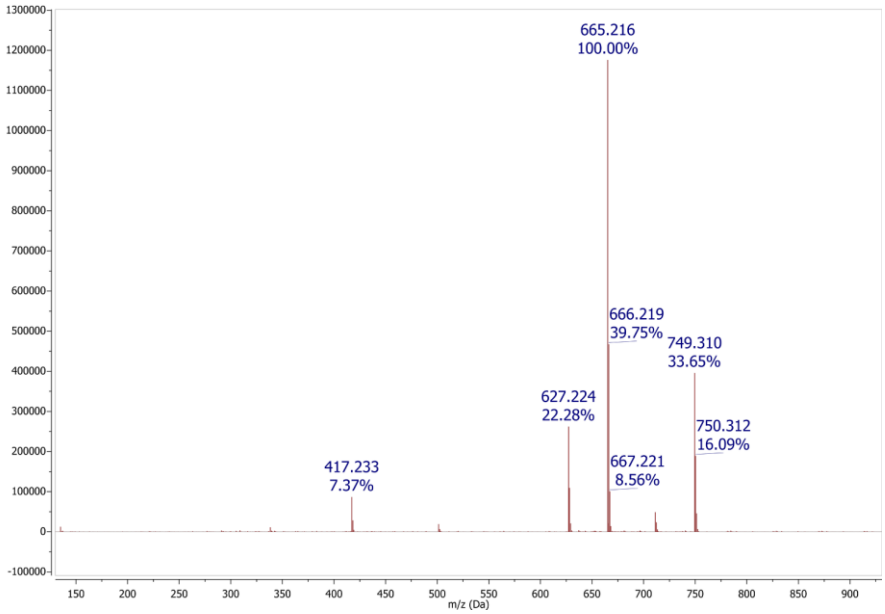

*Figure S40: Mass Spectroscopy spectrum of **3b** recorded in methanol: Positive mode, Electron Spray Ionisation.*

MS (ESI+, CH_3OH): m/z [**3b**]$^+$ calculated 749.311; found 749.310.

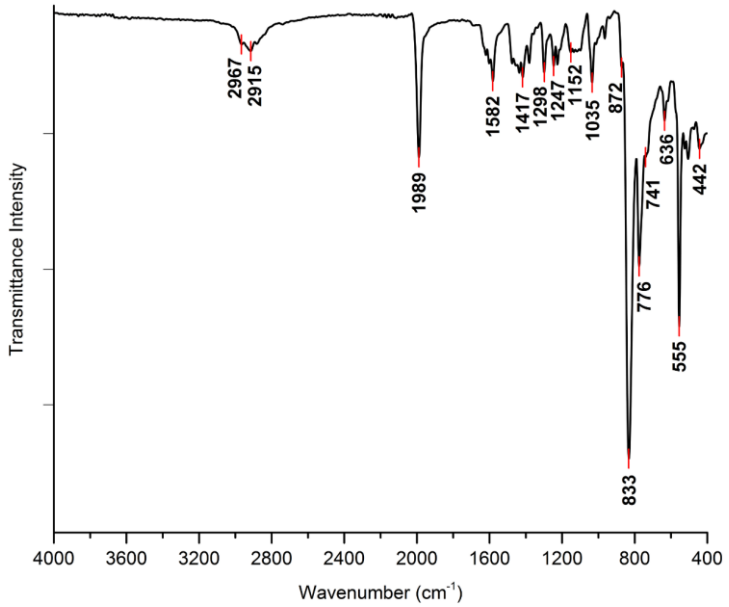

*Figure S41: Solid state infrared transmittance spectrum of **3b** recorded with a platinum-ATR module (monolithic diamond crystal window).*

IR (cm^{-1}) **ν(CO)** 1989 (m); **ν(C=N)** 1652–1524 (w); **ν(P–F)** 833 (vs); **δ(P–F)** 555 (s).

S1.11) Complex **4a** [RhDB(cod)Cl]

0.220 g (0.44 mmol, 1.01eq) $[Rh(cod)Cl]_2$, 0.432 g (0.87 mmol, 2eq) DippBIAN were dissolved in *ca.* 20 mL degassed CH_2Cl_2 and stirred for 24 hours at RT. The orange suspension slowly changed to a dark green solution and was dried *in vacuo*. The resulting green-brown solid was purified by column chromatography (aluminium oxide resin), eluting residual starting material with CH_2Cl_2, thereafter flushing the product from the column with EtOH:CH_2Cl_2 (1:15). The dark brown ethanolic fractions were combined and dried *in vacuo* to yield **4a** as a dark green solid. (0.302 g, 46 % yield).

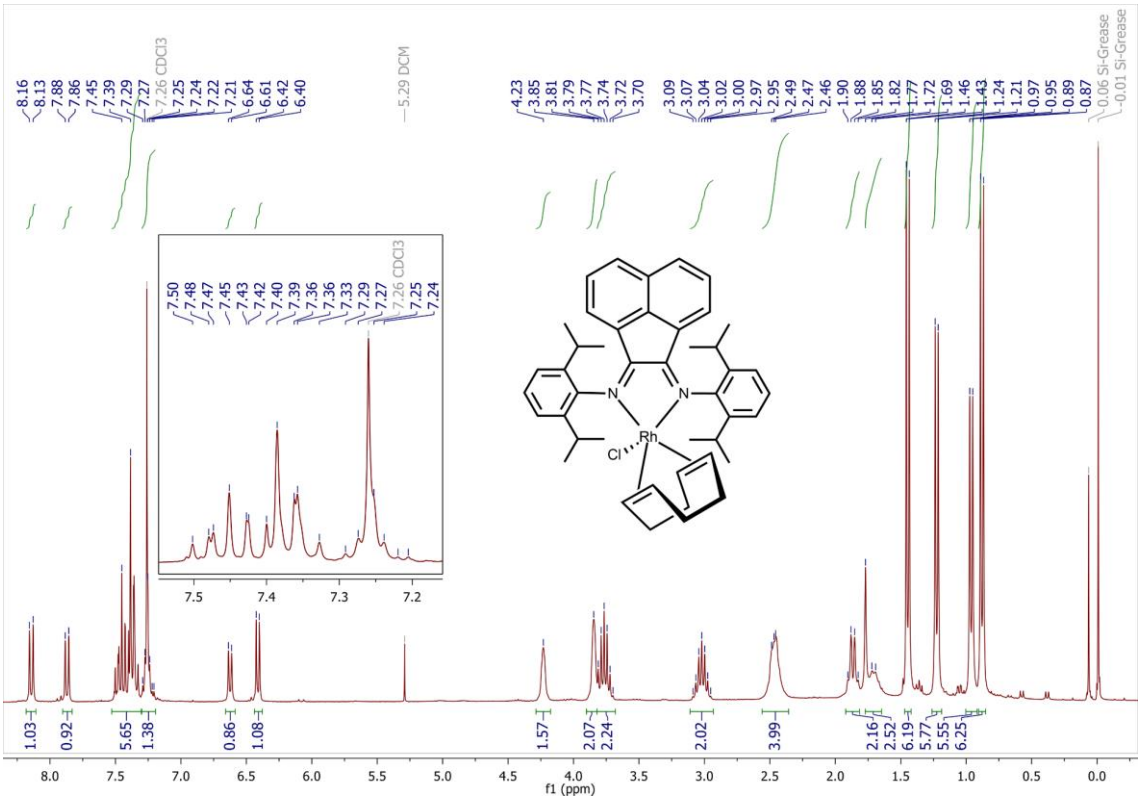

*Figure S42: ^{1}H NMR spectrum of complex **4a** in $CDCl_3$.*

^{1}H NMR (300 MHz, $CDCl_3$) δ 8.14 (d, *J* = 8.3 Hz, 1H, BIAN-C**H**), 7.87 (d, *J* = 8.3 Hz, 1H, BIAN-C**H**), 7.42 (br, 6H, Dipp-C**H** and BIAN-C**H**), 7.31–7.19 (m, 1H), 6.62 (d, *J* = 7.2 Hz, 1H, BIAN-C**H**), 6.41 (d, *J* = 7.3 Hz, 1H, BIAN-C**H**), 4.23 (br, 2H, cod-C**H**), 3.85 (s, 2H, cod-C**H**), 3.75 (sept, *J* = 6.7 Hz, 2H, Dipp(iso)C**H**), 3.02 (sept, *J* = 6.7 Hz, 2H, Dipp(iso)C**H**), 2.55–2.36 (m, 4H, cod-C$\mathbf{H}_2$), 1.93–1.81 (m, 2H, cod-C$\mathbf{H}_2$), 1.77–1.64 (m, 2H, cod-C$\mathbf{H}_2$), 1.45 (d, *J* = 6.8 Hz, 6H, Dipp(iso)C$\mathbf{H}_3$), 1.23 (d, *J* = 6.9 Hz, 6H, Dipp(iso)C$\mathbf{H}_3$), 0.96 (d, *J* = 6.9 Hz, 6H, Dipp(iso)C$\mathbf{H}_3$), 0.88 (d, *J* = 6.8 Hz, 6H, Dipp(iso)C$\mathbf{H}_3$).

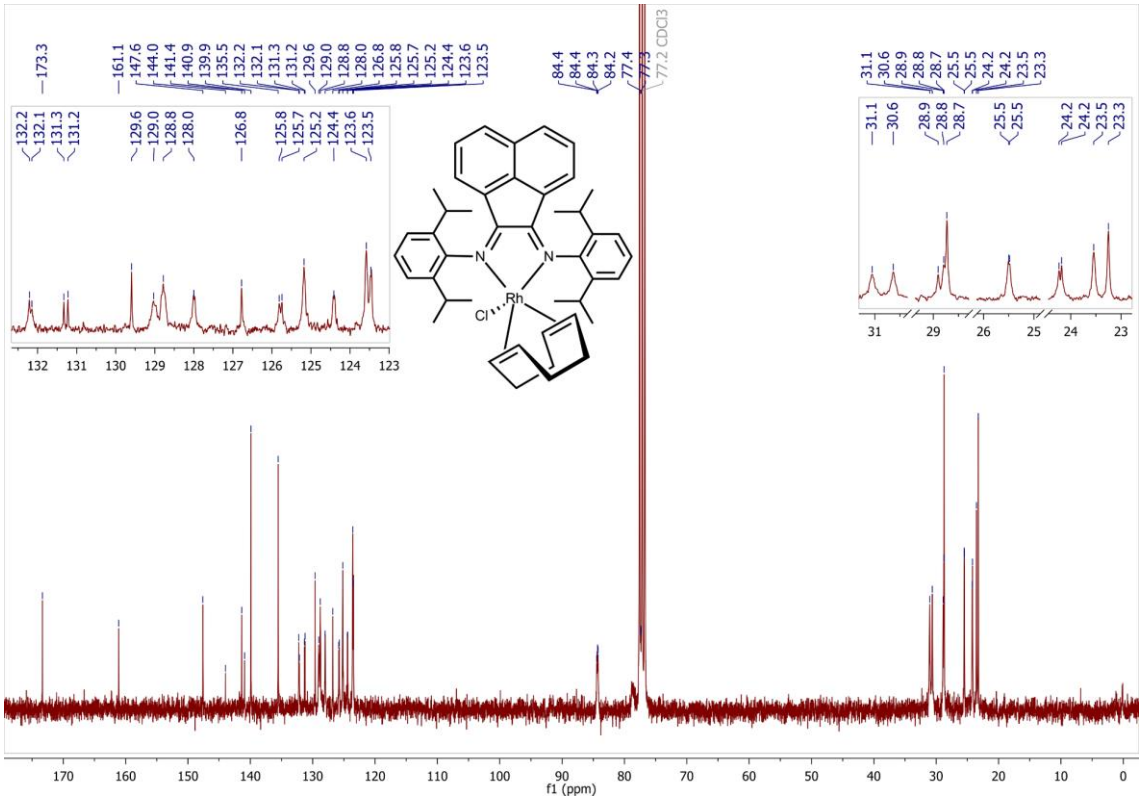

*Figure S43: ^{13}C NMR spectrum of complex **4a** in $CDCl_3$.*

^{13}C NMR (75 MHz, $CDCl_3$) δ 173.3 (BIAN-N=**C**$_q$), 161.1 (BIAN-N=**C**$_q$), 147.6 (Dipp-N-**C**$_q$), 144.0 (Dipp-N-**C**$_q$), 141.4 (BIAN-**C**$_q$), 140.9 (BIAN-**C**$_q$), 139.9 (**C**$_q$), 135.5 (**C**$_q$), 132.2, 132.1 (BIAN-**C**H), 131.3, 131.2 (Dipp(iso)-**C**$_q$), 129.6 (**C**$_q$), 129.0, 128.8 (Dipp-**C**H), 128.0 (BIAN-**C**H), 126.8 (**C**$_q$), 125.8, 125.7 (Dipp-**C**H), 125.2, 124.4 (BIAN-**C**H), 123.6, 123.5 (Dipp-**C**H), 84.35 (dd, $J_{C\text{-}Rh}$ = 10.9, 4.9 Hz, cod-**C**H), 77.36 (d, $J_{C\text{-}Rh}$ = 4.8 Hz, cod-**C**H), 31.1 (cod-**C**H$_2$), 30.6 (cod-**C**H$_2$), 28.9, 28.8, 28.7 (Dipp(iso)-**C**H), 25.5 (cod-**C**H$_2$), 25.5 (Dipp(iso)-**C**H$_3$), 24.2 (cod-**C**H$_2$), 24.2, 23.5, 23.3 (Dipp(iso)-**C**H$_3$).

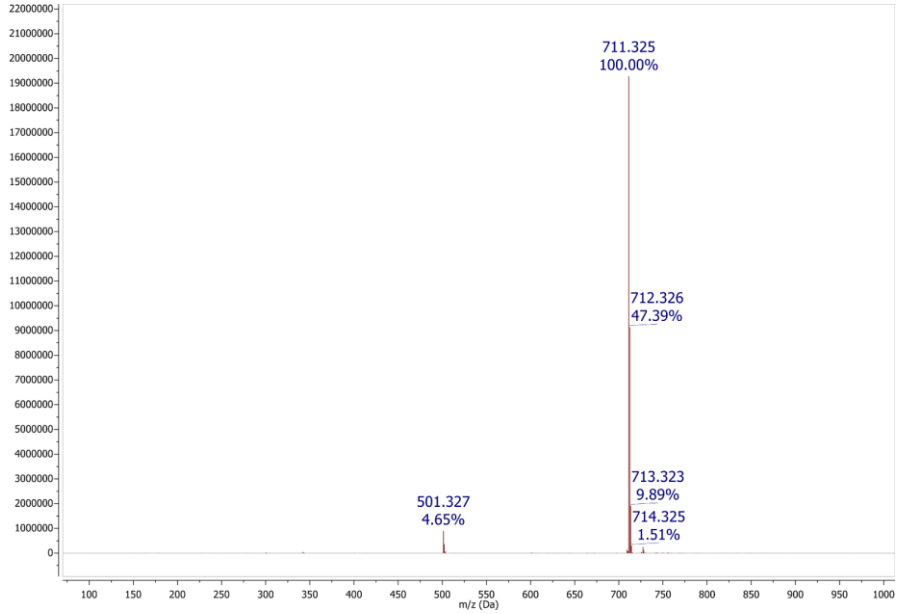

*Figure S44: Mass Spectroscopy spectrum of **4a** recorded in methanol: Positive mode, Electron Spray Ionisation.*

MS (ESI+, CH_3OH): m/z [**4a**-Cl]$^+$ calculated 711.3186; found 711.325.

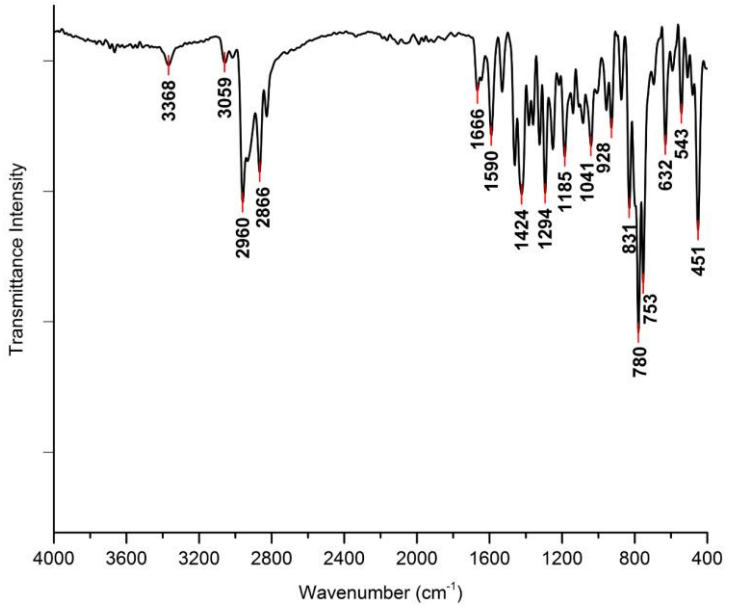

*Figure S45: Solid state infrared transmittance spectrum of **4a** recorded with a platinum-ATR module (monolithic diamond crystal window).*

IR (cm^{-1}) **ν(C=N)** 1689–1619 (w), 1590 (m).

S1.12) Complex **4b** [RhMB(cod)Cl]

Complex **4b** was prepared in a procedure similar to that reported for **4a**. 0.246 g (0.5 mmol, 1.01eq) $[Rh(cod)Cl]_2$ and 0.404 g (0.98 mmol, 2eq) MesBIAN were employed, and **4b** isolated as a dark green solid. (0.469 g, 72 % yield).

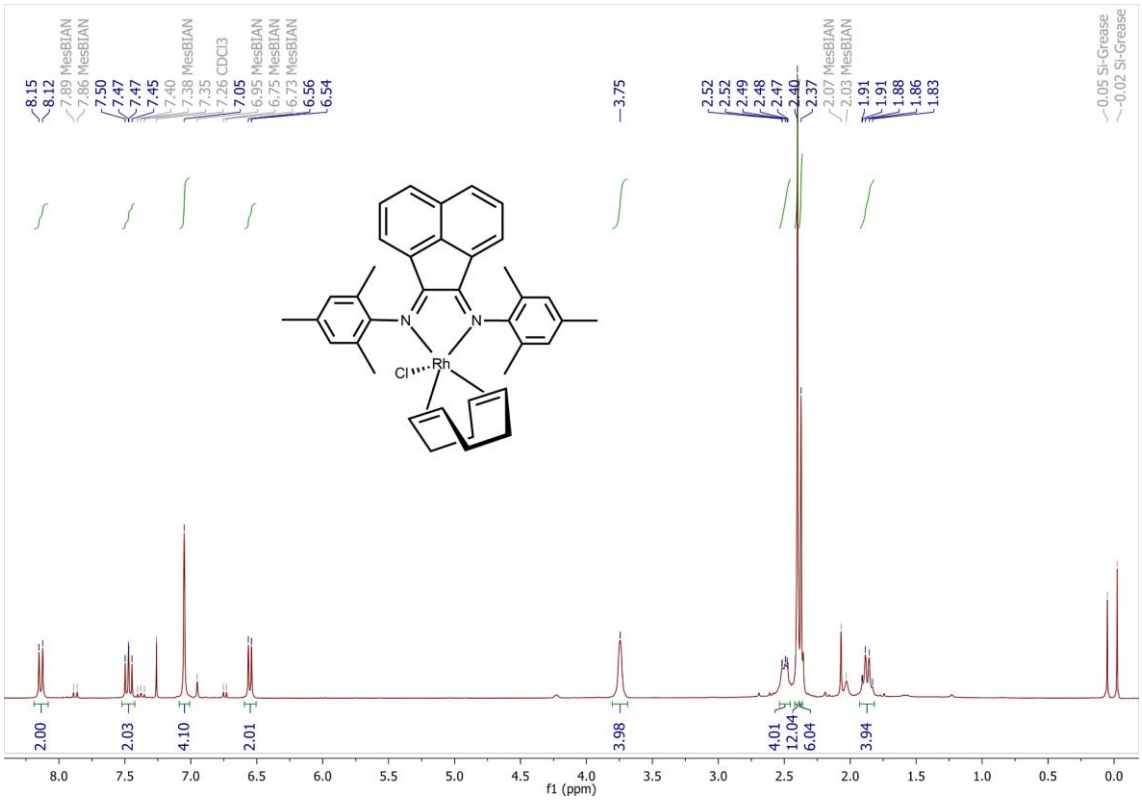

*Figure S46: ^1H NMR spectrum of complex **4b** in $CDCl_3$. A small amount of the MesBIAN ligand dissociates from the complex over time, and the associated peaks have been marked as "MesBIAN".*

^{1}H NMR (300 MHz, $CDCl_3$) δ 8.14 (d, *J* = 8.3 Hz, 2H, BIAN-C**H**), 7.47 (dd, *J* = 8.3, 7.3 Hz, 2H, BIAN-C**H**), 7.05 (s, 4H, Mes-C**H**), 6.55 (d, *J* = 7.2 Hz, 2H, BIAN-C**H**), 3.75 (br, 4H, cod-C**H**), 2.52–2.47 (m, 4H, cod-C$\mathbf{H}_2$), 2.40 (s, 12H, Mes-C$\mathbf{H}_3$), 2.37 (s, 6H, Mes-C$\mathbf{H}_3$), 1.98–1.81 (m, 4H, cod-C$\mathbf{H}_2$).

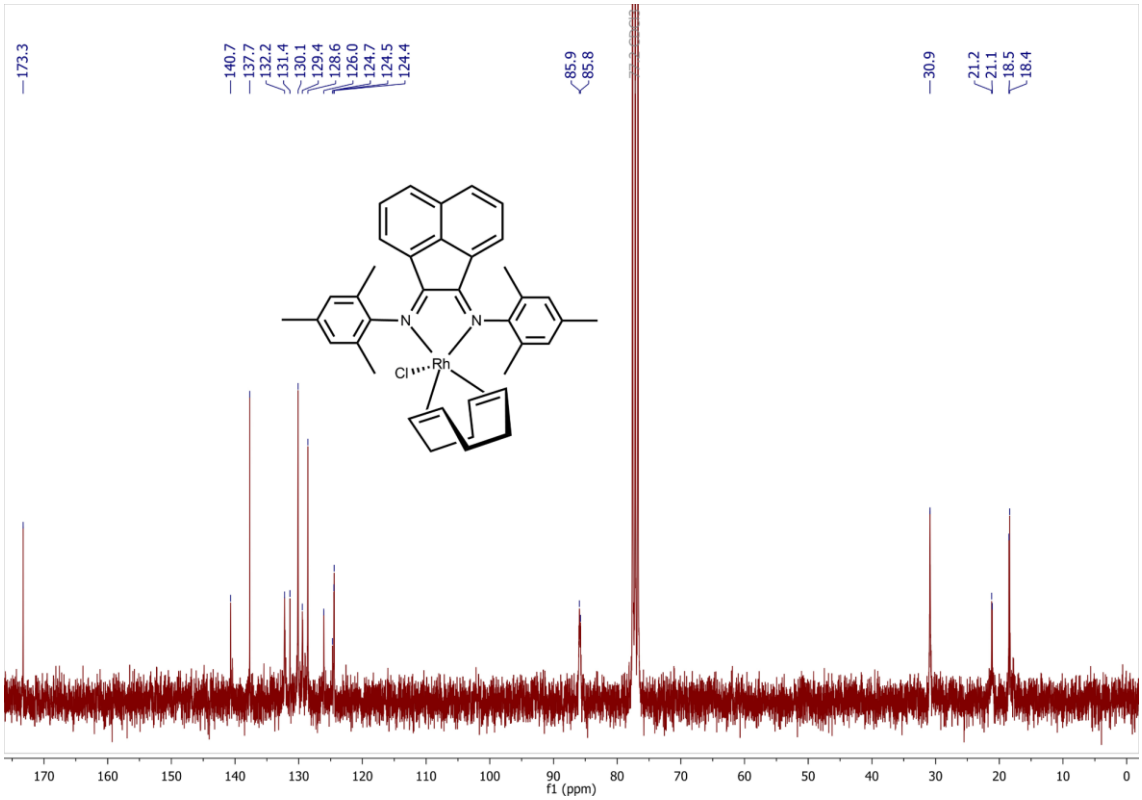

*Figure S47: ^{13}C NMR spectrum of complex **4b** in $CDCl_3$.*

^{13}C NMR (75 MHz, $CDCl_3$) δ 173.3 (BIAN-N=**C**$_q$), 140.7 (Mes-N-**C**$_q$), 137.7 (BIAN-**C**H), 132.2 (BIAN-**C**$_q$), 132.2 (BIAN-**C**$_q$), 131.4 (**C**$_q$), 130.1 (Mes-**C**H), 129.4 (**C**$_q$), 128.6 (BIAN-**C**H), 126.0 (**C**$_q$), 124.7 (BIAN-**C**$_q$), 124.5 (BIAN-**C**H), 124.4 (BIAN-**C**H), 85.9 (d, $J_{C\text{-}Rh}$ = 11.0 Hz, cod-**C**H), 30.9 (cod-**C**H_2), 21.2, 21.1, 18.5, 18.4 (Mes-**C**H_3).

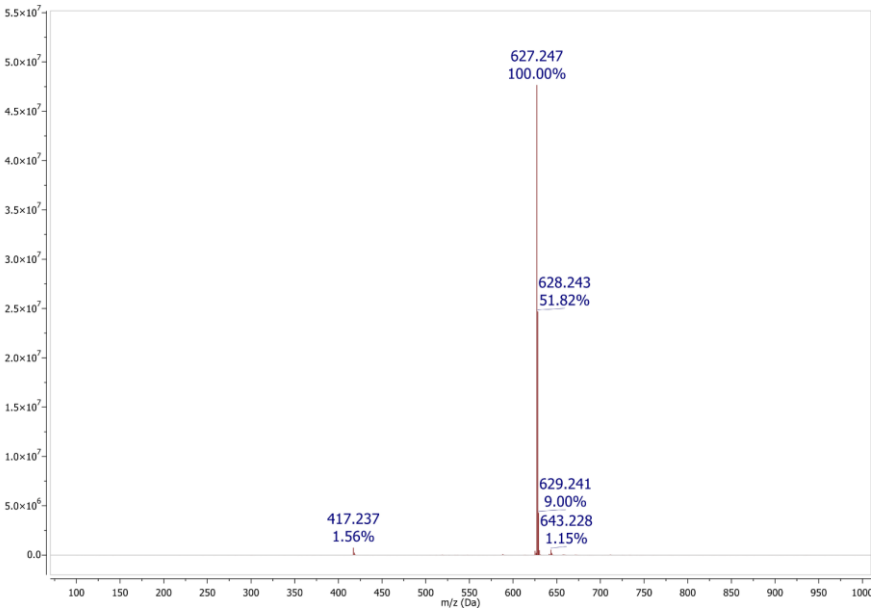

*Figure S48: Mass Spectroscopy spectrum of **4b** recorded in methanol: Positive mode, Electron Spray Ionisation.*

MS (ESI+, CH_3OH): m/z [**4b**-Cl]$^+$ calculated 627.225; found 627.247.

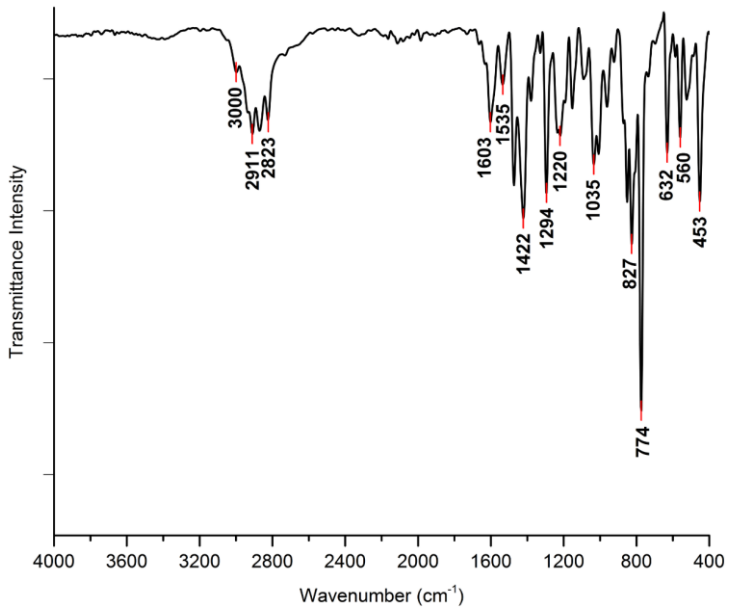

*Figure S49: Solid state infrared transmittance spectrum of **4b** recorded with a platinum-ATR module (monolithic diamond crystal window).*

IR (cm^{-1}) **ν(C=N)** 1620–1530 (w).

S1.13) Complex **4c** [IrDB(cod)Cl]

Complex **4c** was prepared in a procedure similar to that reported for **4a**. 0.245 g (0.4 mmol, 1.01 eq) $[Ir(cod)Cl]_2$, 0.359 g (0.7 mmol, 2 eq) DippBIAN were employed, and **4c** isolated as a dark blue solid. (0.394 g, 66 % yield).

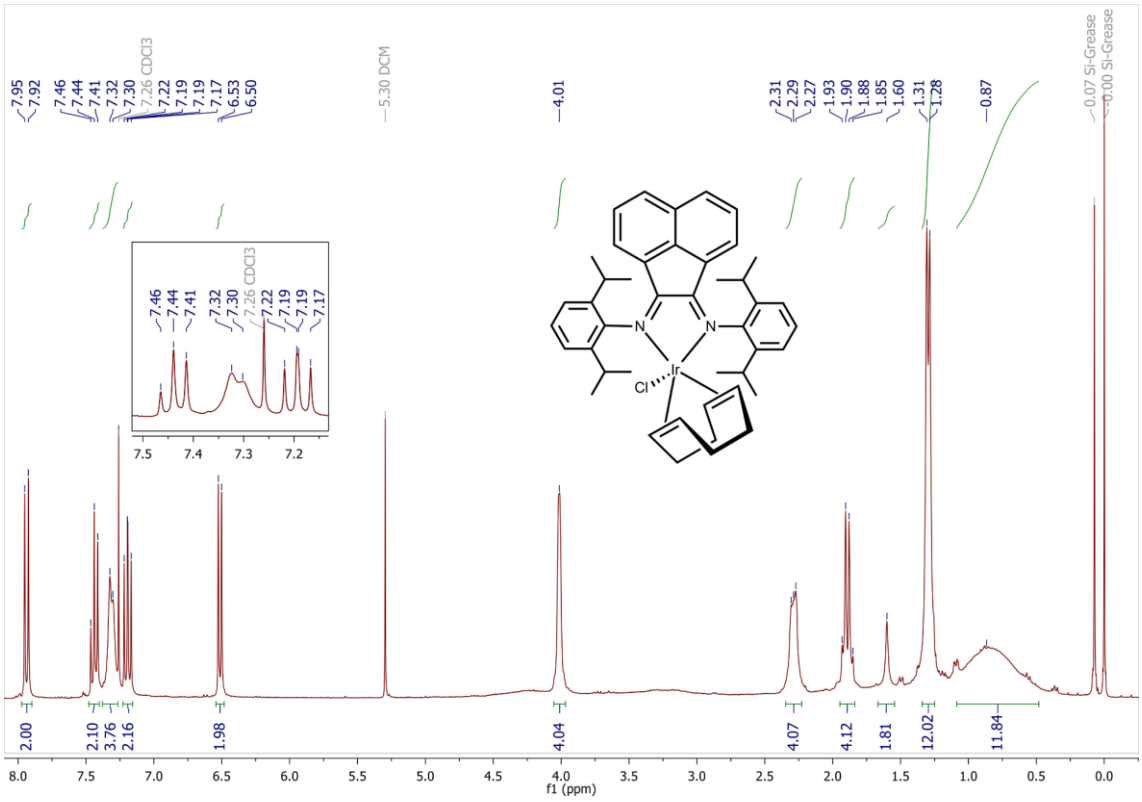

*Figure S50: ^{1}H NMR spectrum of complex **4c** in $CDCl_3$.*

^{1}H NMR (300 MHz, $CDCl_3$) δ 7.94 (d, *J* = 8.2 Hz, 2H, BIAN-C**H**), 7.44 (dd, *J* = 7.6 Hz, 2H, Dipp-C**H**), 7.31 (br, 4H, Dipp-C**H**), 7.19 (dd, *J* = 8.3, 7.2 Hz, 2H, 2H, BIAN-C**H**), 6.51 (d, *J* = 7.2 Hz, 2H, BIAN-C**H**), 4.01 (br, 4H, cod-C**H**), 2.29 (br, 4H, Dipp(iso)C**H**), 1.95–1.84 (m, 4H, cod-C$\mathbf{H}_2$), 1.60 (br, 2H, cod-C$\mathbf{H}_2$), 1.30 (d, *J* = 6.7 Hz, 12H, Dipp(iso)C$\mathbf{H}_3$), 0.87 (br, 12H, Dipp(iso)C$\mathbf{H}_3$).

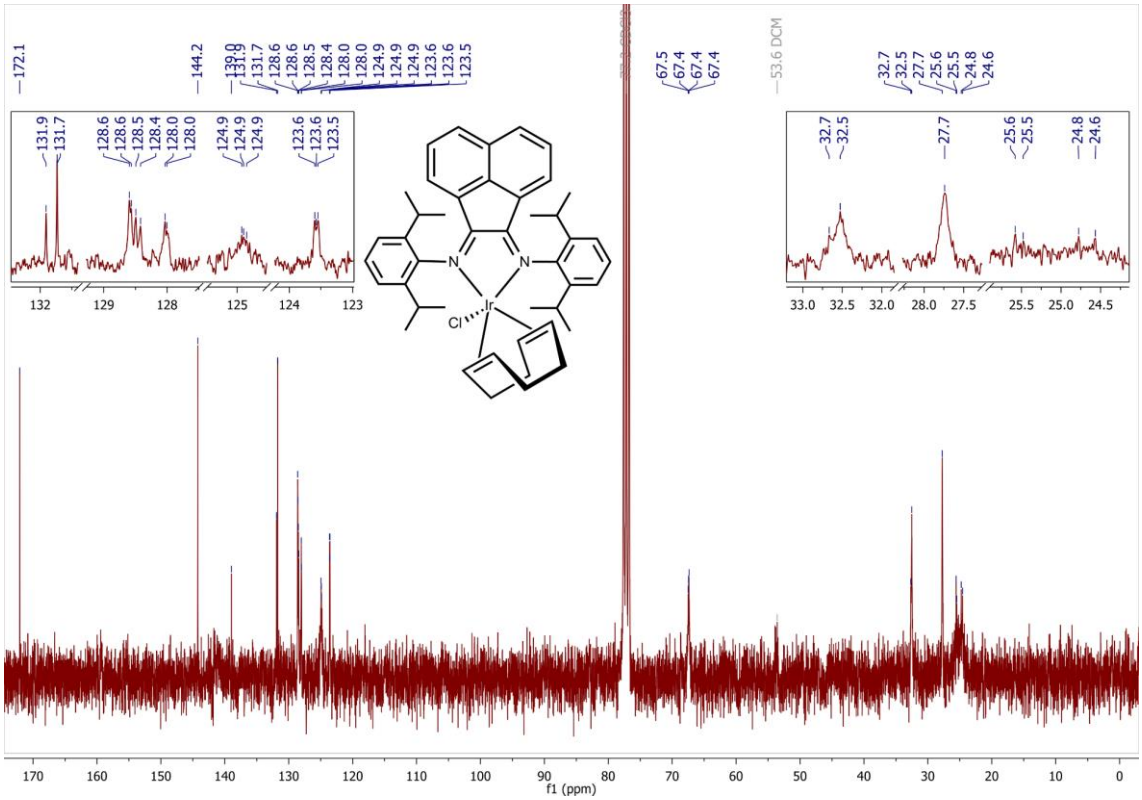

*Figure S51: ^{13}C NMR spectrum of complex **4c** in $CDCl_3$.*

^{13}C NMR (75 MHz, $CDCl_3$) δ 172.1 (BIAN-N=**C**$_q$), 144.2 (Dipp-N-**C**$_q$), 139.0 (BIAN-**C**$_q$), 131.9, 131.7 (Dipp(iso)-**C**$_q$), 128.59, 128.57 (BIAN-**C**H), 128.5, 128.4 (BIAN-**C**$_q$), 128.03, 128.00 (BIAN-**C**H), 124.93, 124.90, 124.85 (Dipp-**C**H), 123.6 (BIAN-**C**H), 123.6 (BIAN-**C**$_q$), 123.5 (BIAN-**C**H), 67.4 (br, cod-**C**H), 32.7 (cod-**C**H_2), 32.5 (br, Dipp(iso)-**C**H), 27.7 (br, cod-**C**H_2), 25.6, 25.5, 24.8, 24.6 (Dipp(iso)-**C**H_3).

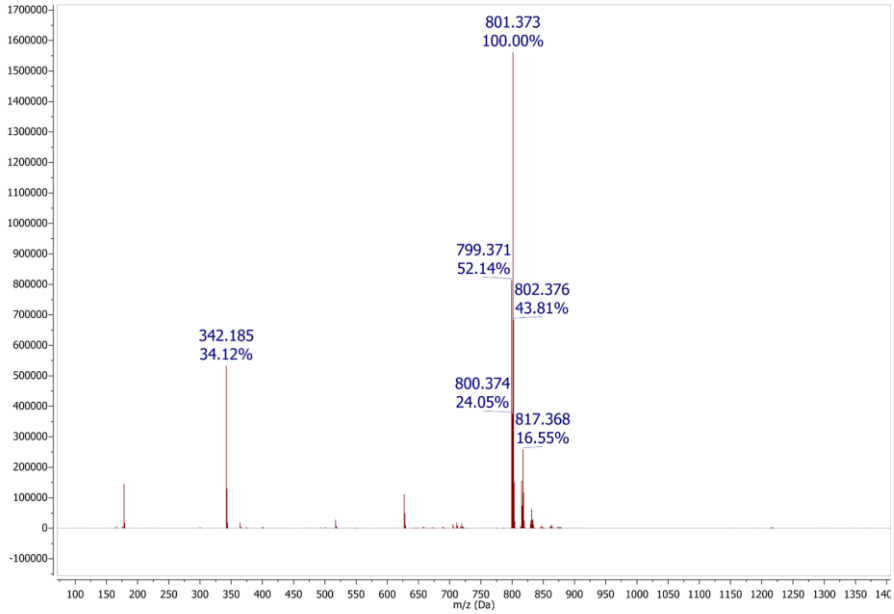

*Figure S52: Mass Spectroscopy spectrum of **4c** recorded in methanol: Positive mode, Electron Spray Ionisation.*

MS (ESI+, CH_3OH): m/z [**4c**-Cl]$^+$ calculated 801.376; found 801.373.

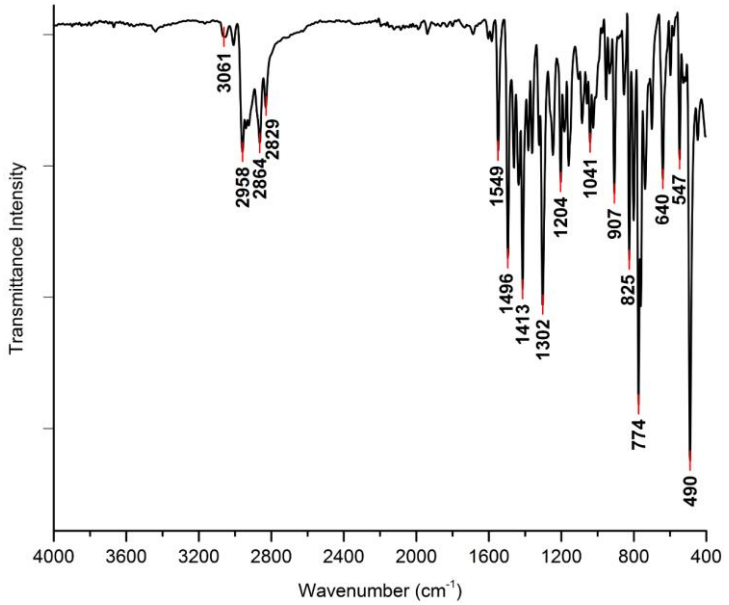

*Figure S53: Solid state infrared transmittance spectrum of **4c** recorded with a platinum-ATR module (monolithic diamond crystal window).*

IR (cm^{-1}) **ν(C=N)** 1603 (vw), 1584 (vw), 1549 (w).

S1.14) Complex **4d** [IrMB(cod)Cl]

Complex **4d** was prepared in a procedure similar to that reported for **4a**. 0.298 g (0.4 mmol, 1.01 eq) $[Ir(COD)Cl]_2$, 0.358 g (0.7 mmol, 2 eq) MesBIAN were employed, and **4d** isolated as a dark blue solid. (0.565 g, 87 % yield).

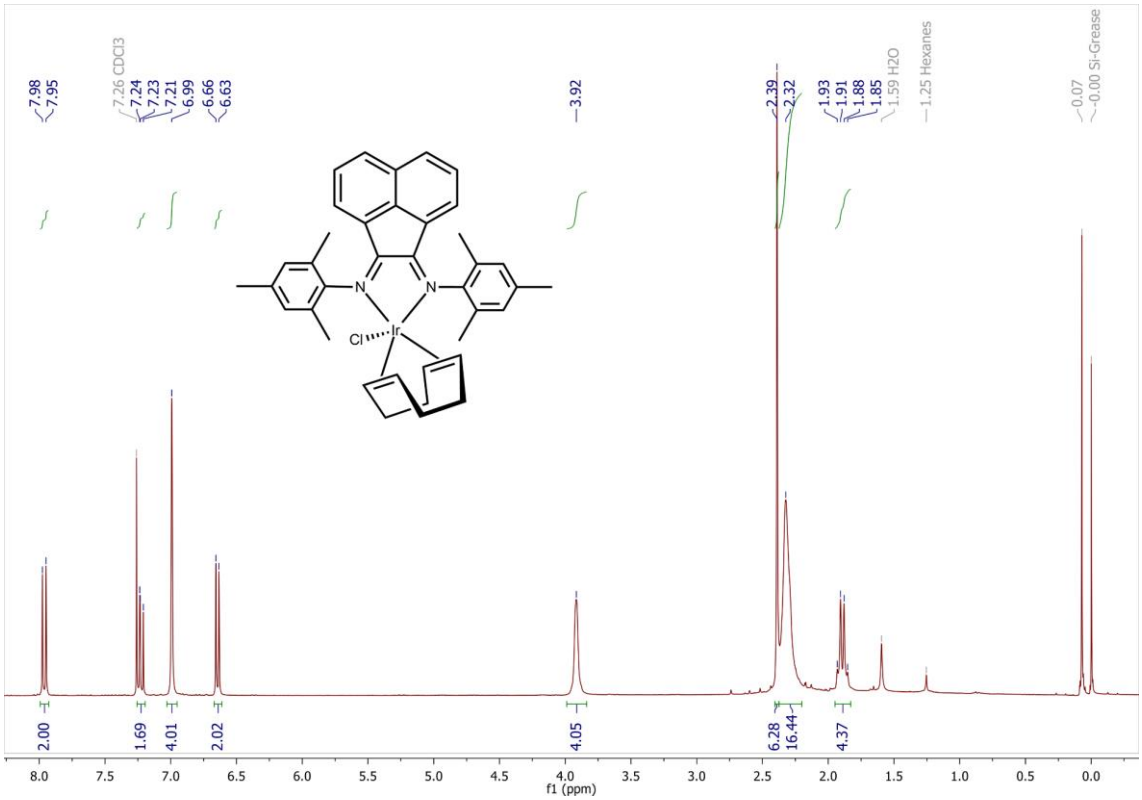

*Figure S54: ^{1}H NMR spectrum of complex **4d** in $CDCl_3$.*

^{1}H NMR (300 MHz, $CDCl_3$) δ 7.96 (d, *J* = 8.2 Hz, 2H, BIAN-C**H**), 7.26–7.20 (m, 2H, BIAN-C**H**), 6.99 (s, 4H, Mes-C**H**), 6.64 (d, *J* = 7.1 Hz, 2H, BIAN-C**H**), 3.92 (br, 4H, cod-C**H**), 2.39 (s, 6H, Mes-C**H**$_3$), 2.32 (br, 16H, Mes-C**H**$_3$ and cod-C**H**$_2$), 1.95–1.83 (m, 4H, cod-C**H**$_2$).

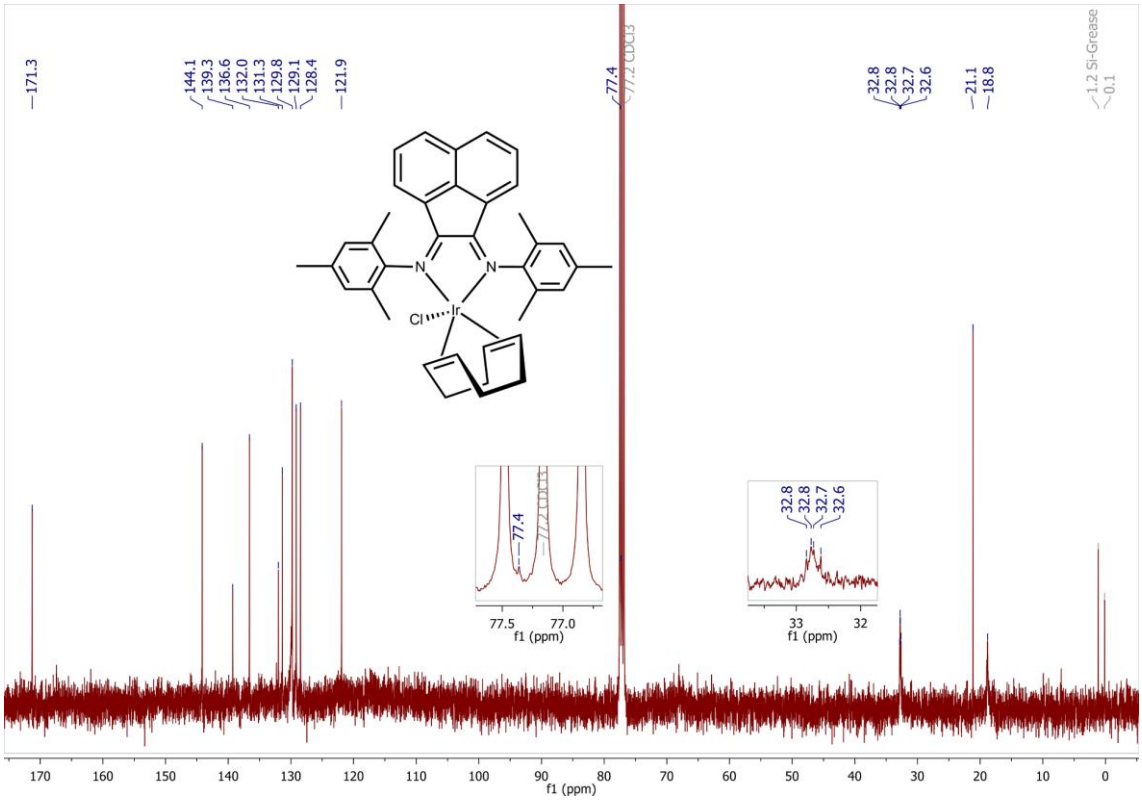

*Figure S55: ^{13}C NMR spectrum of complex **4d** in $CDCl_3$.*

^{13}C NMR (75 MHz, $CDCl_3$) δ 171.3 (BIAN-N=**C_q**), 144.1 (Mes-N-**C_q**), 139.3 (BIAN-**C_q**), 136.6, 132.0 (BIAN-**C_q**), 131.3, 129.8 (Mes-**C**H), 129.1 (BIAN-**C**H), 128.4 (BIAN-**C**H), 121.9 (BIAN-**C**H), 77.4 (cod-**C**H), 32.8, 32.8, 32.7, 32.6 (cod-**C**H_2), 21.1, 18.8 (Mes-**C**H_3).

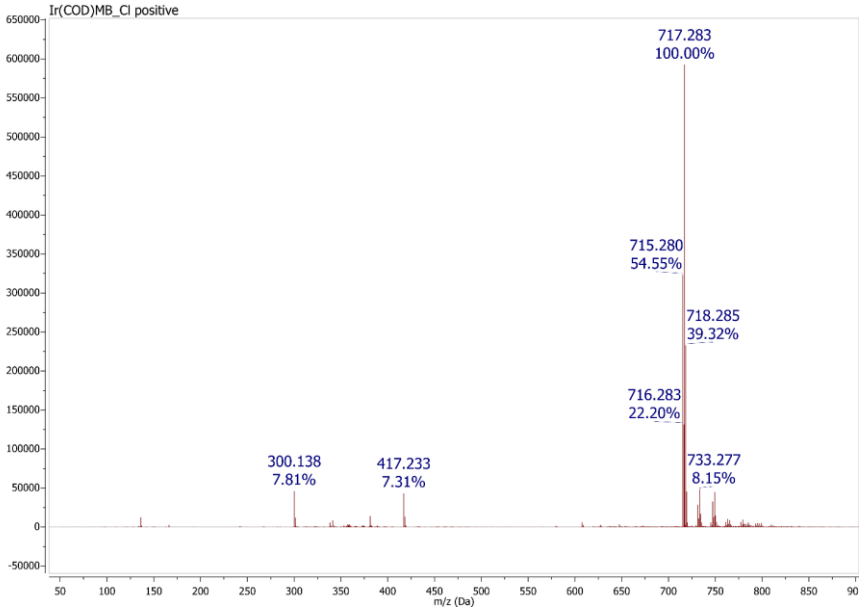

*Figure S56: Mass Spectroscopy spectrum of **4d** recorded in methanol: Positive mode, Electron Spray Ionisation.*

MS (ESI+, CH_3OH): m/z [**4d**-Cl]$^+$ calculated 717.282; found 717.283.

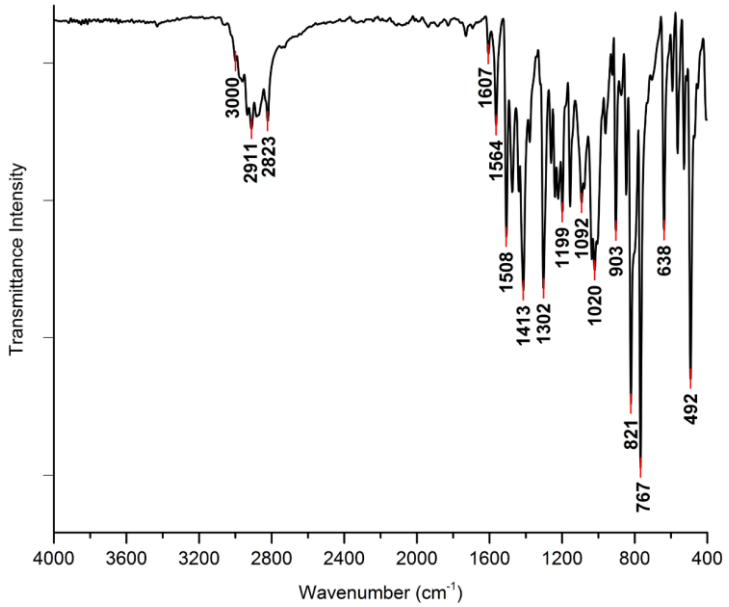

*Figure S57: Solid state infrared transmittance spectrum of **4d** recorded with a platinum-ATR module (monolithic diamond crystal window).*

IR (cm^{-1}) **ν(C=N)** 1610–1550 (m).

S2) SINGLE CRYSTAL X-RAY DIFFRACTION DATA

S2.1) Complex **1b** [RhMB(cod)]PF_6

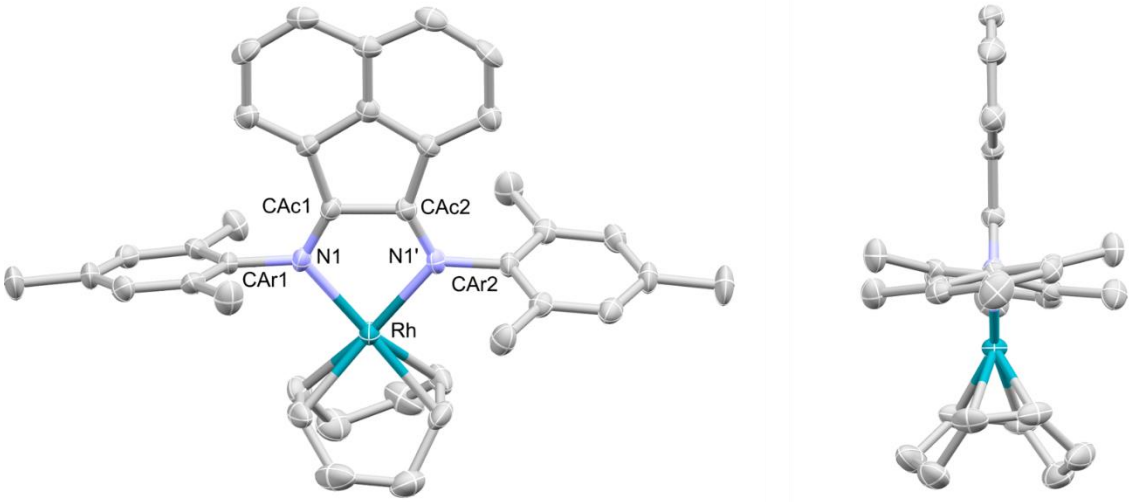

*Figure S58: The molecular structure of **1b** [RhMB(cod)]PF_6 with partial atom-numbering scheme (left), and side-on view (right), thermal ellipsoids shown at 50 % probability. Hydrogen atoms, PF_6 counterion and CH_2Cl_2 solvent molecule are omitted for clarity. The atomic lables C_{Ac1}/C_{Ac2} and C_{Ar1}/C_{Ar2} used above correspond to the symmetry-adapted atom numbers C6/C6' and C13/C13' as depicted in the cif-file.*

$C_{38.91}H_{41.82}Cl_{1.82}F_6N_2PRh$ (*M* = 849.74 g/mol): hexagonal, space group *P6₅22*, *a* = 12.2066(7) Å, *b* = 12.2066(7) Å, *c* = 43.710(3) Å, *γ* = 120°, V = 5640.3(8) Å^3, *Z* = 6, *T* = 150(2) K, μ(MoKα) = 0.687 mm^{-1}, *Dcalc* = 1.501 g/cm^3, 166775 reflections measured (4.28° ≤ 2Θ ≤ 52.742°), 3853 unique (R_{int} = 0.0575, R_{sigma} = 0.0146) which were used in all calculations. The final R_1 was 0.0442 (I > 2σ(I)) and wR_2 was 0.1059 (all data). CCDC 2161247.

Complex **1b** is accompanied by one molecule of CH_2Cl_2 in the unit cell, along with one PF_6^- counter ion.

S2.2) Complex **1d** [IrMB(cod)]PF_6

$C_{40}H_{42}Cl_6F_6IrN_2P$ (*M* = 1100.62 g/mol): monoclinic, space group *P2₁/n*, *a* = 12.0546(7) Å, *b* = 22.1106(11) Å, *c* = 15.8673(9) Å, *β* = 100.789(2)°, V = 4154.4(4) Å^3, *Z* = 4, *T* = 150(2) K, μ(MoKα) = 3.698 mm^{-1}, *Dcalc* = 1.760 g/cm^3, 25383 reflections measured (4.694° ≤ 2Θ ≤ 52.74°), 8202 unique (R_{int} = 0.0912, R_{sigma} = 0.0963) which were used in all calculations. The final R_1 was 0.0639 (I > 2σ(I)) and wR_2 was 0.1624 (all data). CCDC 2161249.

Complex **1d** is accompanied by two molecules of $CDCl_3$ in the unit cell, along with one PF_6^- counter ion.

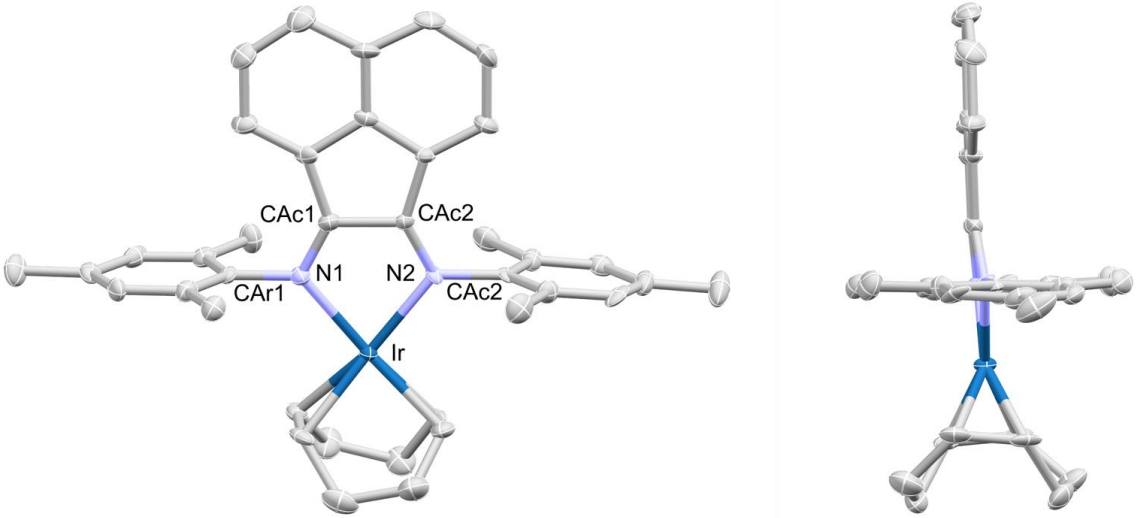

*Figure S59: The molecular structure of **1d** [IrMB(cod)]PF_6 with partial atom-numbering scheme (left), and side-on view (right), thermal ellipsoids shown at 50 % probability. Hydrogen atoms, PF_6 counterion and two $CDCl_3$ solvent molecules are omitted for clarity. The atomic lables C_{Ac1}/C_{Ac2} and C_{Ar1}/C_{Ar2} used above correspond to the atom numbers C20/C9 and C30/C21 as depicted in the cif-file.*

S2.3) Complex **2a** [RhDB$(CO)_2$]PF_6

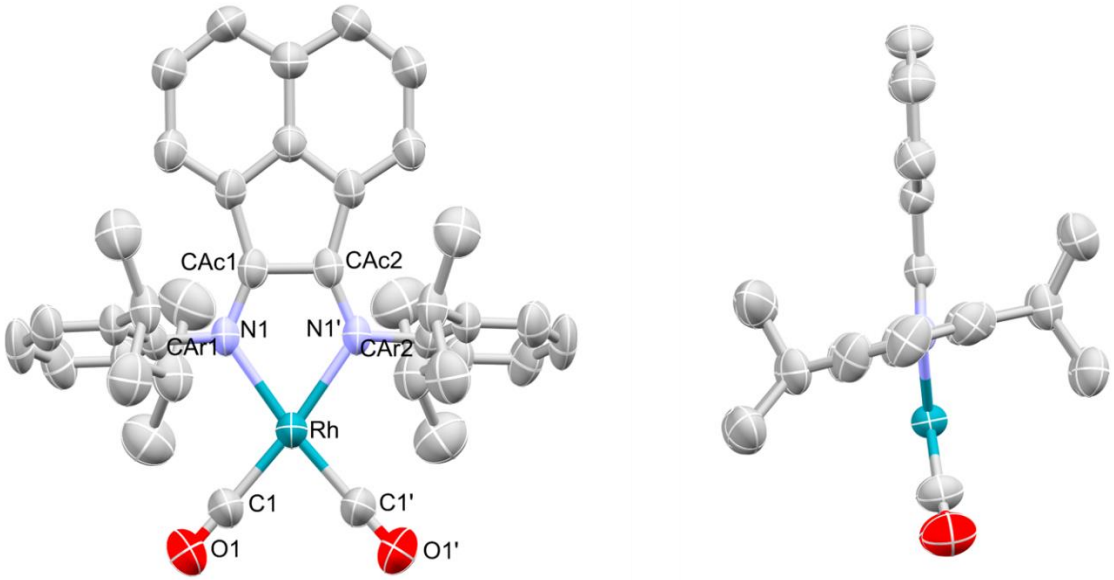

*Figure S60: The molecular structure of **2a** [RhDB$(CO)_2$]PF_6 with partial atom-numbering scheme (left), and side-on view (right), thermal ellipsoids shown at 50 % probability. Hydrogen atoms and PF_6 counterion are omitted for clarity. The atomic lables C_{Ac1}/C_{Ac2} and C_{Ar1}/C_{Ar2} used above correspond to the symmetry-adapted atom numbers C2/C2' and C9/C9' as depicted in the cif-file.*

$C_{38}H_{40}F_6N_2O_2PRh$ (*M* = 804.60 g/mol): orthorhombic, space group *Pnma*, *a* = 16.6885(3) Å, *b* = 14.9252(3) Å, *c* = 16.2846(3) Å, V = 4056.16(13) Å^3, *Z* = 4, *T* = 149.98(10) K, μ(MoKα) = 4.296 mm^{-1}, *Dcalc* = 1.318 g/cm^3, 13585 reflections measured (7.936° ≤ 2Θ ≤ 151.48°), 4009 unique (R_{int} = 0.1612, R_{sigma} = 0.0564) which were used in all calculations. The final R_1 was 0.0698 (I > 2σ(I)) and wR_2 was 0.2070 (all data). CCDC 2161246.

S2.4) Complex **2b** [RhMB(CO)$_2$]PF$_6$

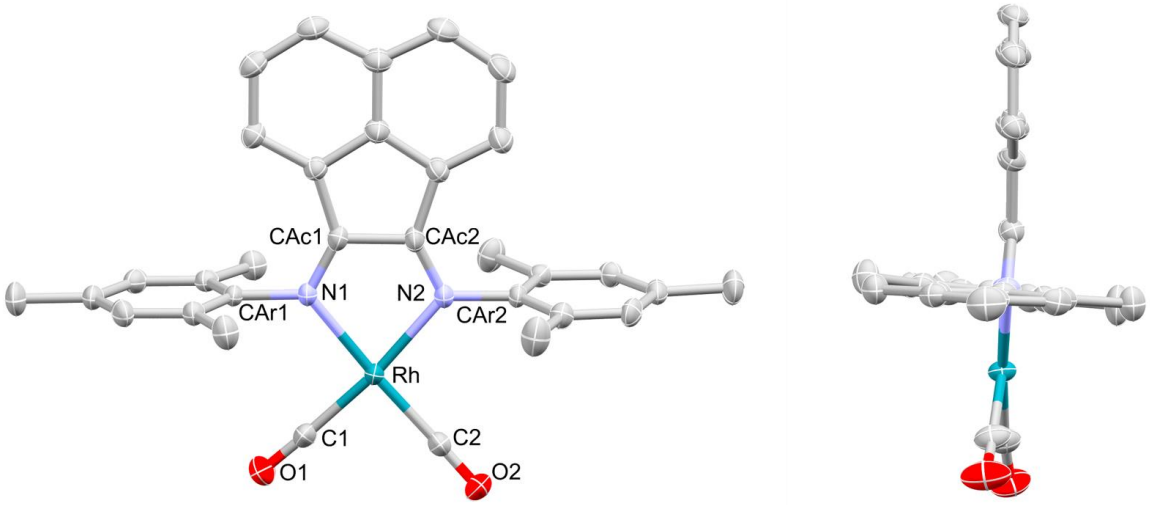

*Figure S61: The molecular structure of **2b** [RhMB(CO)$_2$]PF$_6$ with partial atom-numbering scheme (left), and side-on view (right), thermal ellipsoids shown at 50 % probability. Hydrogen atoms and PF$_6$ counterion are omitted for clarity. The atomic lables C_{Ac1}/C_{Ac2} and C_{Ar1}/C_{Ar2} used above correspond to the symmetry-adapted atom numbers C3/C14 and C15/C23 as depicted in the cif-file.*

$C_{32}H_{28}F_6N_2O_2PRh$ (*M* = 720.44 g/mol): orthorhombic, space group *Pbcn*, *a* = 25.6796(4) Å, *b* = 10.7759(2) Å, *c* = 21.8263(3) Å, V = 6039.79(17) Å^3, *Z* = 8, *T* = 150(2) K, μ(MoKα) = 0.689 mm^{-1}, *Dcalc* = 1.585 g/cm^3, 98928 reflections measured (4.1° ≤ 2Θ ≤ 52.744°), 6173 unique (R_{int} = 0.1040, R_{sigma} = 0.0344) which were used in all calculations. The final R_1 was 0.0294 (I > 2σ(I)) and wR_2 was 0.0835 (all data). CCDC 2161251.

S2.5) Complex **2c** [IrDB(CO)$_2$]PF$_6$

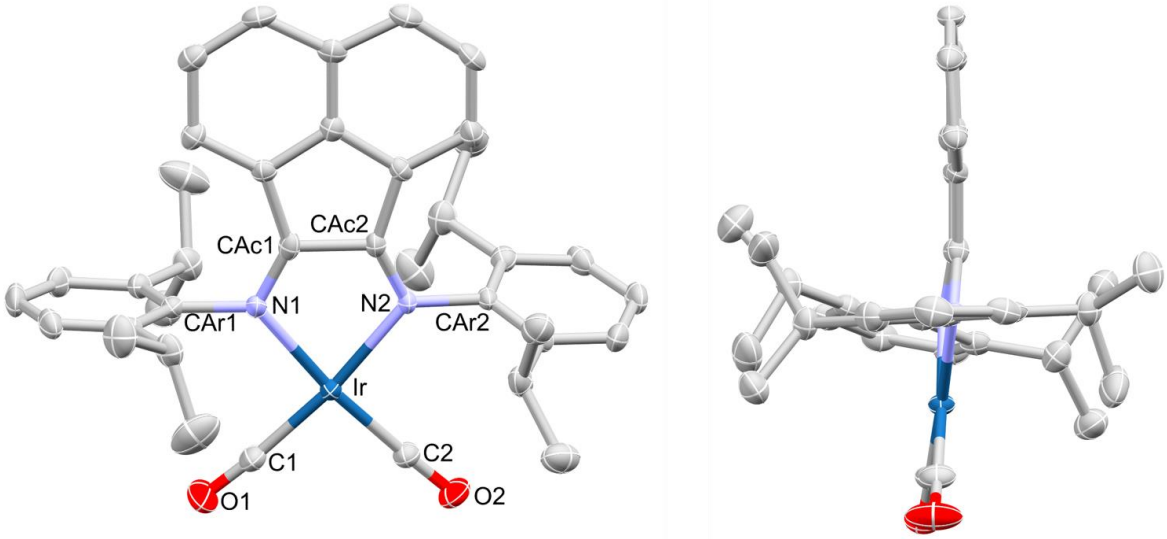

*Figure S62: The molecular structure of **2c** [IrDB(CO)$_2$]PF$_6$ with partial atom-numbering scheme (left), and side-on view (right), thermal ellipsoids shown at 50 % probability. Hydrogen atoms and PF$_6$ counterion are omitted for clarity. The atomic lables C_{Ac1}/C_{Ac2} and C_{Ar1}/C_{Ar2} used above correspond to the symmetry-adapted atom numbers C3/C14 and C15/C27 as depicted in the cif-file.*

$C_{38}H_{40}F_6IrN_2O_2P$ (*M* = 893.91 g/mol): orthorhombic, space group $P2_12_12_1$, *a* = 12.5684(2) Å, *b* = 12.6901(2) Å, *c* = 22.7161(3) Å, V = 3623.09(9) Å^3, *Z* = 4, *T* = 149.98(10) K, μ(MoKα) = 3.796 mm^{-1}, *Dcalc* = 1.639 g/cm^3, 74771 reflections measured (3.74° ≤ 2Θ ≤ 62.522°), 7400 unique (R_{int} = 0.0731, R_{sigma} = 0.0319) which were used in all calculations. The final R_1 was 0.0200 (I > 2σ(I)) and wR_2 was 0.0459 (all data). CCDC 2161248.

S2.6) Complex **3a** [RhDB(CO)(PEt$_3$)]PF$_6$

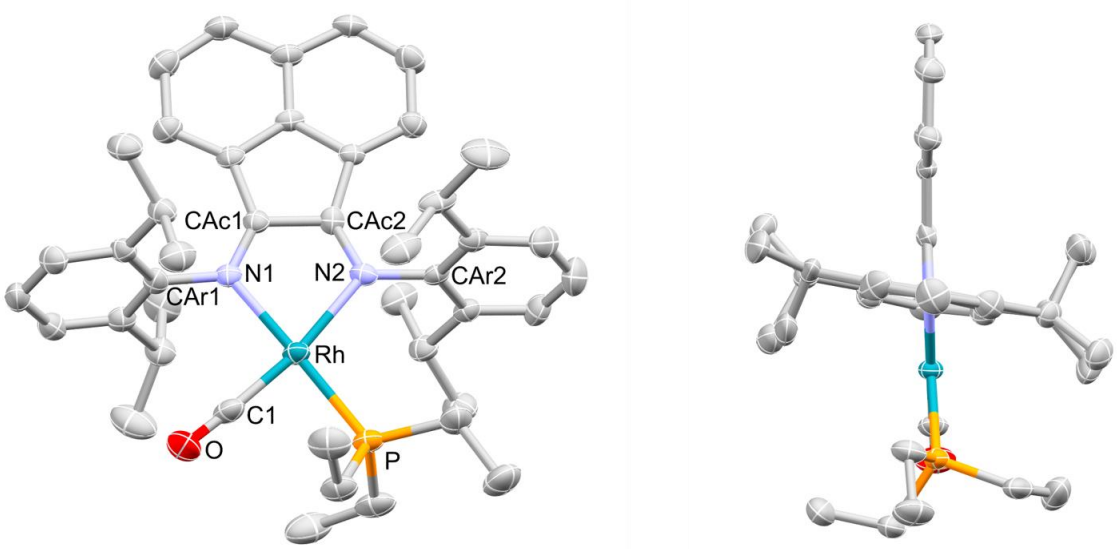

*Figure S63: The molecular structure of **3a** [RhDB(CO)(PEt$_3$)]PF$_6$ with partial atom-numbering scheme (left), and side-on view (right), thermal ellipsoids shown at 50 % probability. Hydrogen atoms and PF$_6$ counterion are omitted for clarity. The atomic lables C_{Ac1}/C_{Ac2} and C_{Ar1}/C_{Ar2} used above correspond to the symmetry-adapted atom numbers C2/C13 and C14/C26 as depicted in the cif-file.*

$C_{43}H_{55}F_6N_2OP_2Rh$ (*M* = 894.74 g/mol): orthorhombic, space group *Pbca*, *a* = 17.3549(15) Å, *b* = 15.2081(15) Å, *c* = 33.675(3) Å, V = 8888.0(14) Å^3, *Z* = 8, *T* = 150(2) K, μ(MoKα) = 0.515 mm^{-1}, *Dcalc* = 1.337 g/cm^3, 546214 reflections measured (5.08° ≤ 2Θ ≤ 52.76°), 9113 unique (R_{int} = 0.0650, R_{sigma} = 0.0128) which were used in all calculations. The final R_1 was 0.0647 (I > 2σ(I)) and wR_2 was 0.1446 (all data). CCDC 2161252.

S2.7) Complex **4c** [IrDB(cod)Cl]

$C_{44}H_{52}ClIrN_2$ (*M* = 836.55 g/mol): orthorhombic, space group *Pnma*, *a* = 18.6186(3) Å, *b* = 19.3903(3) Å, *c* = 10.2238(2) Å, V = 3691.00(11) Å^3, *Z* = 4, *T* = 149.99(10) K, μ(MoKα) = 3.723 mm^{-1}, *Dcalc* = 1.505 g/cm^3, 60960 reflections measured (4.202° ≤ 2Θ ≤ 52.74°), 3889 unique (R_{int} = 0.0804, R_{sigma} = 0.0282) which were used in all calculations. The final R_1 was 0.0250 (I > 2σ(I)) and wR_2 was 0.0622 (all data). CCDC 2161250.

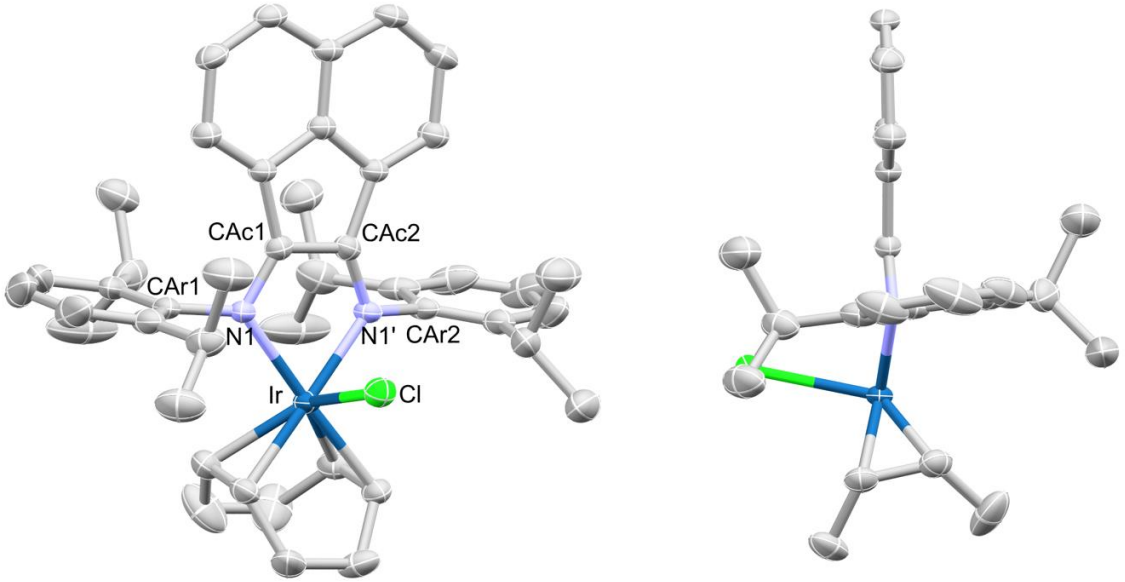

*Figure S64: The molecular structure of **4c** [IrDB(cod)Cl] with partial atom-numbering scheme (left), and side-on view (right), thermal ellipsoids shown at 50 % probability. Hydrogen atoms are omitted for clarity. The atomic lables C_{Ac1}/C_{Ac2} and C_{Ar1}/C_{Ar2} used above correspond to the symmetry-adapted atom numbers C5/C5' and C12/C12' as depicted in the cif-file.*

S2.8) General Notes

The two Dipp-substituents of **2a** are co-planar with one another (0.91°) but slanted away from the acenaphthalene plane by 13.3° from the orthogonal (Fig S60), partially shielding the back of the coordination sphere with the two isopropyl groups in close proximity to each other. The aryl substituents of complexes **1d** (Fig S59), **2b** (Fig S61), **3a** (Fig S63) and **4c** (Fig S64) are nearly co-planar as well (7.31°, 5.18°, 7.30° and 5.27° respectively), but do not deviate from orthogonality with the acenaphthalene plane as much as **2a**. The aryl substituents of **1b** (Fig S58) and **2c** (Fig S62) show the largest degree of rotation relative to one another (23.97° and 17.41° respectively). The Mes-substituents of **1b** are equivalently slanted away from the acenaphthalene plane (10.4°), the dihedral of the two Dipp-substituents of **2c** are markedly different – the C_{Ar1}–substituent being orthogonal to the acenaphthalene plane whereas the C_{Ar2}–substituent is slanted by 14.6°.

The coordination centre of **2a** displays an almost rectangular geometry due to the small bite angle enforced by coordination to the rigid bisimine ligand (N1–Rh–N1' 69.4(2)°) as well as the small angle between the two carbonyl ligands (C1–Rh–C1' 80.8(4)°). This, in turn, impacts the planarity of the coordination sphere as illustrated by the angle between the bisimine nitrogens and their *trans* carbonyl carbons (173.9(2)°). The dorsal coordination sites of **2a** are partially shrouded by the close proximity of the two isopropyl groups on the near co-planar Dipp-substituents (0.91°), that are pitched away from the acenaphthalene plane (*ca*. 13.3°). A number of aryl-aryl, and alkyl-alkyl C–C bond lengths in the ligand also show a *ca*. 0.1 Å deviation from values previously reported for similar

compounds [1–4]. These distortions are likely the result of steric constraints imposed on the bulky Dipp-substituents by crystal packing effects, as the unit cell parameters of **2a** still compare relatively well with those of the other reported structures. While the magnitude of the angular distortions in **2b** is less pronounced than in **2a**, it should be noted that the two carbonyl ligands are not repositioned equivalently around the coordination sphere as seen by the –7.3(4)° dihedral angle between the two carbonyls.

The Rh–C bonds in **2a** (1.897(6) Å) are slightly longer than those in both **2b** and **3a** (av. 1.873(2) and 1.814(6) Å respectively). The Rh–C bond lengths of **2a**–**b** are within the value range for various literature reported Rh(I) dicarbonyl complexes [5–7]. The two carbonyl ligands in **2c** show slightly different Ir–C bond lengths (Ir–C1 1.873(5) and Ir–C2 1.861(4) Å), and bond angles (O1–C1–Ir 175.8(4)° and O2–C2–Ir 177.9(4)°) indicating a distortion of the coordination sphere to adapt to the steric demands of twisted C_{Ar2} Dipp-substituent. The Ir–C bond lengths are at the upper limit of values previously reported for similar iridium dicarbonyl-bisimine complexes [7,8]. The Rh–P bond length (2.3053(13) Å) is slightly shorter than comparable cationic pentacoordinate Rh(I)-diimine complexes featuring phosphine co-ligands, but still within the known range of previously reported Rh–P bond lengths [9–12].

S2.9) Crystallographic Data

Table S1: Selected bond lengths (Å) from XRD data. M=Metal; Ac = Acenaphthalene imine carbon; Ar = Aromatic substituent carbon, i.e. Dipp or Mes; L = ancillary ligand. † Half of molecule is present in asymmetric unit, therefore selected bond lengths and angles are duplicated in the complex structure. ‡ Imine-N trans of PEt_3.

Complex	M–N	N–C_{Ac}	N–C_{Ar}	C_{Ac}–C_{Ac}	Miscellaneous
1b	Rh–N 2.100(4)†	N–C_{Ac} 1.276(7)†	N–C_{Ar} 1.445(6)†	C_{Ac1}–C_{Ac2} 1.492(10)	
1d	Ir–N_1 2.100(7) Ir–N_2 2.097(7)	N_1–C_{Ac1} 1.291(11) N_2–C_{Ac2} 1.280(11)	N_1–C_{Ar1} 1.451(11) N_2–C_{Ar2} 1.456(11)	C_{Ac2}–C_{Ac1} 1.495(13)	
2a	Rh–N 2.135(4)†	N–C_{Ac} 1.350(6)†	N–C_{Ar} 1.328(5)†	C_{Ac2}–C_{Ac1} 1.381(9)	Rh–C 1.897(6)† C–O 1.104(7)†
2b	Rh–N_1 2.0728(17) Rh–N_2 2.0898(16)	N_1–C_{Ac1} 1.285(3) N_2–C_{Ac2} 1.289(2)	N_1–C_{Ar1} 1.450(2) N_2–C_{Ar2} 1.451(2)	C_{Ac1}–C_{Ac2} 1.501(3)	Rh–C_1 1.871(2) C_1–O_1 1.124(3) Rh–C_2 1.875(2) C_2–O_2 1.129(3)
2c	Ir–N_1 2.082(3) Ir–N_2 2.083(3)	N_1–C_{Ac1} 1.279(5) N_2–C_{Ac2} 1.277(5)	N_1–C_{Ar1} 1.452(5) N_2–C_{Ar2} 1.455(5)	C_{Ac1}–C_{Ac2} 1.500(5)	Ir–C_1 1.873(5) C_1–O_1 1.124(6) Ir–C_2 1.861(4) C_2–O_2 1.134(5)
3a	Rh–N_1 2.3053(13)‡ Rh–N_2 2.163(4)	N_1–C_{Ac1} 1.278(6) N_2–C_{Ac2} 1.289(6)	N_1–C_{Ar1} 1.443(6) N_2–C_{Ar2} 1.434(6)	C_{Ac1}–C_{Ac2} 1.495(6)	Rh–P 2.3053(13) Rh–C_1 1.814(6) C_1–O 1.155(7)
4c	Ir–N 2.096(2)†	N–C_{Ac} 1.321(4)†	N–C_{Ar} 1.443(4)†	C_{Ac1}–C_{Ac2} 1.447(6)	Ir–Cl 2.4754(11)

Table S2: Selected bond angles (°) from XRD data. M=Metal; Ac = Acenaphthalene imine carbon; Ar = Aromatic substituent carbon, i.e. Dipp or Mes; L = ancillary ligand. † Half of molecule is present in asymmetric unit, therefore selected bond lengths and angles are duplicated in the complex structure.

Complex	N–M–N	N–M–L	L–M–L	Ar–N–Ac	N–Ac–Ac	Miscellaneous
1b	78.9(2)			C_{Ac1}–N_1–C_{Ar1} 120.6(5)†	N_1–C_{Ac1}–C_{Ac2} 117.5(3)†	
1d	78.8(3)			C_{Ac1}–N_1–C_{Ar1} 118.9(7) C_{Ac2}–N_2–C_{Ar2} 120.3(7)	N_1–C_{Ac1}–C_{Ac2} 117.4(8) N_2–C_{Ac2}–C_{Ac1} 116.7(8)	
2a	69.4(2)	C_1–Rh–N_1 104.9(2)† C_1–Rh–N_1′ 173.9(2)†	C_1–Rh–C_2 80.8(4)	C_{Ar1}–N_1–C_{Ac1} 116.0(4)†	N_1–C_{Ac1}–C_{Ac2} 112.9(2)†	O_1–C_1–Rh 177.6(7)†
2b	79.78(6)	C_1–Rh–N_1 94.31(8) C_1–Rh–N_2 172.50(8) C_2–Rh–N_1 174.17(8) C_2–Rh–N_2 96.35(8)	C_1–Rh–C_2 89.89(8)	C_{Ac1}–N_1–C_{Ar1} 119.84(16) C_{Ac2}–N_2–C_{Ar2} 118.96(17)	N_1–C_{Ac1}–C_{Ac2} 116.96(17) N_2–C_{Ac2}–C_{Ac1} 117.04(17)	O_1–C_1–Rh 177.9(2) O_2–C_2–Rh 175.6(2)
2c	78.47(13)	C_1–Ir–N_1 94.74(17) C_1–Ir–N_2 172.92(17) C_2–Ir–N_1 173.47(15) C_2–Ir–N_2 95.07(16)	C_2–Ir–C_1 91.69(19)	C_{Ac1}–N_1–C_{Ar1} 118.9(3) C_{Ac2}–N_2–C_{Ar2} 120.6(3)	N_1–C_{Ac1}–C_{Ac2} 116.5(4) N_2–C_{Ac2}–C_{Ac1} 116.1(4)	O_1–C_1–Ir 175.8(4) O_2–C_2–Ir 177.9(4)
3a	77.30(15)	C_1–Rh–N_1 93.53(19) C_1–Rh–N_2 170.76(19) N_2–Rh–P 103.90(11) N_1–Rh–P 178.38(11)	C_1–Rh–P 85.24(16)	C_{Ac1}–N_1–C_{Ar1} 121.1(4) C_{Ac2}–N_2–C_{Ar2} 118.1(4)	N_1–C_{Ac1}–C_{Ac2} 117.3(4) N_2–C_{Ac2}–C_{Ac1} 117.1(4)	O–C_1–Rh 176.9(5)
4c	78.49(13)	N_1–Ir–Cl 88.32(6)†		C_{Ac1}–N_1–C_{Ar1} 116.8(2)†	N_1–C_{Ac1}–C_{Ac2} 117.14(16)†	Cl–Ir–Ac_{plane} 79.66

Table S3: Selected dihedral angles (°) from XRD data. M=Metal; Ac = Acenaphthalene imine carbon; Ar = Aromatic substituent carbon, i.e. Dipp or Mes; L = ancillary ligand.

Complex	$N–C_{Ac1}–C_{Ac2}–N$	$M–N–C_{Ac1}–C_{Ac2}$	Miscellaneous
1b	–3.0(8)	$Rh–N_1–C_{Ac1}–C_{Ac2}$ 2.2(8) $Rh–N_1'–C_{Ac2}–C_{Ac1}$ –2.2(8)	$Mes_{plane1}–Mes_{plane2}$ 23.97 $Ac_{plane}–Mes_{plane1(CAr1)}$ 79.62 $Ac_{plane}–Mes_{plane2(CAr2)}$ 79.62
1d	2.6(12)	$Ir–N_1–C_{Ac1}–C_{Ac2}$ 2.6(10) $Ir–N_2–C_{Ac2}–C_{Ac1}$ –6.4(10)	$Mes_{plane1}–Mes_{plane2}$ 7.31 $Ac_{plane}–Mes_{plane1(CAr1)}$ 89.60 $Ac_{plane}–Mes_{plane2(CAr2)}$ 87.62
2a	0.0(6)	$Rh–N_1'–C_{Ac2}–C_{Ac1}$ 4.3(4) $Rh–N_1–C_{Ac1}–C_{Ac2}$ –4.3(4)	$O_1–C_1–C_1'–O_1'$ 0.0(1) $Dipp_{plane1}–Dipp_{plane2}$ 0.91 $Ac_{plane}–Dipp_{plane1(CAr1)}$ 76.69 $Ac_{plane}–Dipp_{plane2(CAr2)}$ 76.69
2b	0.4(3)	$Rh–N_1–C_{Ac1}–C_{Ac2}$ 1.5(2) $Rh–N_2–C_{Ac2}–C_{Ac1}$ –2.0(2)	$O_1–C_1–C_2–O_2$ –7.3(4) $Mes_{plane1}–Mes_{plane2}$ 5.18 $Ac_{plane}–Mes_{plane1(CAr1)}$ 87.49 $Ac_{plane}–Mes_{plane2(CAr2)}$ 84.12
2c	2.7(6)	$Ir–N_1–C_{Ac1}–C_{Ac2}$ 0.6(5) $Ir–N_2–C_{Ac2}–C_{Ac1}$ –4.5(5)	$O_1–C_1–C_2–O_2$ –0.7(9) $Dipp_{plane1}–Dipp_{plane2}$ 17.41 $Ac_{plane}–Dipp_{plane(CAr1)}$ 89.34 $Ac_{plane}–Dipp_{plane(CAr2)}$ 75.36
3a	0.2(7)	$Rh–N_1–C_{Ac1}–C_{Ac2}$ –0.2(5) $Rh–N_2–C_{Ac2}–C_{Ac1}$ –0.1(5)	$Dipp_{plane1}–Dipp_{plane2}$ 7.30 $Ac_{plane}–Dipp_{plane1(CO side)}$ 82.04 $Ac_{plane}–Dipp_{plane2(PEt3 side)}$ 81.52
4c	0.0(4)	$Ir–N_1–C_{Ac1}–C_{Ac2}$ 12.12(9) $Ir–N_1'–C_{Ac2}–C_{Ac1}$ –12.12(9)	$Dipp_{plane1}–Dipp_{plane2}$ 5.27 $Ac_{plane}–Dipp_{plane1(CAr1)}$ 83.32 $Ac_{plane}–Dipp_{plane2(CAr2)}$ 83.32

S3) ELECTROCHEMISTRY (CYCLIC VOLTAMMETRY & DIFFERENTIAL PULSE VOLTAMMETRY)

Cyclic voltammograms were recorded between –2.0 and +1.8 V and scan rate of 100 mV s^{-1}. Differential pulse voltammograms were recorded from 0.0 to –2.0 V and 0.0 to +1.8 V, with a step potential of 5 mV, modulation amplitude of 25mV, modulation time of 0.05 s, and interval of 0.5 s. All measurements were made using a three-electrode cell with a platinum wire counter electrode, glassy carbon working electrode (5.0 mm diameter) and silver wire quasi-reference electrode. Sample solutions were prepared using 1.0 mM analyte concentration, 0.1 M tetrabutylammonium hexafluorophosphate ($TBAPF_6$) supporting electrolyte in HPLC grade CH_2Cl_2, deoxygenated with Ar (g) before starting analyses. All potentials from the cyclic voltammograms (CVs) and differential pulse voltammograms (DPVs) are reported relative to the silver wire pseudo-reference electrode, as reactivity and resultant shift of both analyte and internal standard peak potentials with ferrocene-based internal standards precluded their use.

S3.1) DippBIAN; 1,2-bis[(2,6-diisopropylphenyl)imino]acenaphthalene (DB)

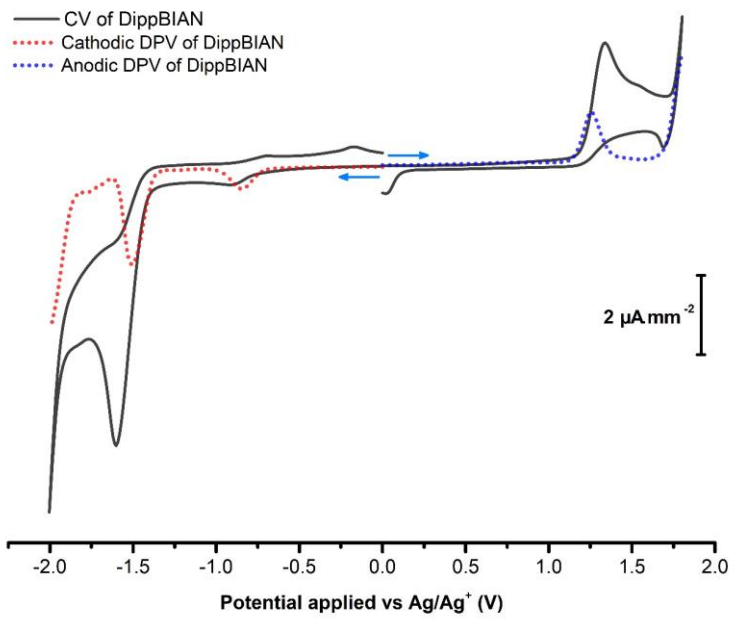

*Figure S65: CV and DPV of **DippBIAN**, recorded in CH_2Cl_2 with 1.0 mM analyte and 0.1 M $TBAPF_6$ supporting electrolyte.*

S3.2) MesBIAN; 1,2-bis[(2,4,6-trimethylphenyl)imino]acenaphthalene (MB)

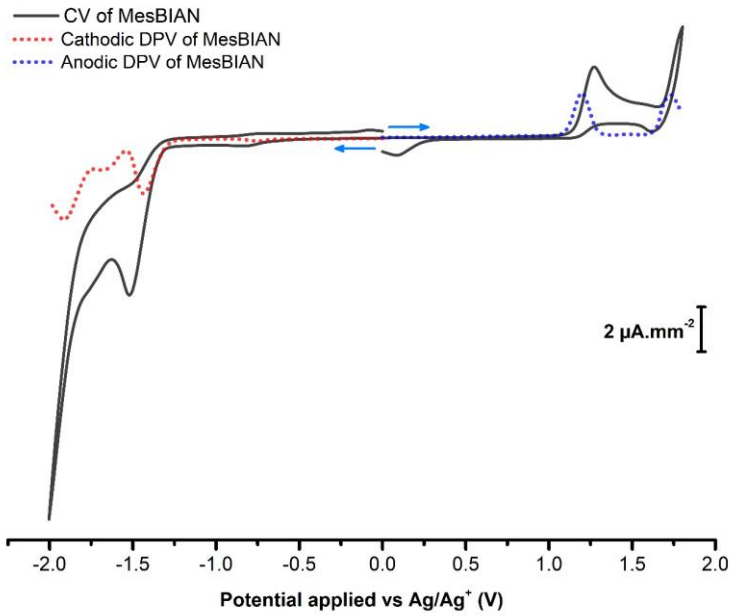

*Figure S66: CV and DPV of **MesBIAN**, recorded in CH_2Cl_2 with 1.0 mM analyte and 0.1 M $TBAPF_6$ supporting electrolyte.*

S3.3) Complex **1b** [RhMB(cod)]PF_6

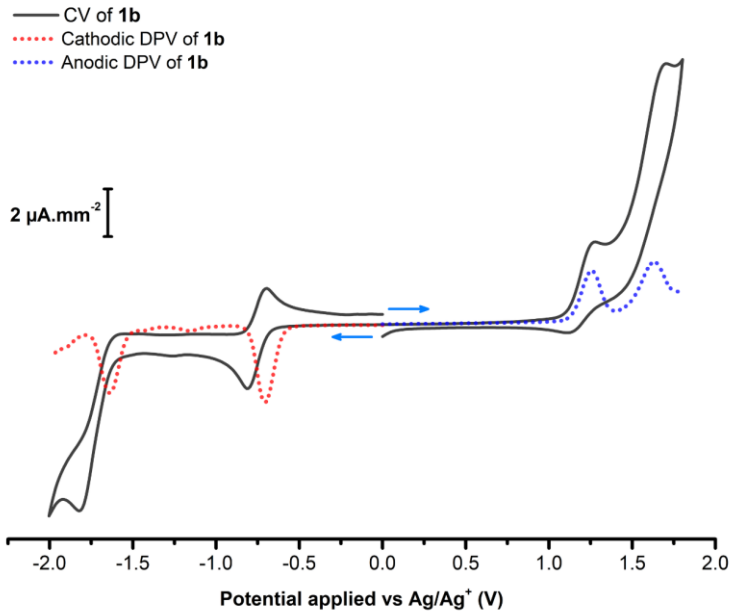

*Figure S67: CV and DPV of **1b** [RhMB(cod)]PF_6 recorded in CH_2Cl_2 with 1.0 mM analyte and 0.1 M $TBAPF_6$ supporting electrolyte.*

S3.4) Complex **1c** [IrDB(cod)]PF_6

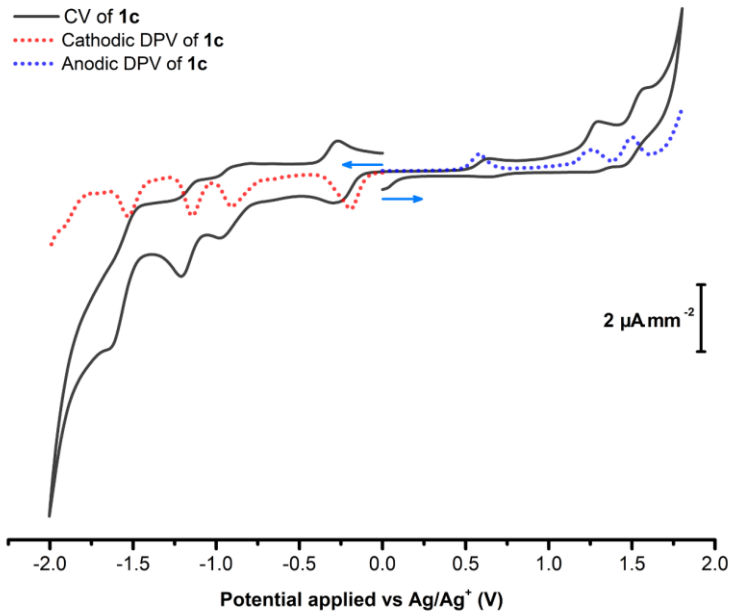

*Figure S68: CV and DPV of **1c** [IrDB(cod)]PF_6 recorded in CH_2Cl_2 with 1.0 mM analyte and 0.1 M $TBAPF_6$ supporting electrolyte.*

S3.5) Complex **1d** [IrMB(cod)]PF_6

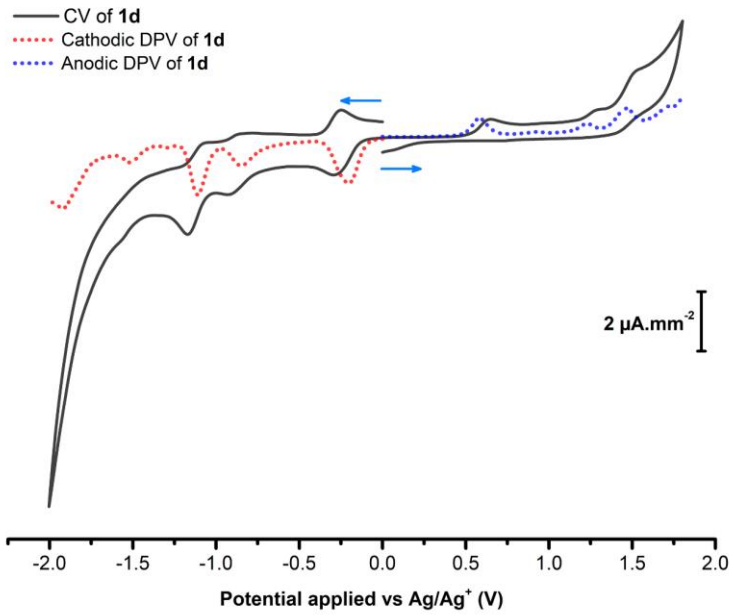

*Figure S69: CV and DPV of **1d** [IrMB(cod)]PF_6 recorded in CH_2Cl_2 with 1.0 mM analyte and 0.1 M $TBAPF_6$ supporting electrolyte.*

S3.6) Complex **2a** $[RhDB(CO)_2]PF_6$

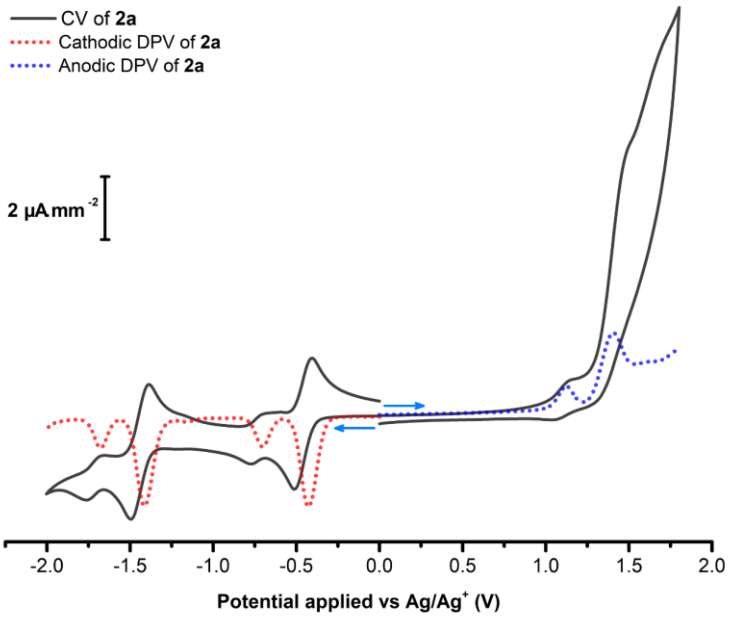

*Figure S70: CV and DPV of **2a** $[RhDB(CO)_2]PF_6$ recorded in CH_2Cl_2 with 1.0 mM analyte and 0.1 M $TBAPF_6$ supporting electrolyte.*

S3.7) Complex **2b** $[RhMB(CO)_2]PF_6$

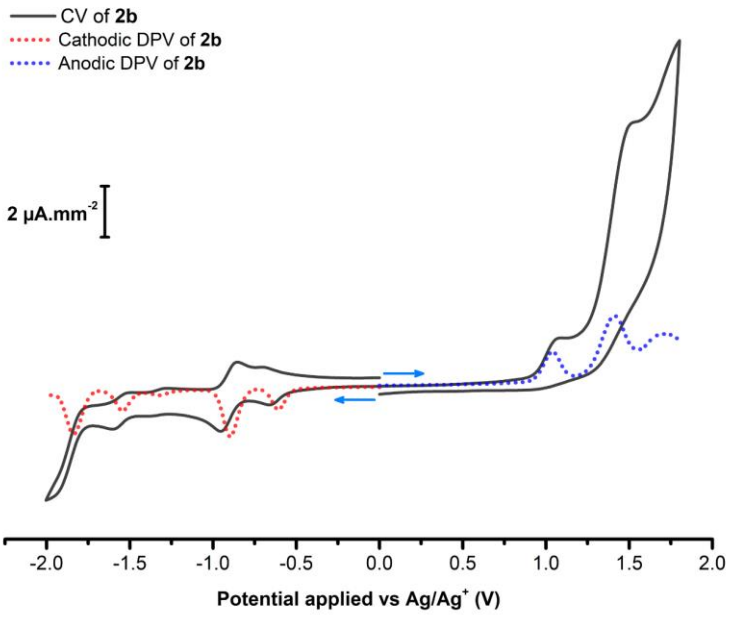

*Figure S71: CV and DPV of **2b** $[RhMB(CO)_2]PF_6$ recorded in CH_2Cl_2 with 1.0 mM analyte and 0.1 M $TBAPF_6$ supporting electrolyte.*

S3.8) Complex **2c** [IrDB(CO)$_2$]PF$_6$

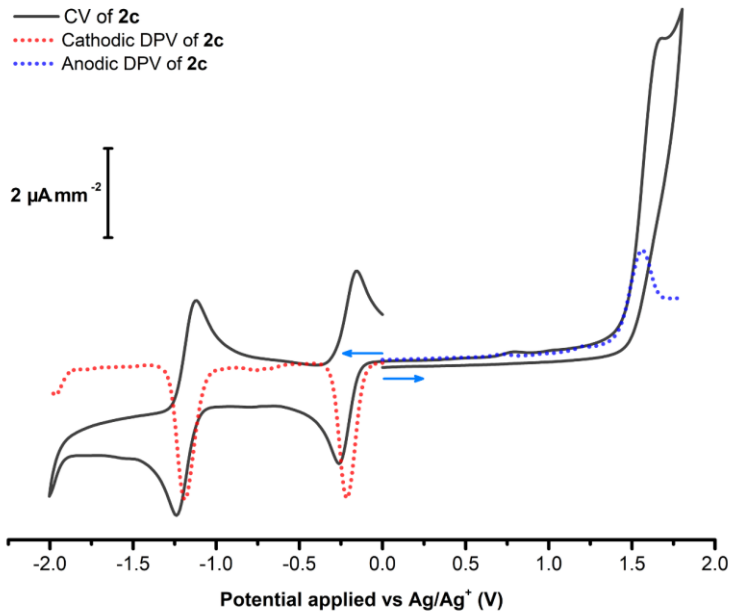

*Figure S72: CV and DPV of **2c** [IrDB(CO)$_2$]PF$_6$ recorded in CH_2Cl_2 with 1.0 mM analyte and 0.1 M TBAPF$_6$ supporting electrolyte.*

S3.9) Complex **3b** [RhMB(CO)(PEt$_3$)]PF$_6$

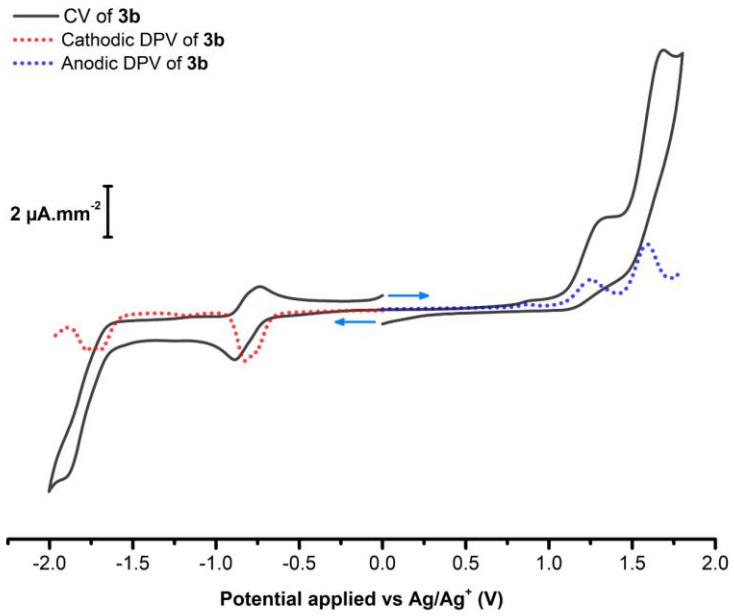

*Figure S73: CV and DPV of **3b** [RhMB(CO)(PEt$_3$)]PF$_6$ recorded in CH_2Cl_2 with 1.0 mM analyte and 0.1 M TBAPF$_6$ supporting electrolyte.*

S3.10) Complex **4b** [RhMB(cod)Cl]

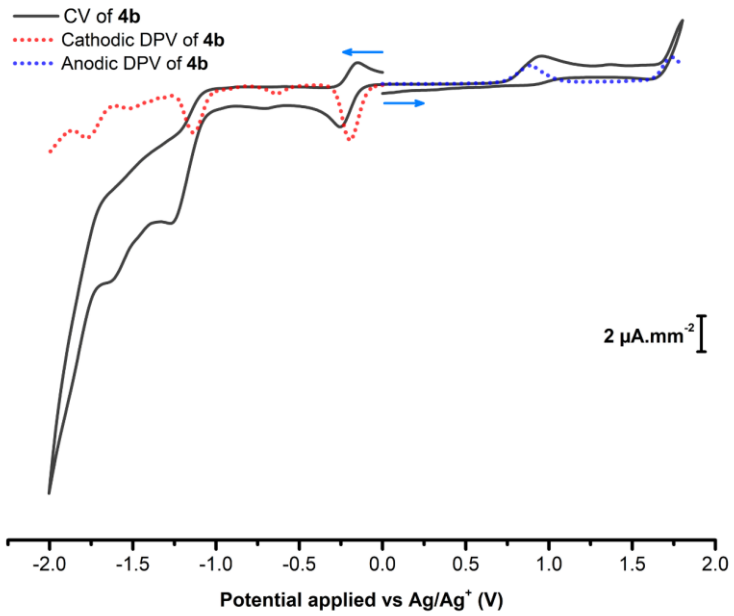

*Figure S74: CV and DPV of **4b** [RhMB(cod)Cl] recorded in CH_2Cl_2 with 1.0 mM analyte and 0.1 M $TBAPF_6$ supporting electrolyte.*

S3.11) Complex **4d** [IrMB(cod)Cl]

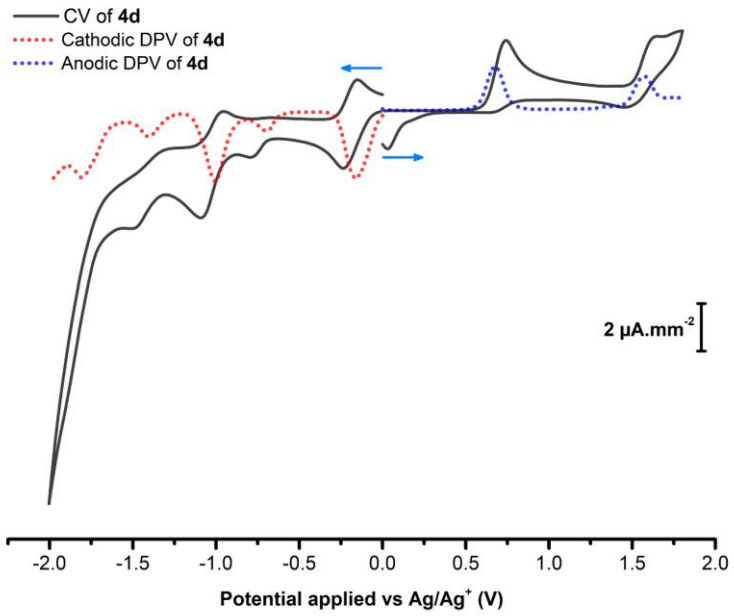

*Figure S75: CV and DPV of **4d** [IrMB(cod)Cl] recorded in CH_2Cl_2 with 1.0 mM analyte and 0.1 M $TBAPF_6$ supporting electrolyte.*

S4) ELECTROCHEMICAL CO_2 REACTIVITY SCREENING (CYCLIC VOLTAMMETRY & DIFFERENTIAL PULSE VOLTAMMETRY)

S4.1) Complex **1b** [RhMB(cod)]PF_6

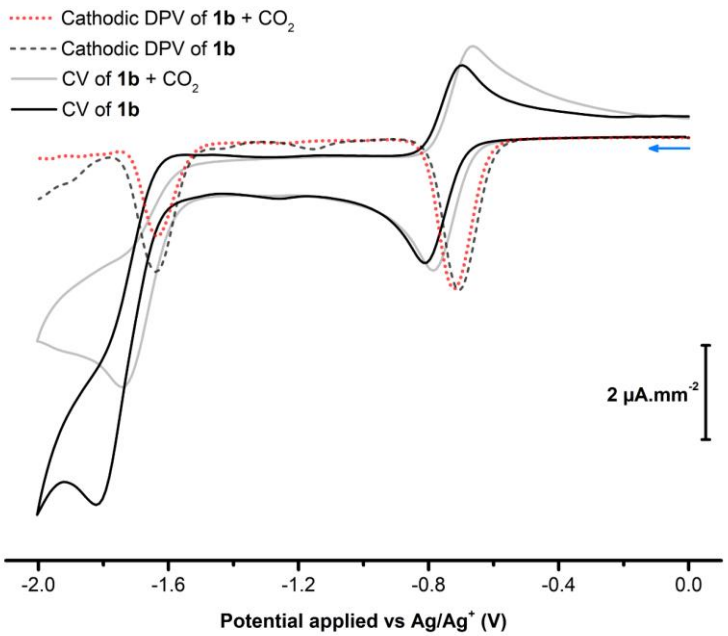

*Figure S76: CV and DPV of **1b** [RhMB(cod)]PF_6 in the presence of CO_2 or Ar, recorded in CH_2Cl_2 with 1.0 mM analyte and 0.1 M $TBAPF_6$ supporting electrolyte.*

S4.2) Complex **1c** [IrDB(cod)]PF_6

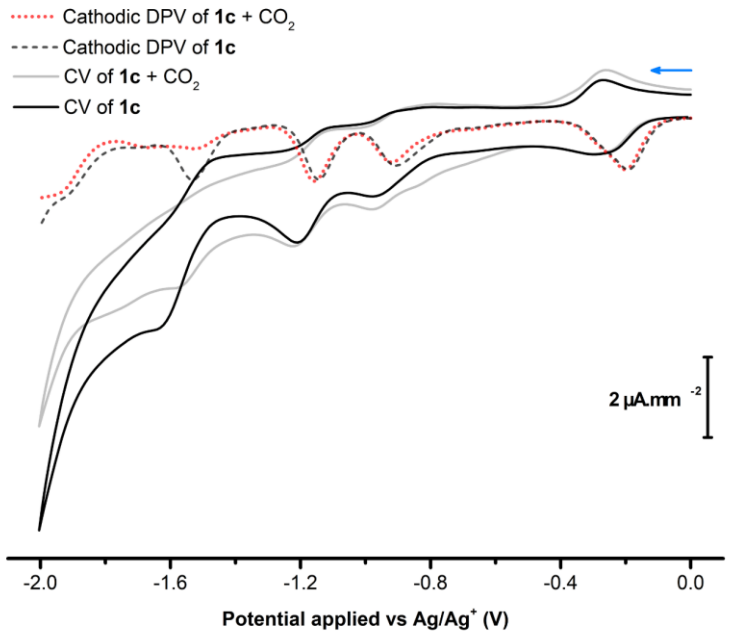

*Figure S77: CV and DPV of **1c** [IrDB(cod)]PF_6 in the presence of CO_2 or Ar, recorded in CH_2Cl_2 with 1.0 mM analyte and 0.1 M $TBAPF_6$ supporting electrolyte.*

S4.3) Complex **1d** [IrMB(cod)]PF_6

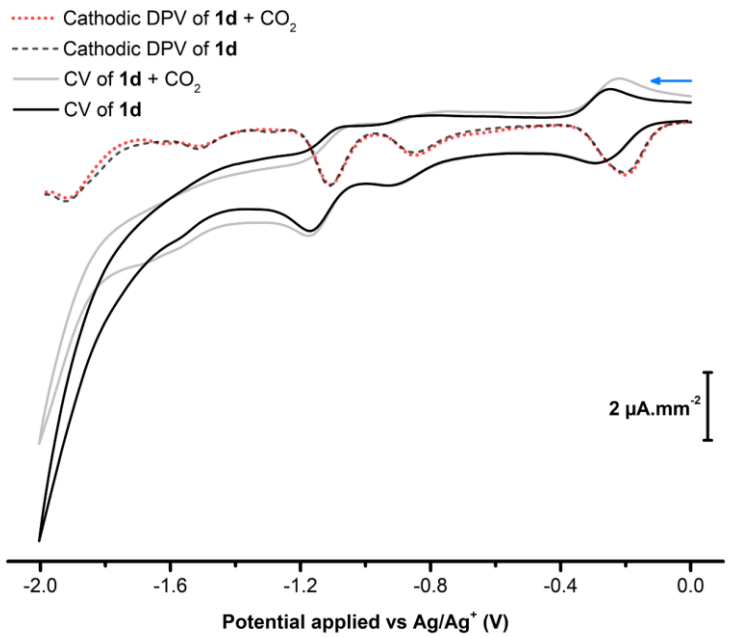

*Figure S78: CV and DPV of **1d** [IrMB(cod)]PF_6 in the presence of CO_2 or Ar, recorded in CH_2Cl_2 with 1.0 mM analyte and 0.1 M $TBAPF_6$ supporting electrolyte.*

S4.4) Complex **2a** $[RhDB(CO)_2]PF_6$

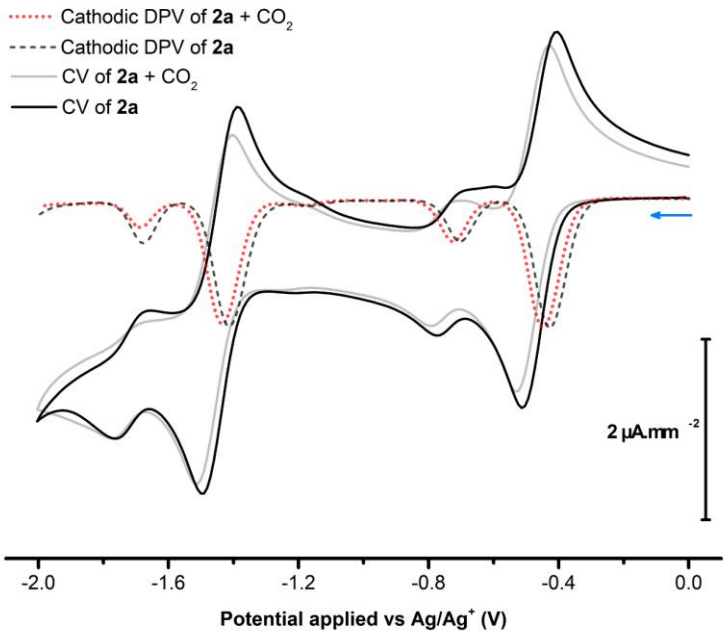

*Figure S79: CV and DPV of **2a** $[RhDB(CO)_2]PF_6$ in the presence of CO_2 or Ar, recorded in CH_2Cl_2 with 1.0 mM analyte and 0.1 M $TBAPF_6$ supporting electrolyte.*

S4.5) Complex **2b** $[RhMB(CO)_2]PF_6$

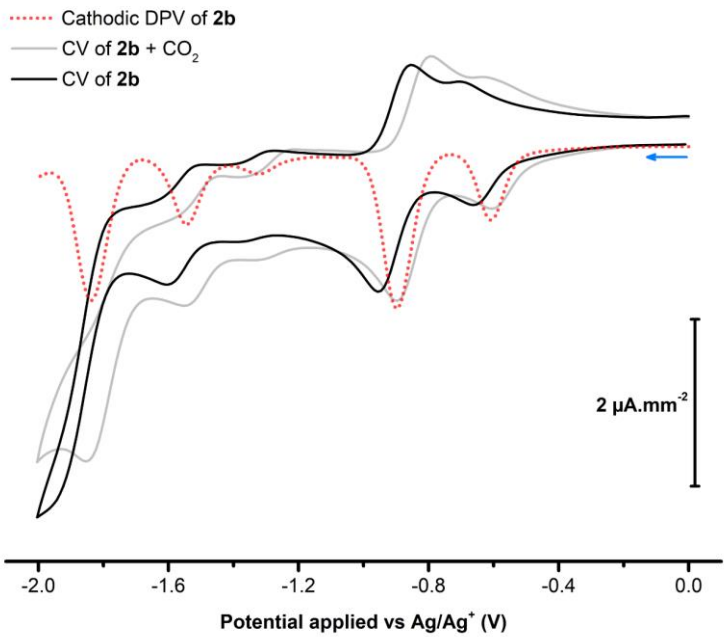

*Figure S80: CV and DPV of **2b** $[RhMB(CO)_2]PF_6$ in the presence of CO_2 or Ar, recorded in CH_2Cl_2 with 1.0 mM analyte and 0.1 M $TBAPF_6$ supporting electrolyte.*

S4.6) Complex **2c** $[IrDB(CO)_2]PF_6$

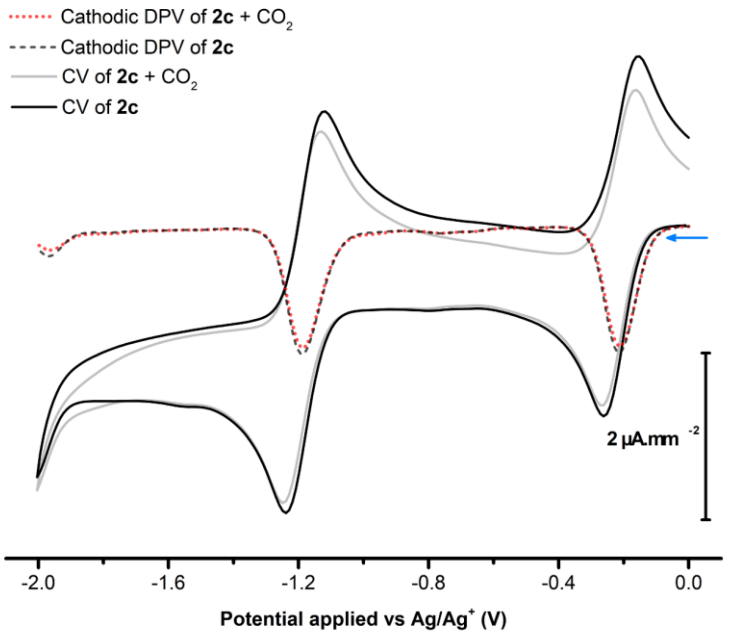

*Figure S81: CV and DPV of **2c** $[IrDB(CO)_2]PF_6$ in the presence of CO_2 or Ar, recorded in CH_2Cl_2 with 1.0 mM analyte and 0.1 M $TBAPF_6$ supporting electrolyte.*

S4.7) Complex **3b** $[RhMB(CO)(PEt_3)]PF_6$

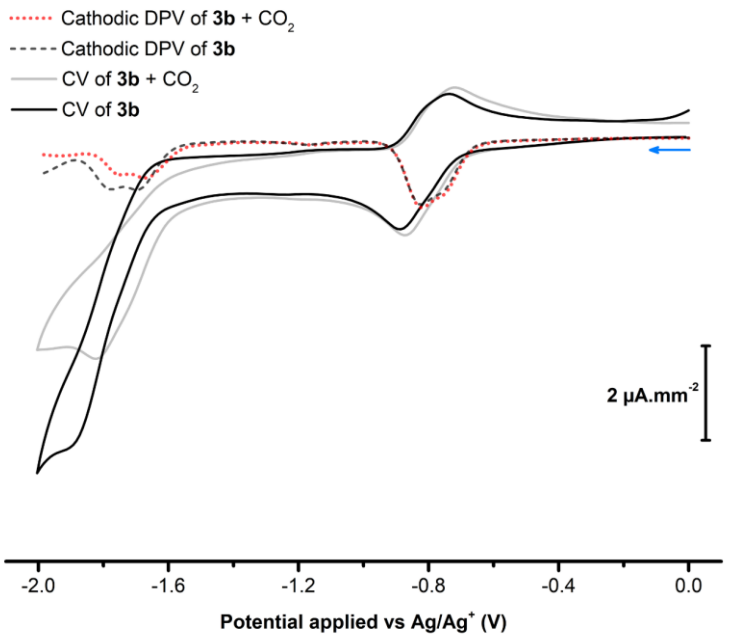

*Figure S82: CV and DPV of **3b** $[RhMB(CO)(PEt_3)]PF_6$ in the presence of CO_2 or Ar, recorded in CH_2Cl_2 with 1.0 mM analyte and 0.1 M $TBAPF_6$ supporting electrolyte.*

S4.8) Complex **4b** [RhMB(cod)Cl]

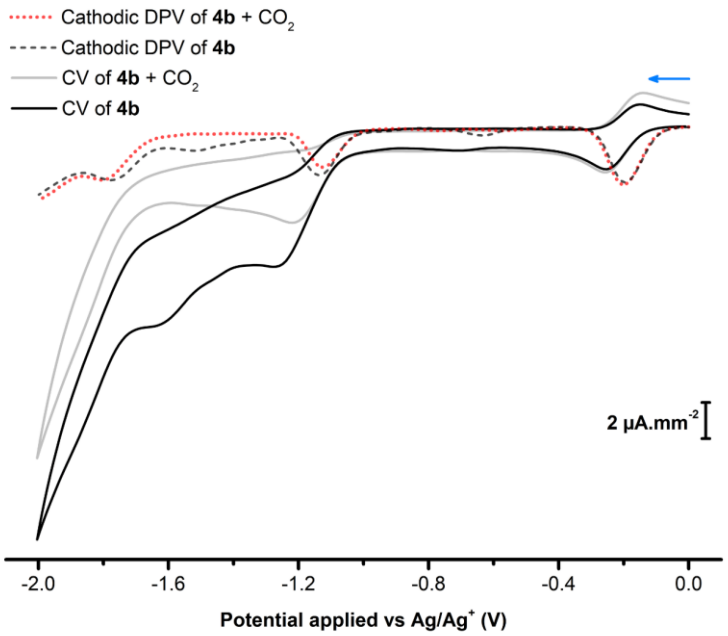

*Figure S83: CV and DPV of **4b** [RhMB(cod)Cl] in the presence of CO_2 or Ar, recorded in CH_2Cl_2 with 1.0 mM analyte and 0.1 M $TBAPF_6$ supporting electrolyte.*

S4.9) Complex **4d** [IrMB(cod)Cl]

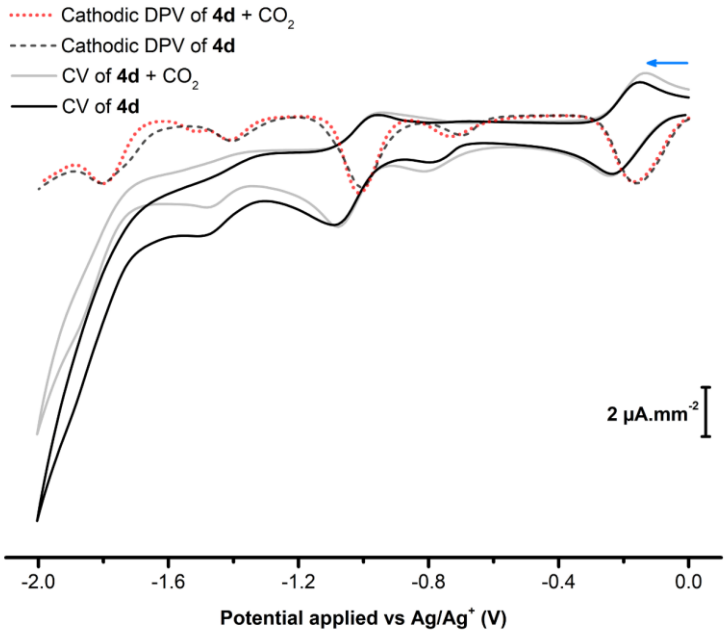

*Figure S84: CV and DPV of **4d** [IrMB(cod)Cl] in the presence of CO_2 or Ar, recorded in CH_2Cl_2 with 1.0 mM analyte and 0.1 M $TBAPF_6$ supporting electrolyte.*

S5) COMPUTATIONAL CALCULATIONS – COMPUTED FRONTIER ORBITALS

S5.1) Complex **1a** [RhDB(cod)]PF_6

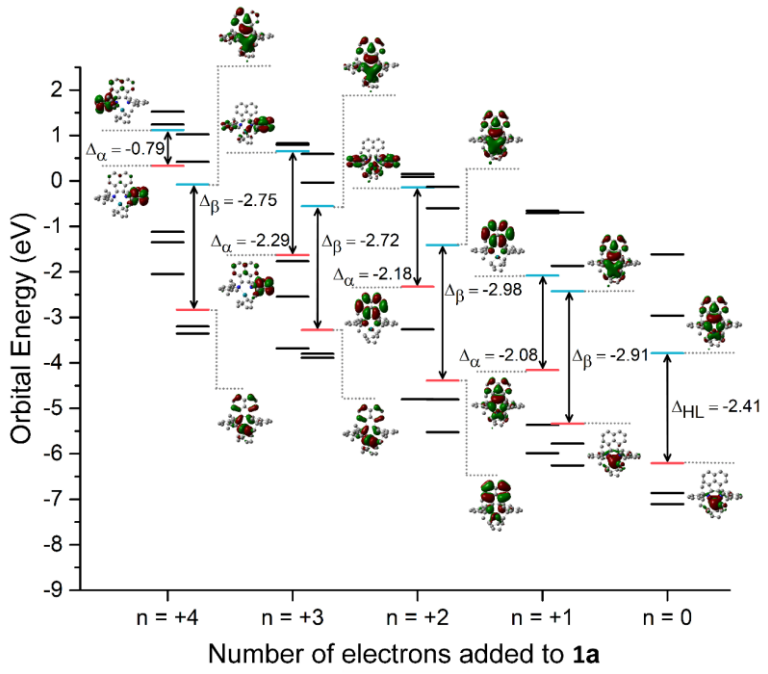

*Figure S85: Frontier orbital energies, HOMO-LUMO gap (Δ in eV), and HOMO and LUMO visualisations as calculated for **1a** [RhDB(cod)]PF_6 modelled in different reduced states. Integer "n" indicates the number of electrons added to **1a**'s initial state (n = 0). Calculated at B3LYP-D3/def2-SVP level of theory in CH_2Cl_2 using cPCM.*

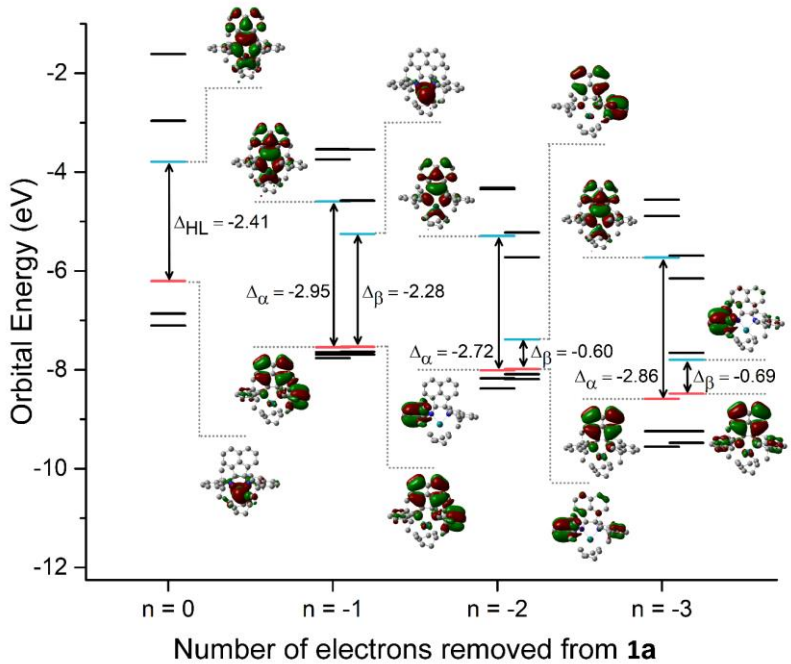

*Figure S86: Frontier orbital energies, HOMO-LUMO gap (Δ in eV), and HOMO and LUMO visualisations as calculated for **1a** [RhDB(cod)]PF_6 modelled in different oxidised states. Integer "n" indicates the number of electrons removed from **1a**'s initial state (n = 0). Calculated at B3LYP-D3/def2-SVP level of theory in CH_2Cl_2 using cPCM.*

S5.2) Complex **1b** [RhMB(cod)]PF_6

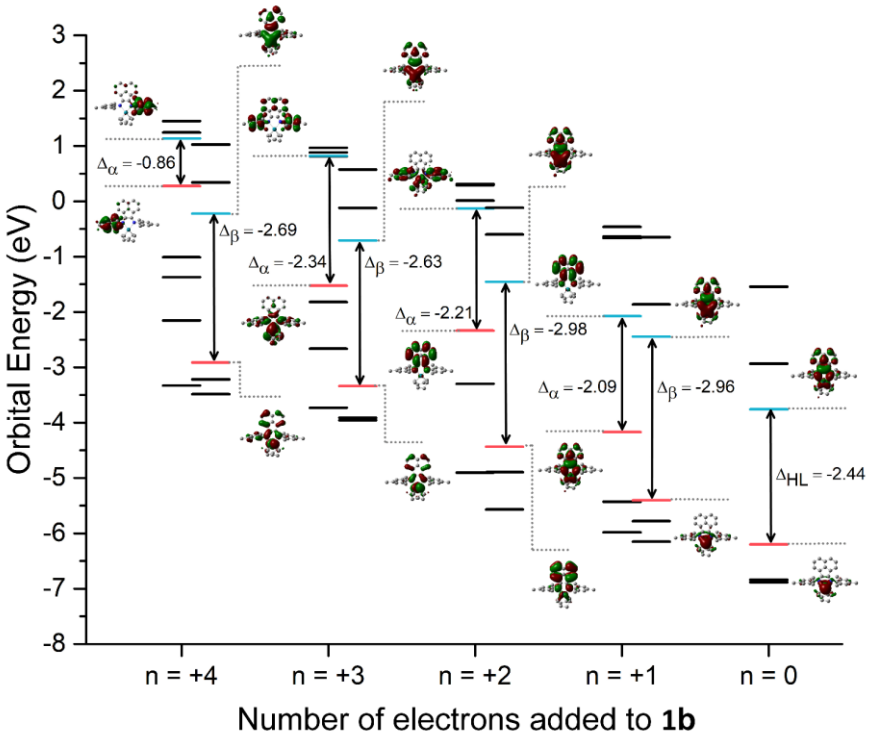

*Figure S87: Frontier orbital energies, HOMO-LUMO gap (Δ in eV), and HOMO and LUMO visualisations as calculated for **1b** [RhMB(cod)]PF_6 modelled in different reduced states. Integer "n" indicates the number of electrons added to **1b**'s initial state (n = 0). Calculated at B3LYP-D3/def2-SVP level of theory in CH_2Cl_2 using cPCM.*

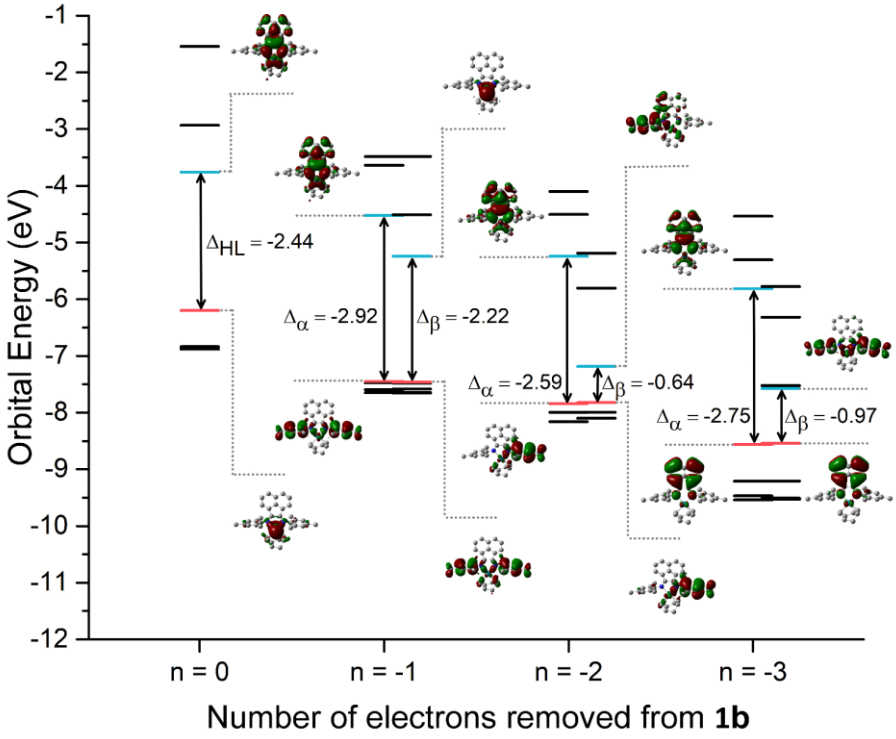

*Figure S88: Frontier orbital energies, HOMO-LUMO gap (Δ in eV), and HOMO and LUMO visualisations as calculated for **1b** [RhMB(cod)]PF_6 modelled in different oxidised states. Integer "n" indicates the number of electrons removed from **1b**'s initial state (n = 0). Calculated at B3LYP-D3/def2-SVP level of theory in CH_2Cl_2 using cPCM.*

S5.3) Complex **1c** [IrDB(cod)]PF_6

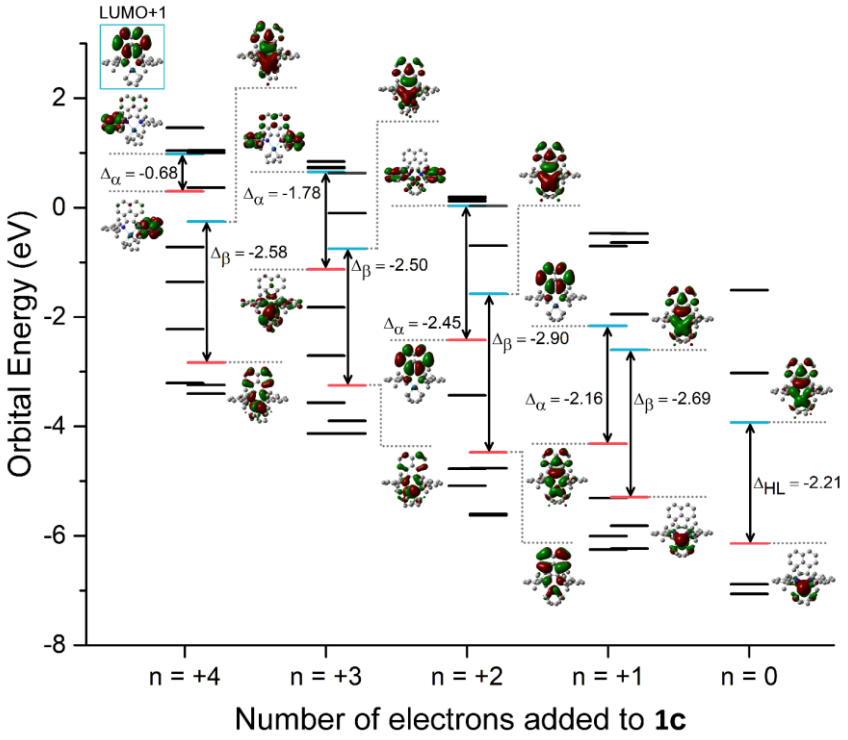

*Figure S89: Frontier orbital energies, HOMO-LUMO gap (Δ in eV), and HOMO and LUMO visualisations as calculated for **1c** [IrDB(cod)]PF_6 modelled in different reduced states. Integer "n" indicates the number of electrons added to **1c**'s initial state (n = 0). Calculated at B3LYP-D3/def2-SVP level of theory in CH_2Cl_2 using cPCM.*

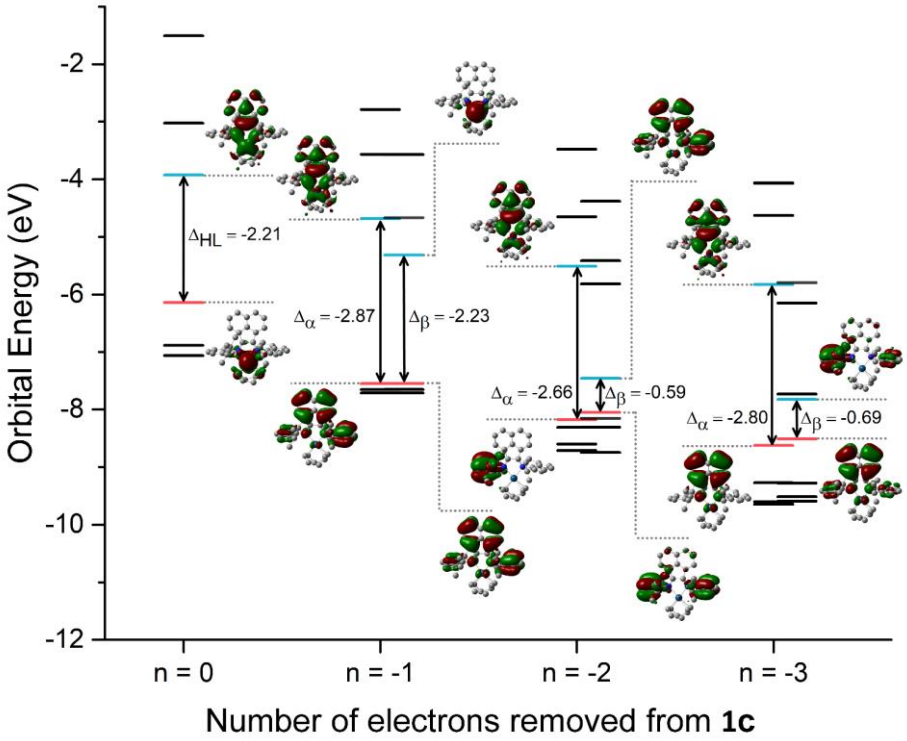

*Figure S90: Frontier orbital energies, HOMO-LUMO gap (Δ in eV), and HOMO and LUMO visualisations as calculated for **1c** [IrDB(cod)]PF_6 modelled in different oxidised states. Integer "n" indicates the number of electrons removed from **1c**'s initial state (n = 0). Calculated at B3LYP-D3/def2-SVP level of theory in CH_2Cl_2 using cPCM.*

S5.4) Complex **1d** [IrMB(cod)]PF_6

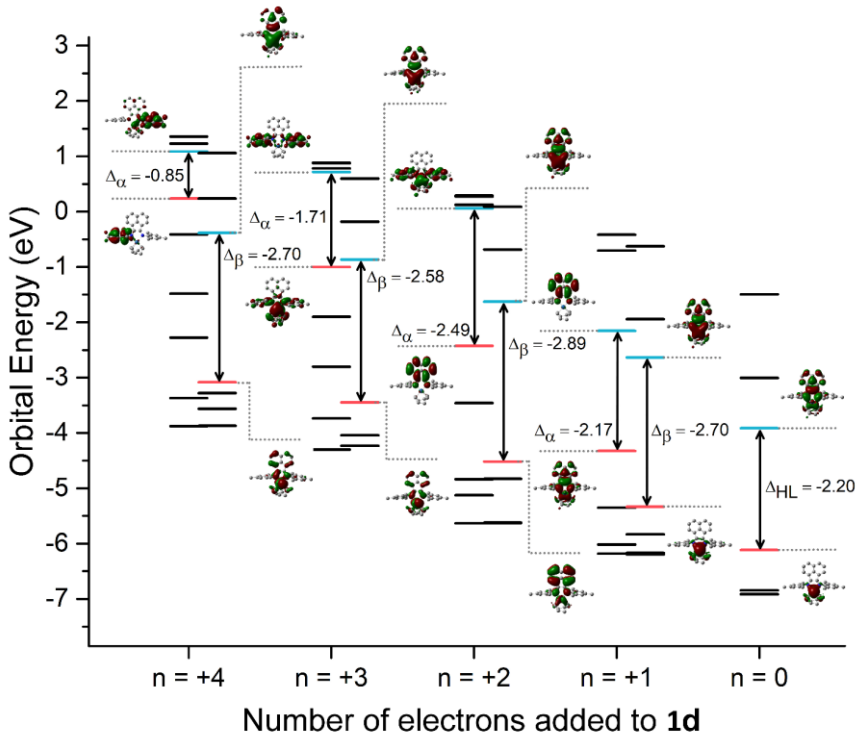

*Figure S91: Frontier orbital energies, HOMO-LUMO gap (Δ in eV), and HOMO and LUMO visualisations as calculated for **1d** [IrMB(cod)]PF_6 modelled in different reduced states. Integer "n" indicates the number of electrons added to **1d**'s initial state (n = 0). Calculated at B3LYP-D3/def2-SVP level of theory in CH_2Cl_2 using cPCM.*

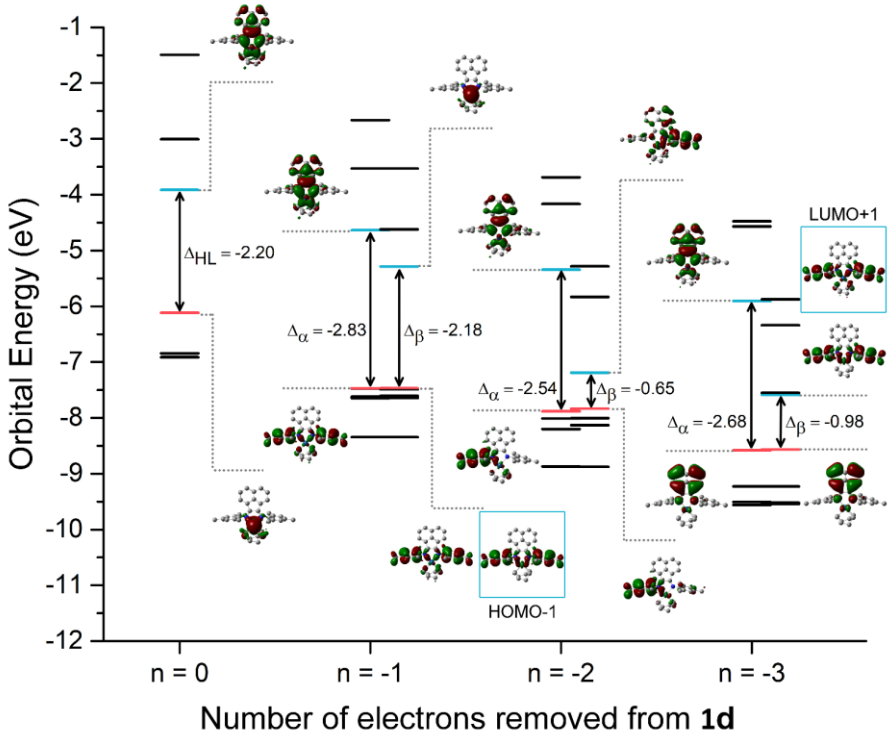

*Figure S92: Frontier orbital energies, HOMO-LUMO gap (Δ in eV), and HOMO and LUMO visualisations as calculated for **1d** [IrMB(cod)]PF_6 modelled in different oxidised states. Integer "n" indicates the number of electrons removed from **1d**'s initial state (n = 0). Calculated at B3LYP-D3/def2-SVP level of theory in CH_2Cl_2 using cPCM.*

S5.5) Complex **2a** [RhDB(CO)$_2$]PF$_6$

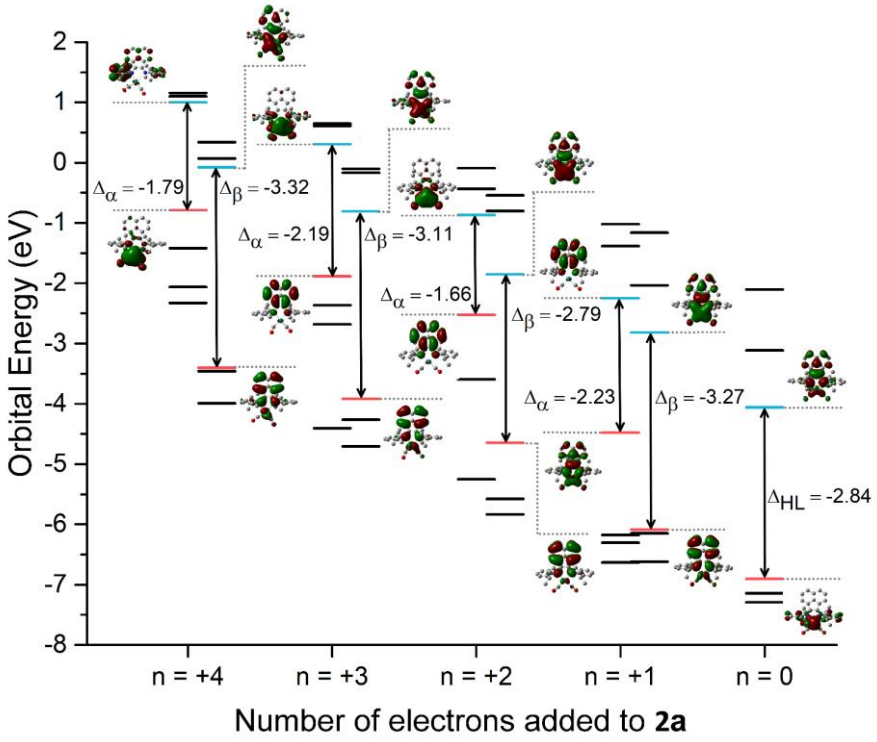

*Figure S93: Frontier orbital energies, HOMO-LUMO gap (Δ in eV), and HOMO and LUMO visualisations as calculated for **2a** [RhDB(CO)$_2$]PF$_6$ modelled in different reduced states. Integer "n" indicates the number of electrons added to **2a**'s initial state (n = 0). Calculated at B3LYP-D3/def2-SVP level of theory in CH_2Cl_2 using cPCM.*

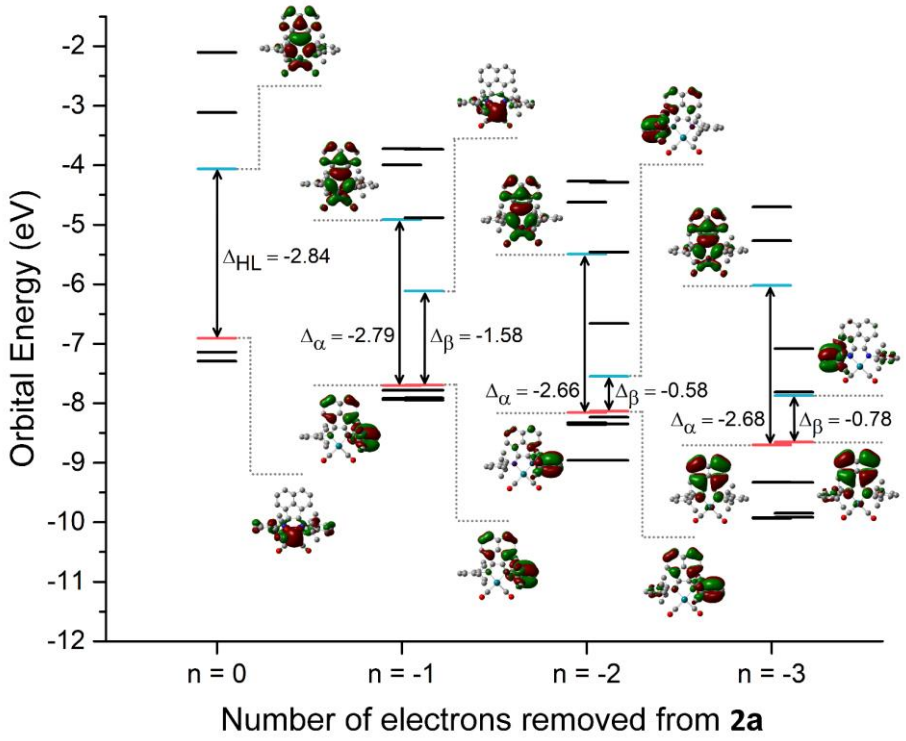

*Figure S94: Frontier orbital energies, HOMO-LUMO gap (Δ in eV), and HOMO and LUMO visualisations as calculated for **2a** [RhDB(CO)$_2$]PF$_6$ modelled in different oxidised states. Integer "n" indicates the number of electrons removed from **2a**'s initial state (n = 0). Calculated at B3LYP-D3/def2-SVP level of theory in CH_2Cl_2 using cPCM.*

S5.6) Complex **2b** [RhMB(CO)$_2$]PF$_6$

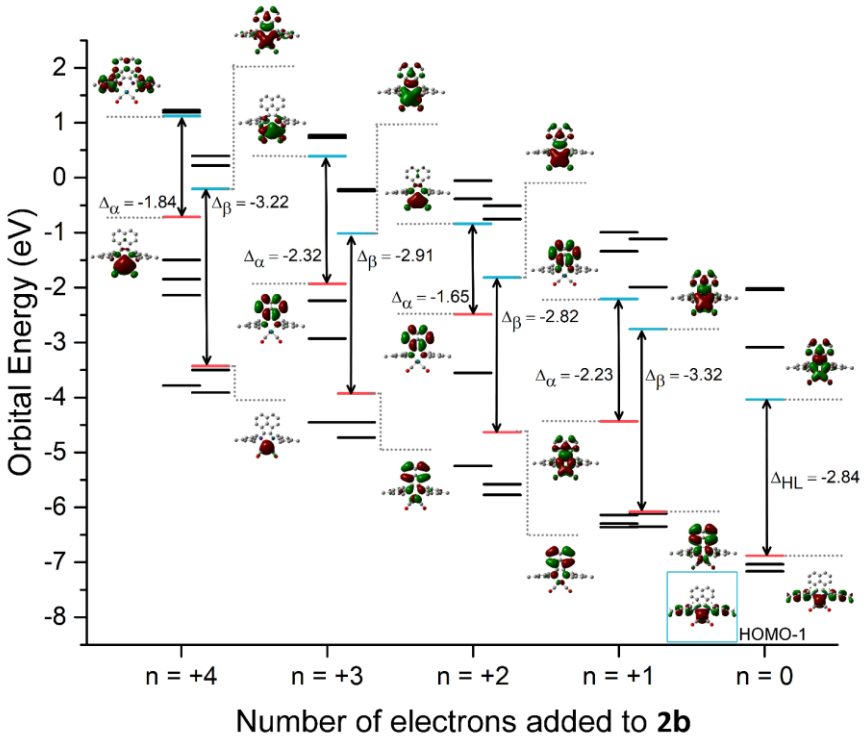

*Figure S95: Frontier orbital energies, HOMO-LUMO gap (Δ in eV), and HOMO and LUMO visualisations as calculated for **2b** [RhMB(CO)$_2$]PF$_6$ modelled in different reduced states. Integer "n" indicates the number of electrons added to **2b**'s initial state (n = 0). Calculated at B3LYP-D3/def2-SVP level of theory in CH$_2$Cl$_2$ using cPCM.*

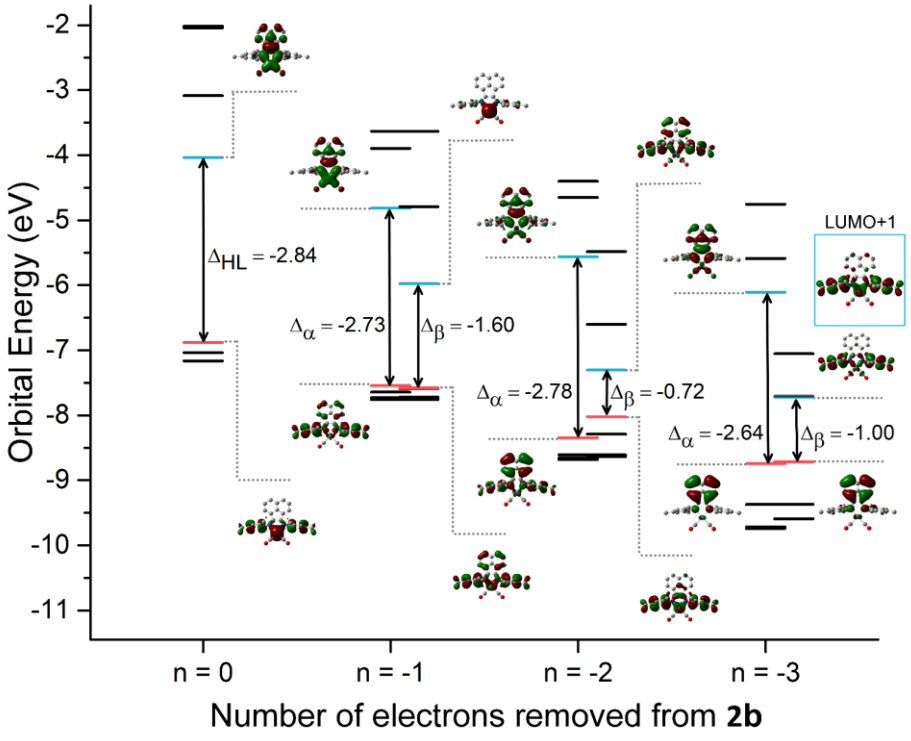

*Figure S96: Frontier orbital energies, HOMO-LUMO gap (Δ in eV), and HOMO and LUMO visualisations as calculated for **2b** [RhMB(CO)$_2$]PF$_6$ modelled in different oxidised states. Integer "n" indicates the number of electrons removed from **2b**'s initial state (n = 0). Calculated at B3LYP-D3/def2-SVP level of theory in CH$_2$Cl$_2$ using cPCM.*

S5.7) Complex **2c** $[IrDB(CO)_2]PF_6$

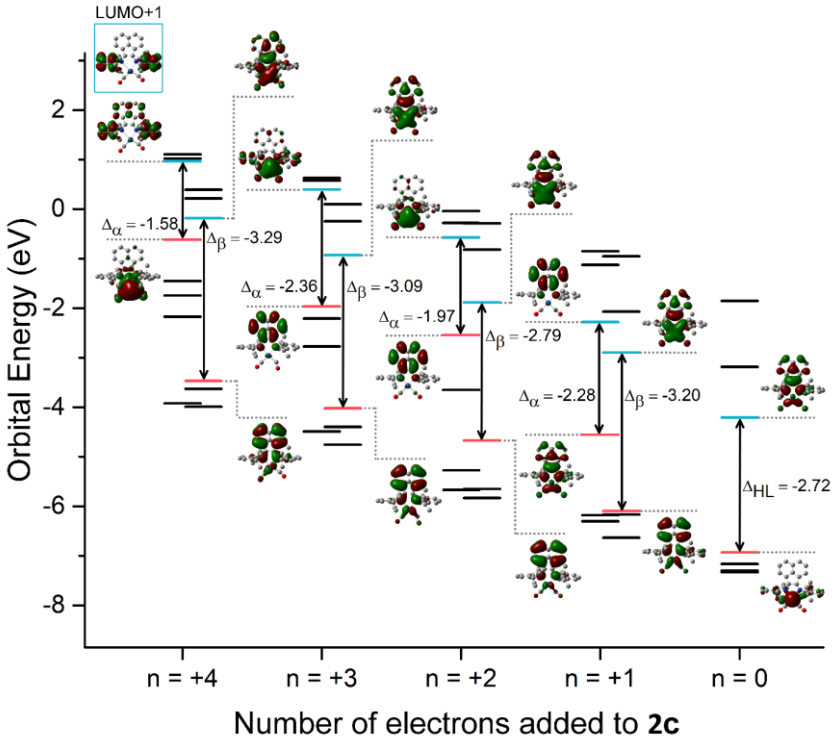

*Figure S97: Frontier orbital energies, HOMO-LUMO gap (Δ in eV), and HOMO and LUMO visualisations as calculated for **2c** $[IrDB(CO)_2]PF_6$ modelled in different reduced states. Integer "n" indicates the number of electrons added to **2c**'s initial state (n = 0). Calculated at B3LYP-D3/def2-SVP level of theory in CH_2Cl_2 using cPCM.*

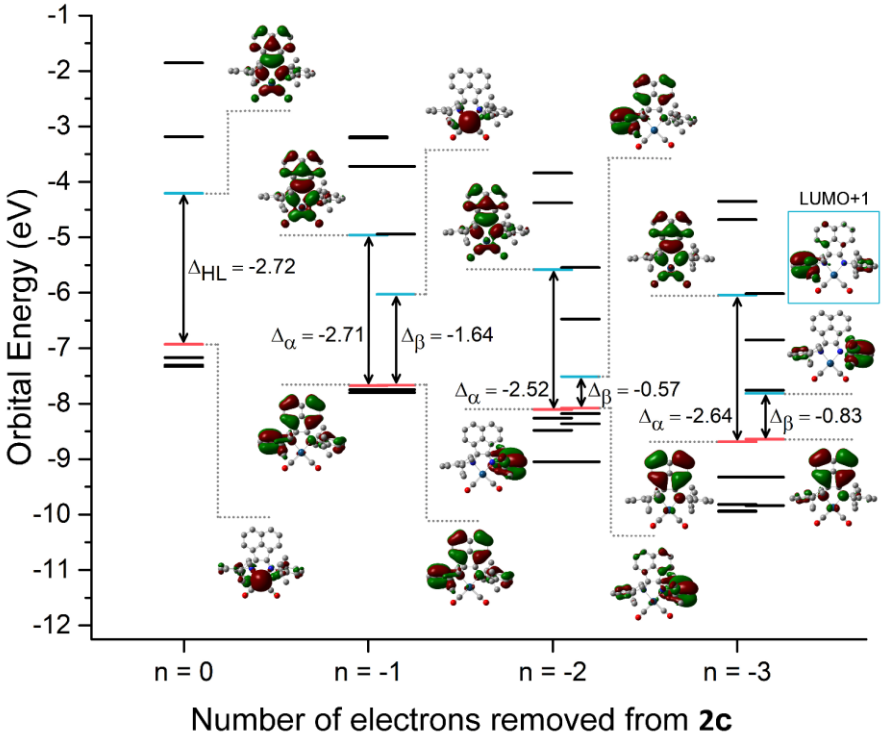

*Figure S98: Frontier orbital energies, HOMO-LUMO gap (Δ in eV), and HOMO and LUMO visualisations as calculated for **2c** $[IrDB(CO)_2]PF_6$ modelled in different oxidised states. Integer "n" indicates the number of electrons removed from **2c**'s initial state (n = 0). Calculated at B3LYP-D3/def2-SVP level of theory in CH_2Cl_2 using cPCM.*

S5.8) Complex **2d** $[IrMB(CO)_2]PF_6$

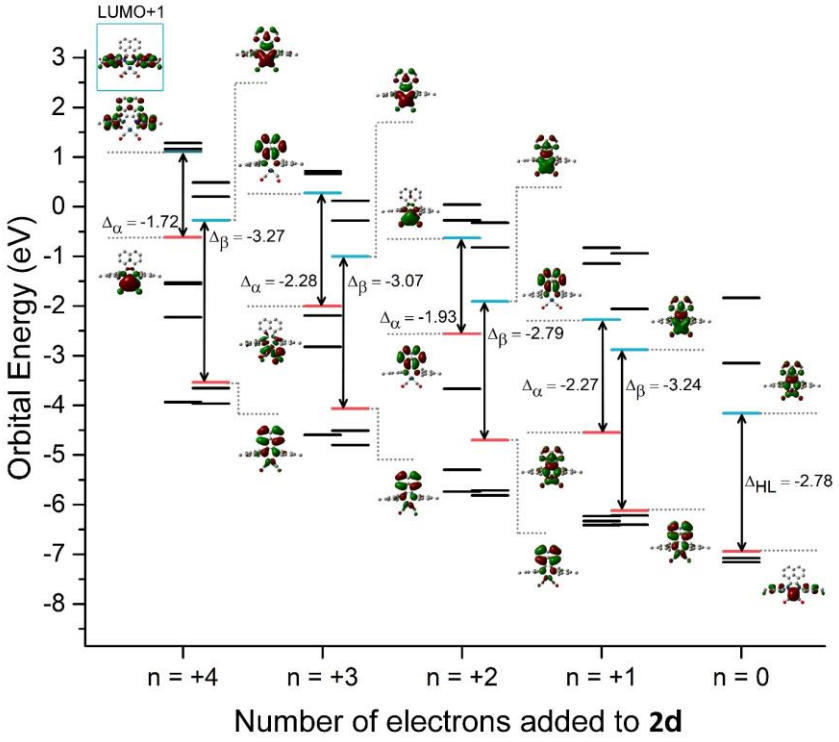

*Figure S99: Frontier orbital energies, HOMO-LUMO gap (Δ in eV), and HOMO and LUMO visualisations as calculated for **2d** $[IrDB(CO)_2]PF_6$ modelled in different reduced states. Integer "n" indicates the number of electrons added to **2d**'s initial state (n = 0). Calculated at B3LYP-D3/def2-SVP level of theory in CH_2Cl_2 using cPCM.*

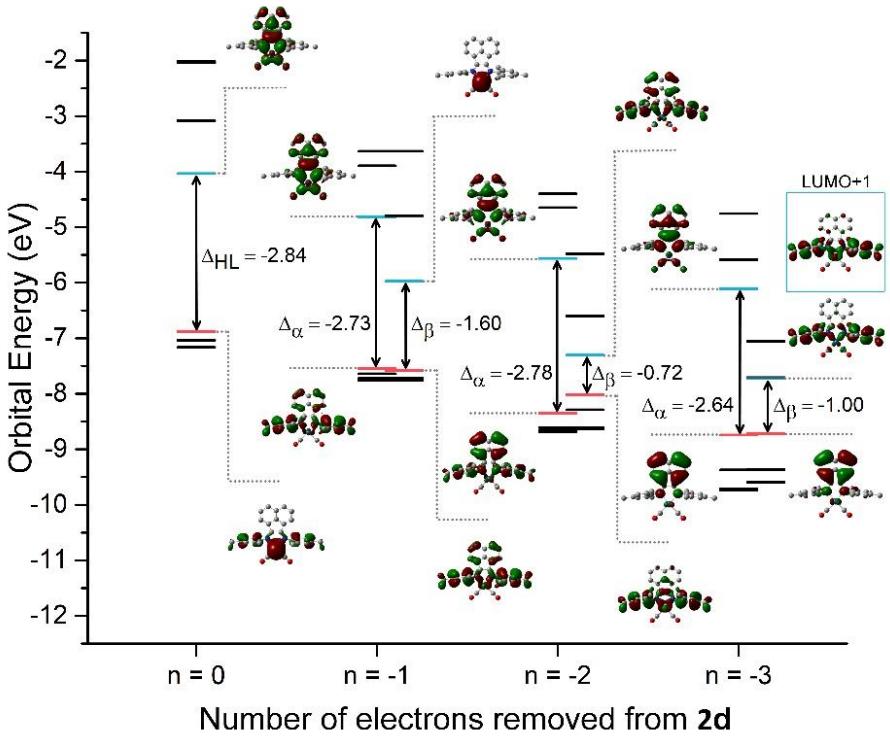

*Figure S100: Frontier orbital energies, HOMO-LUMO gap (Δ in eV), and HOMO and LUMO visualisations as calculated for **2d** $[IrMB(CO)_2]PF_6$ modelled in different oxidised states. Integer "n" indicates the number of electrons removed from **2d**'s initial state (n = 0). Calculated at B3LYP-D3/def2-SVP level of theory in CH_2Cl_2 using cPCM.*

S5.9) Complex **3a** [RhDB(CO)(PEt$_3$)]PF$_6$

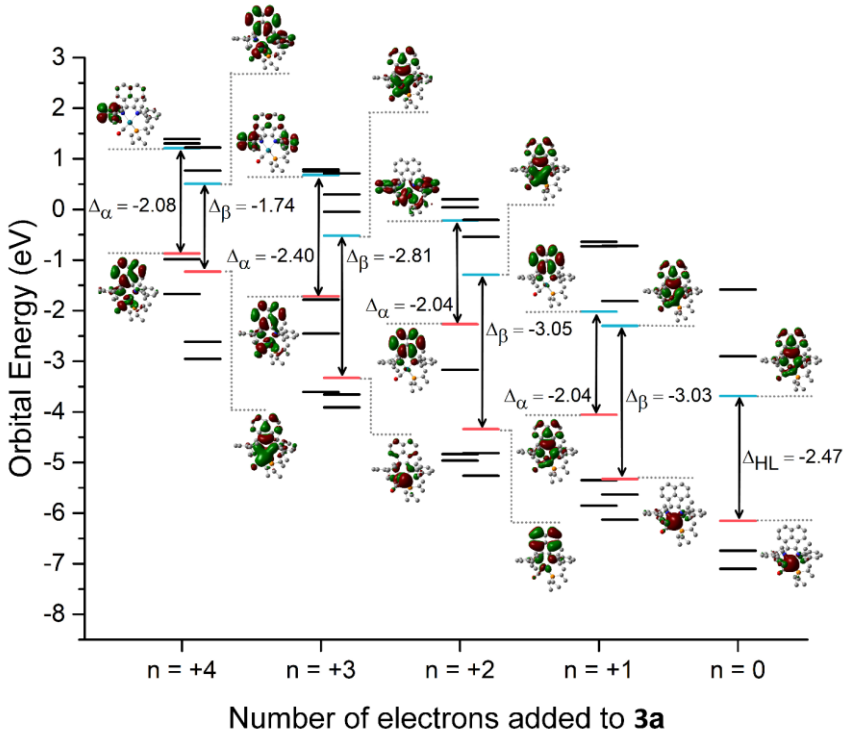

*Figure S101: Frontier orbital energies, HOMO-LUMO gap (Δ in eV), and HOMO and LUMO visualisations as calculated for **3a** [RhDB(CO)(PEt$_3$)]PF$_6$ modelled in different reduced states. Integer "n" indicates the number of electrons removed from **3a**'s initial state (n = 0). Calculated at B3LYP-D3/def2-SVP level of theory in CH_2Cl_2 using cPCM.*

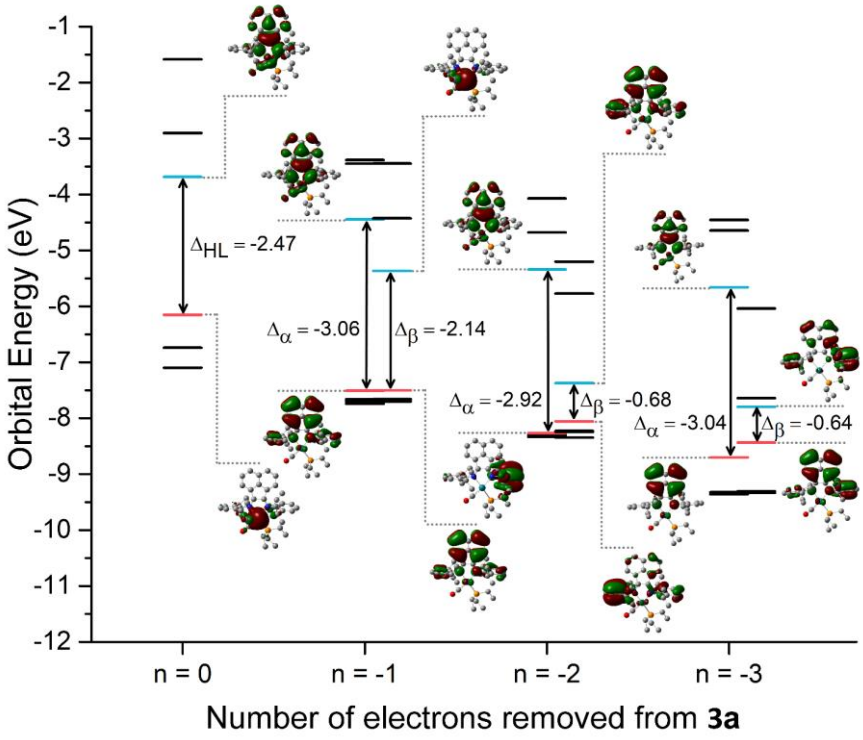

*Figure S102: Frontier orbital energies, HOMO-LUMO gap (Δ in eV), and HOMO and LUMO visualisations as calculated for **3a** [RhDB(CO)(PEt$_3$)]PF$_6$ modelled in different oxidised states. Integer "n" indicates the number of electrons removed from **3a**'s initial state (n = 0). Calculated at B3LYP-D3/def2-SVP level of theory in CH_2Cl_2 using cPCM.*

The (n = +2) α-LUMO, however, is largely restricted to π*-orbitals of the acenaphthalene rings with out-of-phase overlap from the bisimine nitrogens and no visible contributions from the carbonyl ligands. This indicates that the second reduction event favours the delocalisation of the additional charge on the BIAN ligand over increasing the degree of electron density on the metal centre, and consequently the extent of π-backbonding to the carbonyl ligands.

S5.10) Complex **3b** [RhMB(CO)(PEt$_3$)]PF$_6$

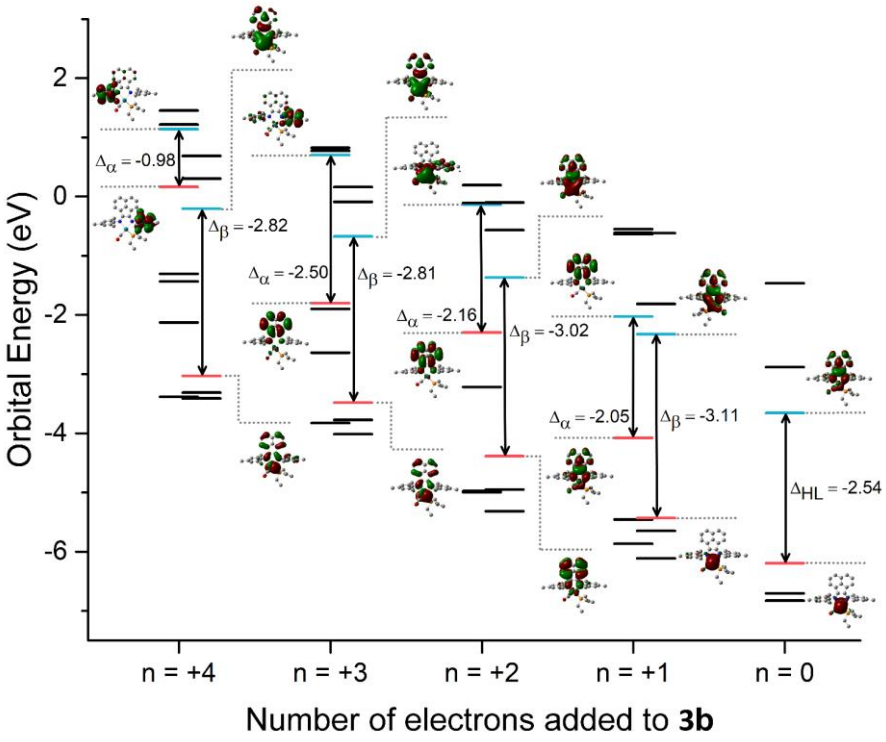

*Figure S103: Frontier orbital energies, HOMO-LUMO gap (Δ in eV), and HOMO and LUMO visualisations as calculated for **3b** [RhMB(CO)(PEt$_3$)]PF$_6$ modelled in different reduced states. Integer "n" indicates the number of electrons added to **3b**'s initial state (n = 0). Calculated at B3LYP-D3/def2-SVP level of theory in CH_2Cl_2 using cPCM.*

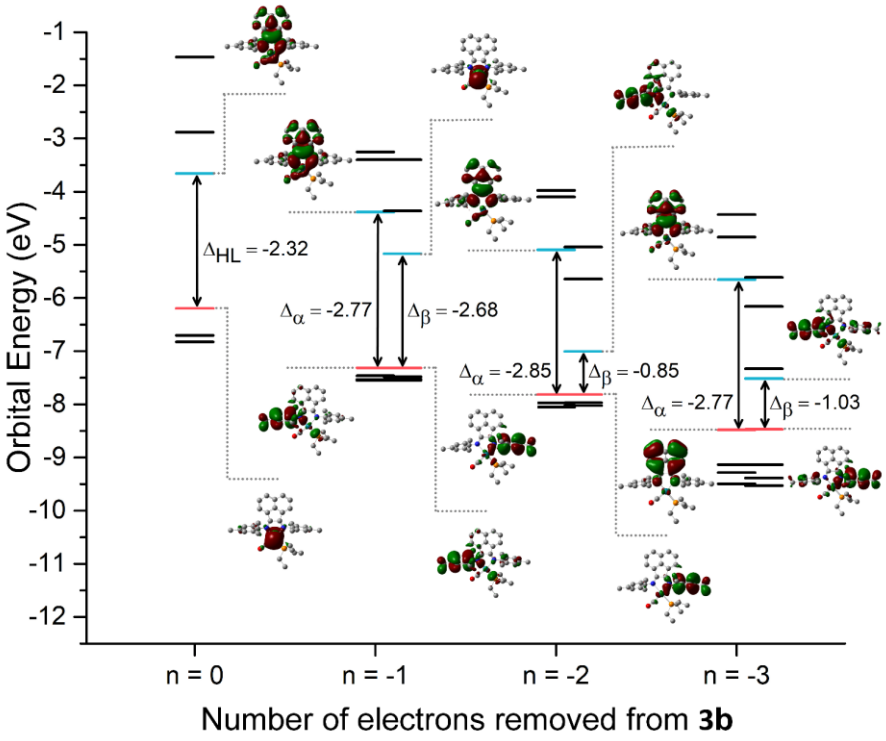

*Figure S104: Frontier orbital energies, HOMO-LUMO gap (Δ in eV), and HOMO and LUMO visualisations as calculated for **3b** [RhMB(CO)(PEt$_3$)]PF$_6$ modelled in different oxidised states. Integer "n" indicates the number of electrons removed from **3b**'s initial state (n = 0). Calculated at B3LYP-D3/def2-SVP level of theory in CH_2Cl_2 using cPCM.*

S5.11) Complex **4a** [RhDB(cod)Cl]

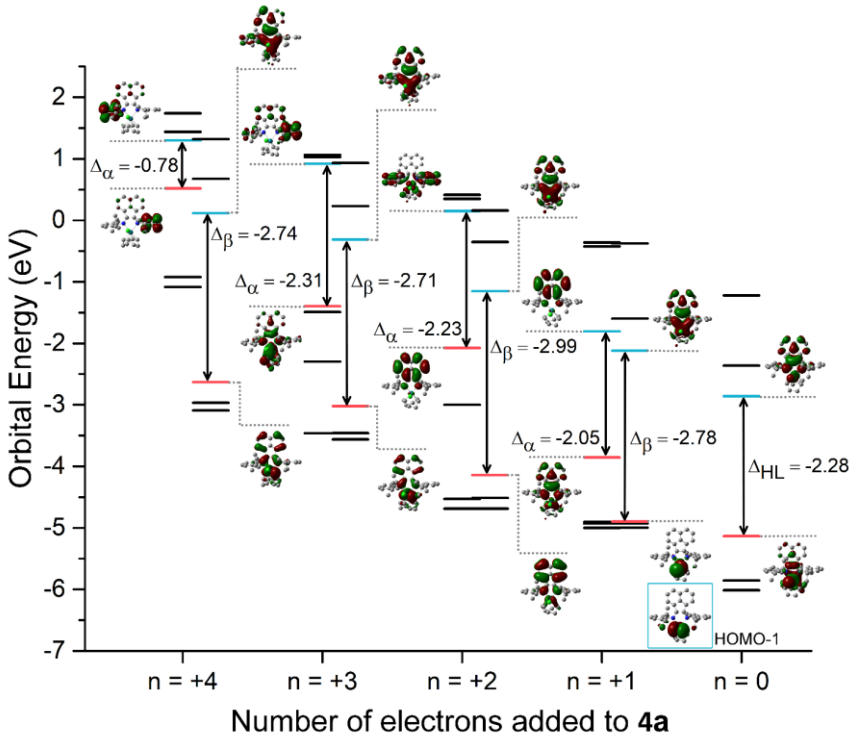

*Figure S105: Frontier orbital energies, HOMO-LUMO gap (Δ in eV), and HOMO and LUMO visualisations as calculated for **4a** [RhDB(cod)Cl] modelled in different reduced states. Integer "n" indicates the number of electrons removed from **4a**'s initial state (n = 0). Calculated at B3LYP-D3/def2-SVP level of theory in CH_2Cl_2 using cPM.*

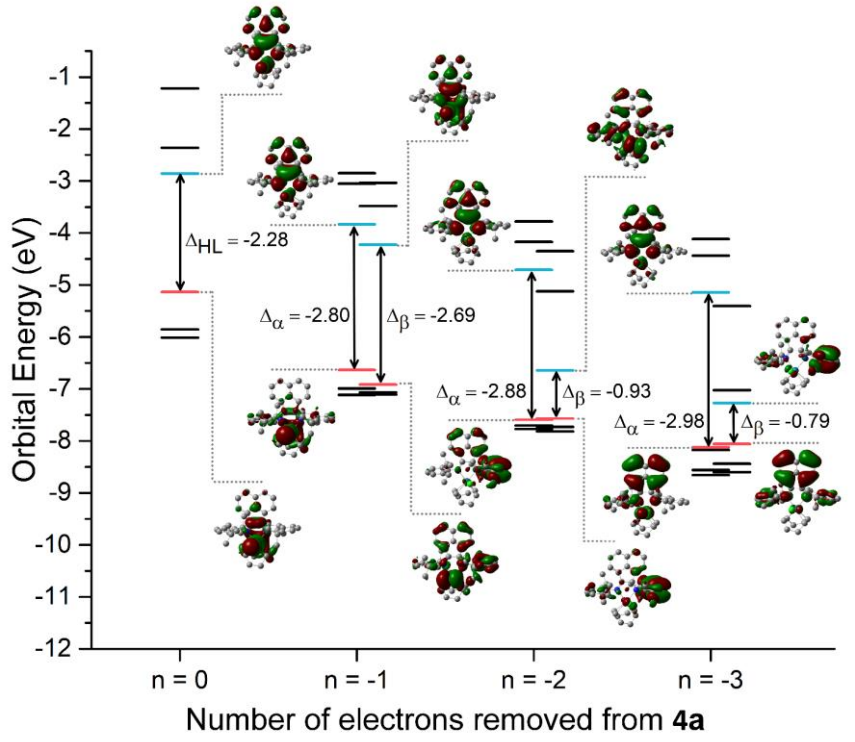

*Figure S106: Frontier orbital energies, HOMO-LUMO gap (Δ in eV), and HOMO and LUMO visualisations as calculated for **4a** [RhDB(cod)Cl] modelled in different oxidised states. Integer "n" indicates the number of electrons removed from **4a**'s initial state (n = 0). Calculated at B3LYP-D3/def2-SVP level of theory in CH_2Cl_2 using cPM.*

S5.12) Complex **4b** [RhMB(cod)Cl]

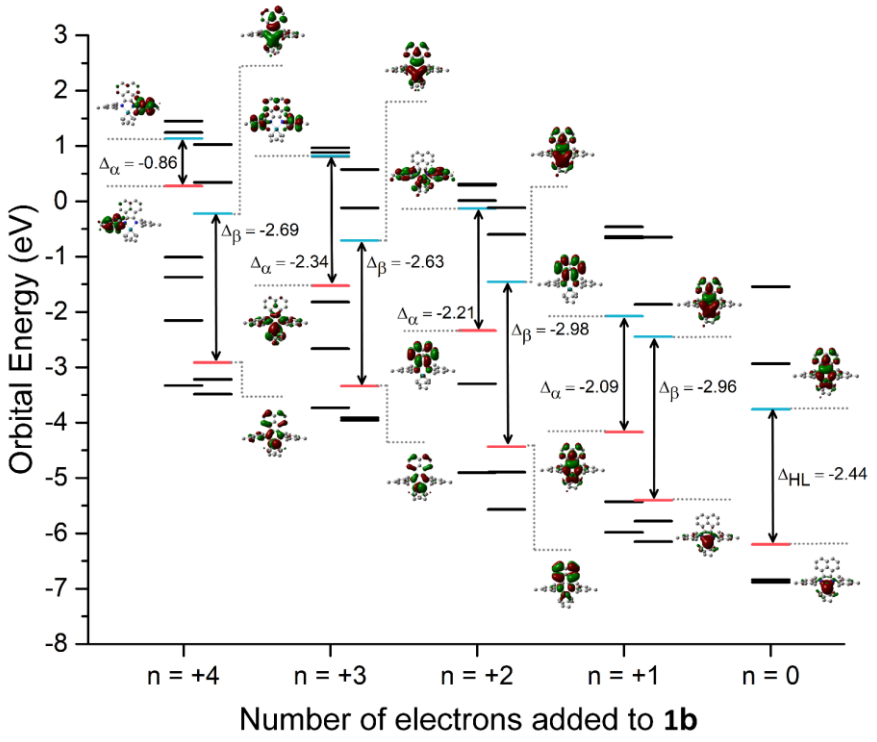

*Figure S107: Frontier orbital energies, HOMO-LUMO gap (Δ in eV), and HOMO and LUMO visualisations as calculated for **4b** [RhMB(cod)Cl] modelled in different reduced states. Integer "n" indicates the number of electrons added to **4b**'s initial state (n = 0). Calculated at B3LYP-D3/def2-SVP level of theory in CH_2Cl_2 using cPCM.*

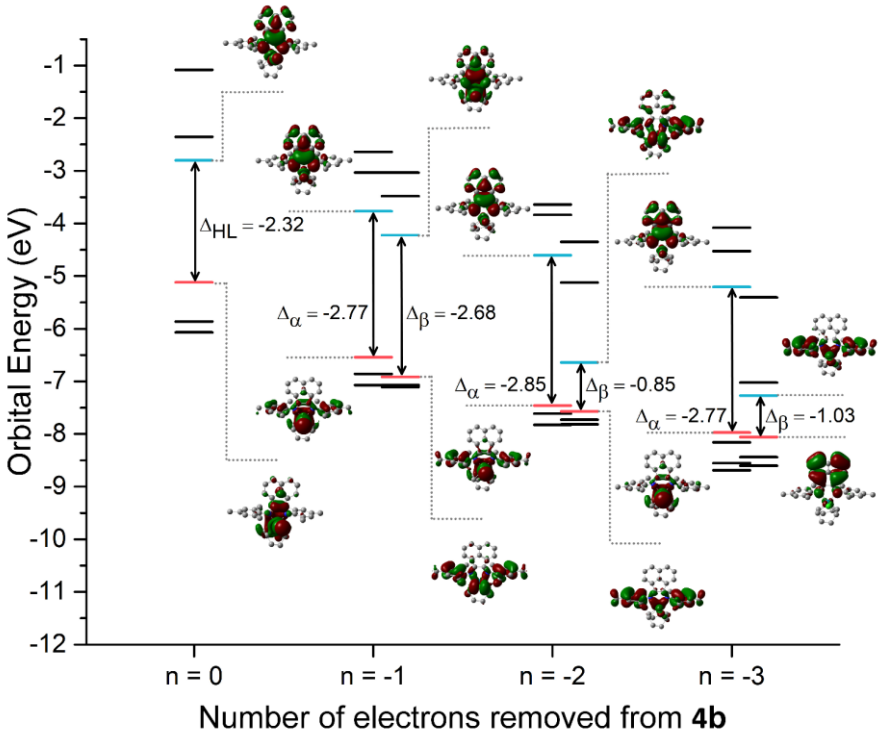

*Figure S108: Frontier orbital energies, HOMO-LUMO gap (Δ in eV), and HOMO and LUMO visualisations as calculated for **4b** [RhMB(cod)Cl] modelled in different oxidised states. Integer "n" indicates the number of electrons removed from **4b**'s initial state (n = 0). Calculated at B3LYP-D3/def2-SVP level of theory in CH_2Cl_2 using cPCM.*

S5.13) Complex **4c** [IrDB(cod)Cl]

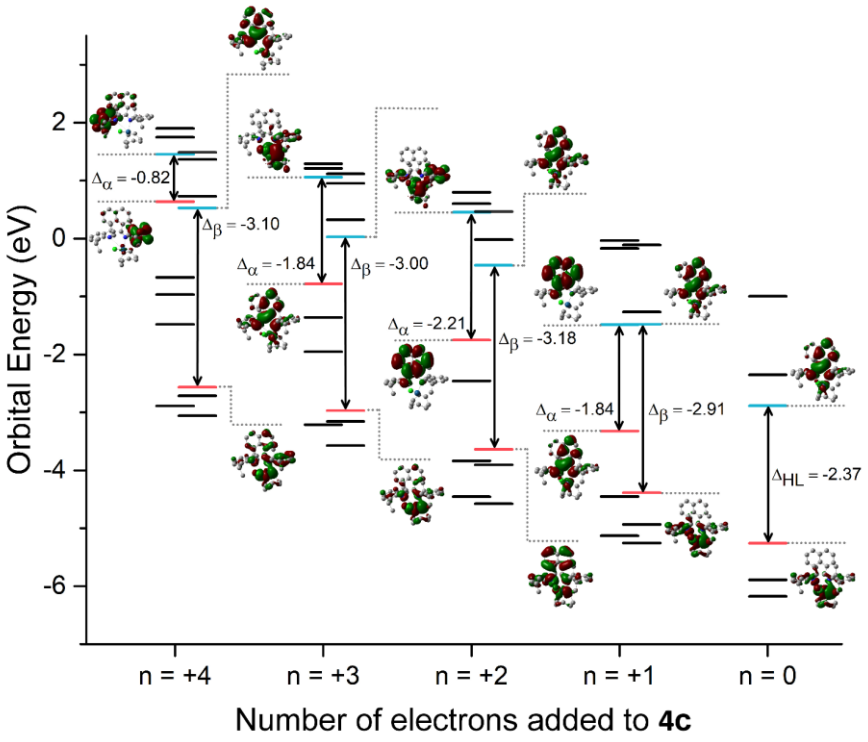

*Figure S109: Frontier orbital energies, HOMO-LUMO gap (Δ in eV), and HOMO and LUMO visualisations as calculated for **4c** [IrDB(cod)Cl] modelled in different reduced states. Integer "n" indicates the number of electrons added to **4c**'s initial state (n = 0). Calculated at B3LYP-D3/def2-SVP level of theory in CH_2Cl_2 using cPCM.*

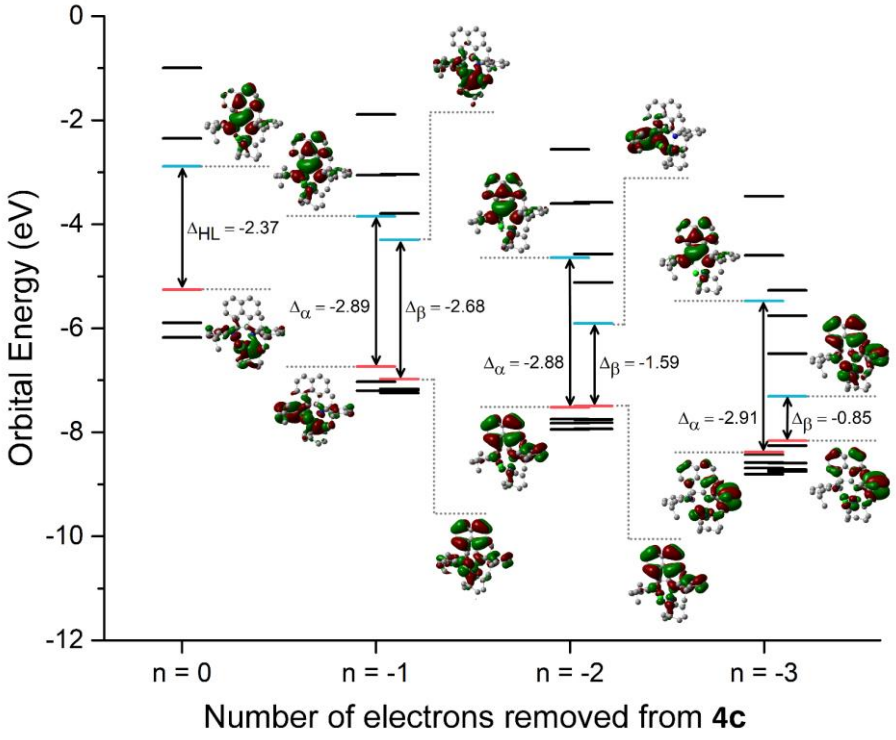

*Figure S110: Frontier orbital energies, HOMO-LUMO gap (Δ in eV), and HOMO and LUMO visualisations as calculated for **4c** [IrDB(cod)Cl] modelled in different oxidised states. Integer "n" indicates the number of electrons removed from **4c**'s initial state (n = 0). Calculated at B3LYP-D3/def2-SVP level of theory in CH_2Cl_2 using cPCM.*

S5.14) Complex **4d** [IrMB(cod)Cl]

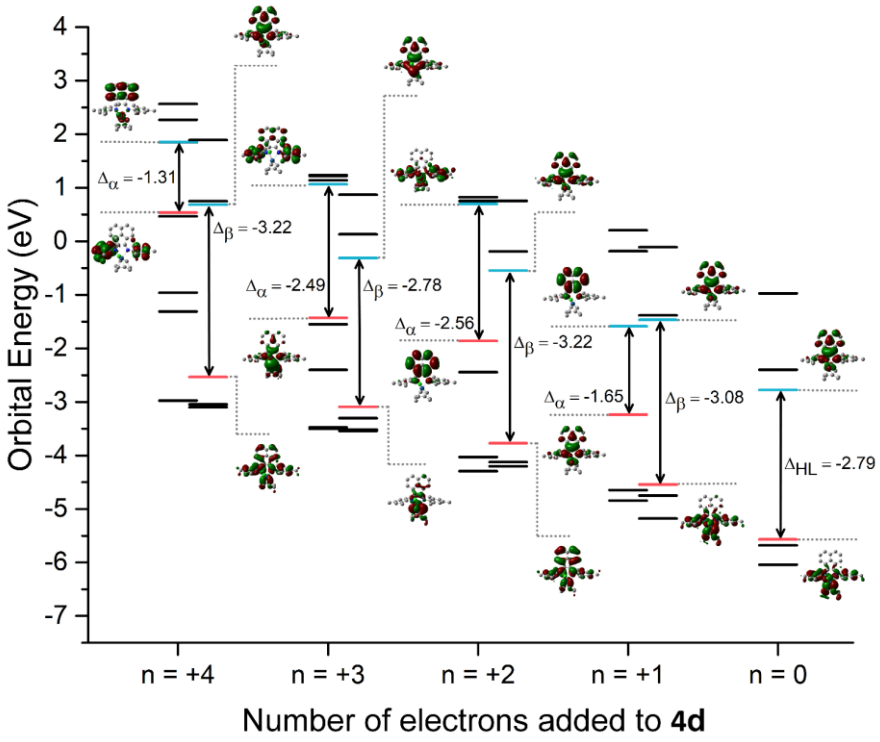

*Figure S111: Frontier orbital energies, HOMO-LUMO gap (Δ in eV), and HOMO and LUMO visualisations as calculated for **4d** [IrMB(cod)Cl] modelled in different reduced states. Integer "n" indicates the number of electrons added to **4d**'s initial state (n = 0). Calculated at B3LYP-D3/def2-SVP level of theory in CH_2Cl_2 using cPCM.*

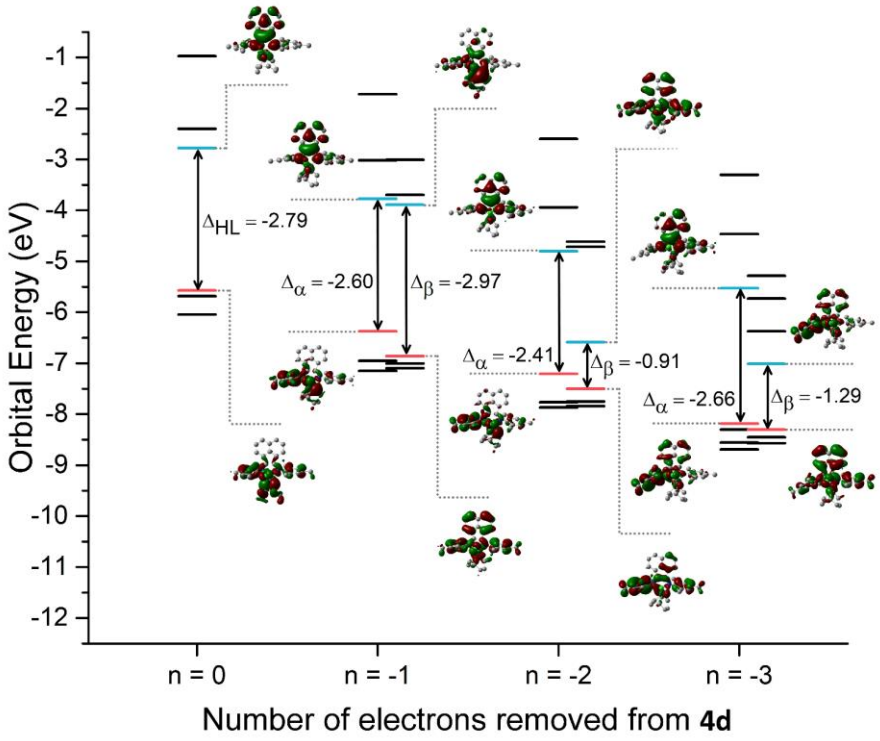

*Figure S112: Frontier orbital energies, HOMO-LUMO gap (Δ in eV), and HOMO and LUMO visualisations as calculated for **4d** [IrMB(cod)Cl] modelled in different oxidised states. Integer "n" indicates the number of electrons removed from **4d**'s initial state (n = 0). Calculated at B3LYP-D3/def2-SVP level of theory in CH_2Cl_2 using cPCM.*

S6) COMPUTATIONAL CALCULATIONS – TOTAL ENERGIES

Total energies in a.u. (including ZPVE and Thermal energy respectively) of all the stationary points discussed and presented in the text and SI. All calculations were performed at B3LYP-D3/def2-SVP level of theory in CH_2Cl_2 using cPCM.

Complex Number	Modelled Charge State	ZPVE	E(Thermal)
1a	(n = +4)	–1926.25	–1926.21
	(n = +3)	–1926.26	–1926.22
	(n = +2)	–1926.23	–1926.18
	(n = +1)	–1926.14	–1926.10
	(n = 0)	–1925.99	–1925.95
	(n = –1)	–1925.78	–1925.74
	(n = –2)	–1925.51	–1925.46
	(n = –3)	–1925.22	–1925.18
1b	(n = +4)	–1690.71	–1690.67
	(n = +3)	–1690.72	–1690.68
	(n = +2)	–1690.69	–1690.65
	(n = +1)	–1690.60	–1690.57
	(n = 0)	–1690.46	–1690.42
	(n = –1)	–1690.24	–1690.20
	(n = –2)	–1689.97	–1689.94
	(n = –3)	–1689.69	–1689.65
1c	(n = +4)	–1920.06	–1920.01
	(n = +3)	–1920.07	–1920.02
	(n = +2)	–1920.05	–1920.01
	(n = +1)	–1919.96	–1919.92
	(n = 0)	–1919.81	–1919.76
	(n = –1)	–1919.59	–1919.55
	(n = –2)	–1919.32	–1919.28
	(n = –3)	–1919.03	–1918.99
1d	(n = +4)	–1684.52	–1684.48
	(n = +3)	–1684.53	–1684.49
	(n = +2)	–1684.51	–1684.47
	(n = +1)	–1684.42	–1684.38
	(n = 0)	–1684.27	–1684.23
	(n = –1)	–1684.05	–1684.02
	(n = –2)	–1683.79	–1683.75
	(n = –3)	–1683.50	–1683.47

Complex Number	Modelled Charge State	ZPVE	E(Thermal)
2a	(n = +4)	–1841.14	–1841.10
	(n = +3)	–1841.13	–1841.09
	(n = +2)	–1841.08	–1841.04
	(n = +1)	–1840.99	–1840.95
	(n = 0)	–1840.82	–1840.78
	(n = –1)	–1840.58	–1840.54
	(n = –2)	–1840.30	–1840.26
	(n = –3)	–1840.01	–1839.97
2b	(n = +4)	–1605.60	–1605.56
	(n = +3)	–1605.59	–1605.55
	(n = +2)	–1605.53	–1605.49
	(n = +1)	–1605.44	–1605.40
	(n = 0)	–1605.28	–1605.24
	(n = –1)	–1605.04	–1605.00
	(n = –2)	–1604.77	–1604.73
	(n = –3)	–1604.48	–1604.45
2c	(n = +4)	–1834.96	–1834.91
	(n = +3)	–1834.95	–1834.91
	(n = +2)	–1834.90	–1834.86
	(n = +1)	–1834.81	–1834.77
	(n = 0)	–1834.65	–1834.61
	(n = –1)	–1834.41	–1834.36
	(n = –2)	–1834.13	–1834.09
	(n = –3)	–1833.84	–1833.80
2d	(n = +4)	–1599.41	–1599.38
	(n = +3)	–1599.40	–1599.37
	(n = +2)	–1599.36	–1599.32
	(n = +1)	–1599.26	–1599.23
	(n = 0)	–1599.10	–1599.07
	(n = –1)	–1598.86	–1598.83
	(n = –2)	–1598.59	–1598.56
	(n = –3)	–1598.30	–1598.27

Complex Number	Modelled Charge State	ZPVE	E(Thermal)
3a	(n = +4)	–2306.51	–2306.46
	(n = +3)	–2306.48	–2306.43
	(n = +2)	–2306.44	–2306.39
	(n = +1)	–2306.36	–2306.31
	(n = 0)	–2306.21	–2306.16
	(n = –1)	–2306.00	–2305.95
	(n = –2)	–2305.73	–2305.68
	(n = –3)	–2305.44	–2305.39
3b	(n = +4)	–2070.92	–2070.88
	(n = +3)	–2070.93	–2070.89
	(n = +2)	–2070.89	–2070.85
	(n = +1)	–2070.81	–2070.76
	(n = 0)	–2070.66	–2070.62
	(n = –1)	–2070.45	–2070.41
	(n = –2)	–2070.19	–2070.15
	(n = –3)	–2069.91	–2069.87

Complex Number	Modelled Charge State	ZPVE	E(Thermal)
4a	(n = +4)	–2386.45	–2386.40
	(n = +3)	–2386.47	–2386.42
	(n = +2)	–2386.44	–2386.39
	(n = +1)	–2386.37	–2386.32
	(n = 0)	–2386.24	–2386.19
	(n = –1)	–2386.07	–2386.02
	(n = –2)	–2385.82	–2385.77
	(n = –3)	–2385.55	–2385.50
4b	(n = +4)	–2150.90	–2150.85
	(n = +3)	–2150.92	–2150.88
	(n = +2)	–2150.90	–2150.86
	(n = +1)	–2150.83	–2150.79
	(n = 0)	–2150.71	–2150.67
	(n = –1)	–2150.54	–2150.50
	(n = –2)	–2150.29	–2150.25
	(n = –3)	–2150.03	–2149.99
4c	(n = +4)	–2380.22	–2380.17
	(n = +3)	–2380.24	–2380.19
	(n = +2)	–2380.24	–2380.19
	(n = +1)	–2380.17	–2380.13
	(n = 0)	–2380.05	–2380.01
	(n = –1)	–2379.87	–2379.83
	(n = –2)	–2379.63	–2379.59
	(n = –3)	–2379.36	–2379.32
4d	(n = +4)	–2144.67	–2144.62
	(n = +3)	–2144.72	–2144.67
	(n = +2)	–2144.70	–2144.66
	(n = +1)	–2144.63	–2144.59
	(n = 0)	–2144.52	–2144.48
	(n = –1)	–2144.34	–2144.30
	(n = –2)	–2144.10	–2144.06
	(n = –3)	–2143.83	–2143.79

S7) REFERENCES

[1] K.M. Clark, J. Bendix, A.F. Heyduk, J.W. Ziller, Synthesis and characterization of a neutral titanium tris(iminosemiquinone) complex featuring redox-active ligands, Inorg. Chem. 51 (2012) 7457–7459. https://doi.org/10.1021/ic301059p.

[2] J. Bendix, K.M. Clark, Delocalization and Valence Tautomerism in Vanadium Tris(iminosemiquinone) Complexes, Angew. Chem Int. Ed. 55 (2016) 2748–2752. https://doi.org/10.1002/anie.201510403.

[3] M.M. Khusniyarov, K. Harms, O. Burghaus, J. Sundermeyer, Molecular and Electronic Structures of Homoleptic Nickel and Cobalt Complexes with Non-Innocent Bulky Diimine Ligands Derived from Fluorinated 1,4-Diaza-1,3-butadiene (DAD) and Bis(arylimino)acenaphthene (BIAN), Eur. J. Inorg. Chem. 2006 (2006) 2985–2996. https://doi.org/10.1002/ejic.200600236.

[4] P.J. Larson, F.S. Wekesa, A. Singh, C.R. Smith, A. Rajput, G.P. McGovern, D.K. Unruh, A.F. Cozzolino, M. Findlater, Synthesis, characterization, electrochemical properties and theoretical calculations of (BIAN) iron complexes, Polyhedron. 159 (2019) 365–374. https://doi.org/10.1016/j.poly.2018.11.060.

[5] I. Strydom, G. Guisado-Barrios, I. Fernández, D.C. Liles, E. Peris, D.I. Bezuidenhout, A Hemilabile and Cooperative N-Donor-Functionalized 1,2,3-Triazol-5-Ylidene Ligand for Alkyne Hydrothiolation Reactions, Chem. Eur. J. 23 (2017) 1393–1401. https://doi.org/10.1002/chem.201604567.

[6] D. Aucamp, T. Witteler, F. Dielmann, S. Siangwata, D.C. Liles, G.S. Smith, D.I. Bezuidenhout, A Triarylated 1,2,3-Triazol-5-ylidene Ligand with a Redox-Active Ferrocenyl Substituent for Rhodium(I)-Catalyzed Hydroformylation of 1-Octene, Eur. J. Inorg. Chem. 2017 (2017) 1227–1236. https://doi.org/10.1002/ejic.201700164.

[7] C. Hua, K.Q. Vuong, M. Bhadbhade, B.A. Messerle, New rhodium(I) and iridium(I) complexes containing mixed pyrazolyl-1,2,3-triazolyl ligands as catalysts for hydroamination, Organometallics. 31 (2012) 1790–1800. https://doi.org/10.1021/om201171b.

[8] D.A.J. Harding, E.G. Hope, K. Singh, G.A. Solan, Cationic rhodium(I) and iridium(I) α-diimine complexes, Polyhedron. 33 (2012) 360–366. https://doi.org/10.1016/j.poly.2011.11.058.

[9] M. Bikrani, M.A. Garralda, L. Ibarlucea, E. Pinilla, M.R. Torres, Pentacoordinated cationic rhodium(I) and iridium(I) organocomplexes with α-diimine ligands derived from glyoxal: Crystal structure of [Rh(norbornadiene) (glyoxalbis(4-dimethylamino-anil))-(PPh3)]BF4·1/2CH2Cl2, Inorganica Chim. Acta. 282 (1998) 230–236. https://doi.org/10.1016/s0020-1693(98)00237-0.

[10] M. Bikrani, R. El Mail, M.A. Garralda, L. Ibarlucea, E. Pinilla, M.R. Torres, Pentacoordinated diolefinic rhodium(I) organocomplexes with α-diimine ligands. Crystal structures of

[Rh(Nbd)(LL)(PPh3)]ClO4 (Nbd=norbornadiene; LL=Bdh, biacetylidihydrazone; Pvdh, pyruvaldihydrazone; Bda, biacetyldianil), J. Organomet. Chem. 601 (2000) 311–319. https://doi.org/10.1016/S0022-328X(00)00090-5.

[11] K. Wajda-Hermanowicz, A. Kochel, R. Wróbel, Coordination studies of nitrogen-containing aryl phosphine ligands PˆN and PˆNˆN with rhodium, J. Organomet. Chem. 860 (2018) 30–48. https://doi.org/10.1016/j.jorganchem.2018.01.060.

[12] L.D. Field, B.A. Messerle, K.Q. Vuong, P. Turner, Rhodium(I) and iridium(I) complexes containing bidentate phosphine-imidazolyl donor ligands as catalysts for the hydroamination and hydrothiolation of alkynes, Dalton Trans. 38 (2009) 3599. https://doi.org/10.1039/b821188d.